MINERALOGY, PETROLOGY AND GEOCHEMISTRY OF CARADOCIAN PHOSPHORITES, N. WALES, U.K.

Neeta Saigal

A Thesis Submitted for the Degree of PhD
at the
University of St Andrews

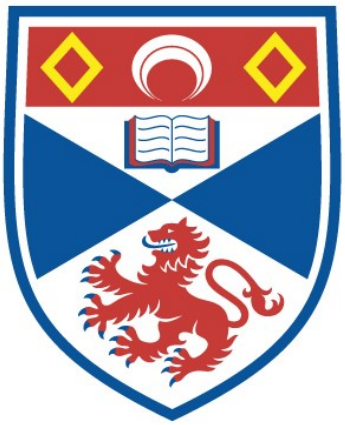

1985

Mineralogy, petrology and geochemistry of Caradocian phosphorites, N. Wales, U.K.

A dissertation submitted for the degree of Ph.D. at the University of St Andrews, February, 1985.

Neeta Saigal

ProQuest LLC.
789 East Eisenhower Parkway
P.O. Box 1346
Ann Arbor, MI 48106 – 1346

ACKNOWLEDGEMENTS

The work pertaining to the present thesis entitled "Mineralogy, petrology and geochemistry of Caradocian phosphorites, N. Wales, U.K.," was carried out during the tenure of research fellowships granted by the St Andrews University, Scotland, U.K.

I am grateful to Professor E.K. Walton, my Research Supervisor for guiding me throughout the course of this investigation, helping me out with stimulating and fruitful discussions and critically reading the manuscript.

I have no words to express my gratefulness towards my husband, Dr G.C. Saigal for his patience, enncouragement and help throughout my studies.

It is my pleasure to record my sincere appreciation for Mr R.A. Batchelor and Dr W.E. Stephens for computing work. Thanks are also due to Mrs J. Galloway, Mr. S. Bateman, Mr D. Herd and Mrs J.A. Kinnaird for general help. Mr A. Mackie for thin section and polished section work, Mr A.J. Reid for help in X.R.D. studies and Mr J. Allan for photography.

I also express my gratitude to every member of this Deparment for their help and co-operation during the day-to-day work.

I am obliged and thankful to Professor J.E. Prentice of the Department of Geology, King's College London, for providing most of the phosphorite samples studied during the present investigation. Significant help was received from Dr J.N. Walsh, King's College, London, for major and trace element analyses of phosphorite samples on

inductively coupled plasma source spectrometer. I am highly obliged for his active co-operation in getting the analyses done in the short duration of my stay with King's College, London.

I am also grateful to Dr A.E. Fallick, S.U.R.R.C., East Kilbride, Glasgow, for many helpful discussions and assistance in analysing the stable carbon and oxygen isotopes. I also acknowledge Mr A.S. Edwards of the Gatty Marine Laboratory, St Andrews, for his help during SEM work. Sincere thanks are due to Dr P.J. Hill of the Grant Institute of Geology, Edinburgh, for electron microprobe analyses.

I owe special thanks to Dr D.M. Banerjee, Department of Geology, Delhi University, India for his constant encouragement throughout my studies.

I gratefully acknowledge the receipt of an Overseas Research Grant and Research Fellowships from St Andrews University, the Continental Oil Company and the Leckie Trust. I thank Marry for typing the manuscript.

CERTIFICATE

I herby certify that NEETA SAIGAL has been engaged in research for nine terms at the University of St Andrews, that she has fulfilled the conditions of Ordinance No 12 and resolution of the University Court, 1967, No 1, and that she is qualified to submit the accompanying thesis in application for the degree of Doctor of Philosophy.

I certify that the following thesis is of my own composition, that it is based on the results of research carried out by me, and that it has not previously been presented in application for a higher degree.

ABSTRACT

Caradocian phosphorite nodules sampled from the Powys county of N. Wales, U.K. have been investigated in order to characterize the deposit geochemically, mineralogically and petrographically and to evaluate their mode of formation. Nodules are the main form of phosphorite although phosphatized organic fragments and oolitic grains are also present. On the basis of petrographic characteristics, nodules are grouped into two types: Type I nodules (with abundant organic material) and Type II nodules (with abundant clay minerals). Mineralogical compositions of the phosphorite nodules reflect varying degrees of dilution of the phosphate material, francolite, by authigenic and detrital minerals. Examination with the scanning electron microscope of freshly fractured surfaces of nodules suggests that the apatite formed authigenically as a direct chemical precipitate. Surfaces of abundant siliceous spicules and other organic fragments as well as some minerals appear to be favoured sites for apatite nucleation. Geochemical studies showed significant impoverishment of lattice elements and enrichment of non-lattice elements in both types of nodules. Chemically the phosphorite nodules may be described in terms of four major components: SiO_2, CaO, P_2O_5 and F. The average concentrations of trace elements present in these

nodular phosphorites were compared with an average concentration in marine shales. The enrichment and/or depletion largely suggested precipitation from sea water.

The proposed model of phosphorite formation involves inorganic (or biochemical) precipitation of apatite within pore waters of anoxic sediments and subsequent concentration of the apatite by physical processes. Oxidation of organic material during sulphate reduction is the main source of phosphate. This is supported by the very light $\delta^{13}C$ isotopic composition of structural carbonate present in the francolites.

These studies have also shown that these phosphorites have undergone differential leaching during weathering processes with the development of secondary phosphate minerals, decarbonation of francolite and removal of many major and minor elements.

CONTENTS

LIST OF FIGURES

LIST OF TABLES

LIST OF APPENDICES

CHAPTER I

INTRODUCTION

Most marine sedimentary rocks contain less than 1% P_2O_5. Phosphorites are sedimentary rocks with a much higher phosphate content; an arbitrary minimum being usually taken at between 15 and 20% P_2O_5 (Bentor, 1980) although it has often been set as low as 5% P_2O_5 (Bushinskii, 1969; Riggs, 1979a). They are practically all marine rocks apart from the rare instances of lacustrine phosphorites and small continental deposits of bird guano (Burnett, 1980). The main P-bearing mineral of phosphorite is apatite, but more specifically it is nearly always francolite $(CaMgNaSr)_{10}(PO_4SO_4CO_3)_6\ F_{2-3}$) which is metastable with respect to fluorapatite ($Ca_{10}\ (PO_4)_6F_2$) (McClellan, 1980).

Phosphorites which are low in gangue minerals and thus high in phosphate content are often mined for commercial use. They are of considerable economic importance representing over 80% of the raw materials used in the manufacture of phosphate fertilizers and many P-based chemicals; an important mineral industry ranking second (if hydrocarbons are excluded) to iron ore, in the world in terms of production and international trade (Notholt, 1980). During beneficiation there are possibilities of extracting further valuable elements such as uranium, rare earths and fluorine which are substituents in the apatite structure. Practically all 'economic phosphorites' are from stratified marine deposits but they are extremely varied in petrography, mineralogy, chemistry, origin and age.

Phosphorites occur in sedimentary deposits of almost all ages from the Precambrian but there are periods when phosphorite formation was particularly common (Cook and McElhinny, 1979). They appear to be forming today as minor deposits in coastal-upwelling regions off Peru/Chile and Namibia and formed in the late Quaternary in the mild seasonal upwelling regions west of South Africa and east of Australia (Burnett and Veeh, 1977; Price and Calvert, 1978; O'Brien and Veeh, 1980; Birch, et al, 1983).

Phosphorites are extremely varied petrographically ranging from microgranular pellets to phosphatized conglomeratic wackestones in the same deposit (Birch, 1980). Pelletal textures are characteristic of most major deposits and are therefore well documented (eg Bushinskii, 1935; Mabie and Hess, 1964; Cook, 1972; Birch, 1979b). There are at least six types of apatite pellets (Mabie and Hess, 1964), the most common being those of a spherical to oval shape with no internal structures. Apatite pellets usually range from 0.06-4 mm in size (Altschuler et al, 1958) but can be as large as 16 mm (Mabie and Hess, 1964).

Modern authigenic phosphorite concretions are friable and exhibit a great variety of morphology and size but can be up to 10 cms in length (Baturin et al, 1970). Elongate, cylindrical coprolite lumps containing fish-scales and small vertebrae are a particularly common form of modern concretionary phosphorite (Bremner, 1980). Authigenic nodules are harder and typically several cms in size (Baturin et al, 1970). Phosphorite pellets, nodules, and concretions may all contain inclusions which often include fossil fragments, quartz, clay minerals, glauconite,

pyrite and organic matter.

Phosphatized carbonates and bone material form a variety of phosphorite types depending on the precursor. Shell debris and bone and teeth fragments can be converted to phosphorite pellets (Reeves and Saadi, 1971; Tankard, 1974), larger carbonate fragments to angular phosphorite nodules (Cullen, 1980) and whole carbonate beds to massive phosphorite sheets and blocks weighing hundreds of kilograms (Manheim et al, 1980) or to extensive phosphatic hardgrounds (Jarvis, 1980). Carbonate cement infillings can also be phosphatized to form phosphatic steinkerns (Kennedy and Garrison, 1975).

Authigenic microcrystalline francolite cement often termed 'microsphorite' or 'collophane mudstone' is an extremely common form of phosphorite. It can occur as burrow infills, steinkerns, disseminated cement or as distinct laminar beds (Riggs, 1979b).

Apatites are capable of concentrating considerable amounts of various trace elements (Cossa, 1878; Swaine, 1962; Tooms et al, 1979; Gulbrandsen, 1966; Altschuler et al, 1967; Kholodov, 1973; Calvert, 1976; Altschuler, 1980; Prevot and Lucas, 1980; McArthur, 1978, 1980). As pointed out by Tooms et al (1969), the trace element pattern is a function of two factors: a crystal chemical one, the capability of the apatite lattice to accept foreign ions and a geochemical one, the availability of these elements in the environment of apatite formation. A good example of an element easily available but not accepted by apatite is iodine (Shishkina and Pavlova, 1973). In a sediment rich in organic matter, it is plentiful, but because of its large ionic size it is rejected by apatite as it cannot be accommodated in

the channels of its structure which contain the much smaller F-ions. On the other hand, there are many elements which, if present in the environment, are readily accepted into the lattice and thus might provide clues for the mode of apatite formation. McArthur (1978) proposed the constant composition hypothesis which suggests that upon formation the chemistry of all marine sedimentary carbonate fluorapatite may be very similar and subaerial weathering systematically reduces the concentrations to a low stable level. McClellan (1983) supported the constant composition hypothesis on the basis of mineralogy and showed how francolite systematically alters towards fluorapatite as a result of variety of geological processes.

The origin of phosphorites has been a matter of dispute for many years and progress in understanding phosphogenesis has been very slow. The main problem which faces phosphorite researchers is that abnormal marine conditions are required for the preferential precipitation of francolite with respect to $CaCO_3$ (Gulbrandsen, 1969). Under normal marine conditions sea water contains 140 ppm bicarbonate (Culkin, 1965) and only 75 ppb phosphate (Birch, 1980) and this is reflected by the average carbonate rock containing only 400 ppm P (Turekian and Wedepohl, 1961). Francolite solubility in sea waters is not well understood owing to complex surface interactions but it would appear that sea water is slightly undersaturated with respect to apatite (Atlas and Pytkowicz, 1977). Possible phosphate precipitation is in any case likely to be swamped by $CaCO_3$ precipitation (Gulbrandsen, 1969). Therefore the enhancement of sea water phosphate concentration is not the sole prerequisite

for phosphorite formation; the formational environment must also favour francolite precipitation over $CaCO_3$ precipitation.

In 1937, Kazakov published the first theory on phosphorite genesis which attempted to explain the preferential precipitation of francolite with respect to $CaCO_3$. He reasoned that below 200 m sea water contained enough CO_2 to be undersaturated with respect to francolite and yet above 50 m in the zone of photosynthesis the available phosphorus is assimilated by phytoplankton at the expense of possible phosphorite formation. He therefore linked phosphorite sedimentation to oceanic upwelling arguing that as deep ocean waters rises to the surface its temperature rises, and as a result of decreasing pressure, CO_2 escapes thereby increasing the pH. At that time the solubility of apatite was thought to decrease with both increasing temperature and pH, so Kazakov (1937) concluded that the upper part of the rising current becomes over saturated with francolite thus resulting in the inorganic precipitation of phosphorites.

Kazakov's theory has now been refuted for CO_2 cannot escape faster than the velocity of the upwelling currents (Bushinskii, 1966) and an increase in pH would in any case increase the solubility of francolite with respect to calcium carbonate (Nathan and Saas, 1981). Furthermore many phosphorite deposits bear sedimentary structures of shallow water (euphotic zone) deposition which is forbidden by Kazakov's theory and faunal features have shown that some phosphorites formed in restricted basins in which no water column phosphate regeneration could have occurred (Kolodny, 1981). However, many workers still believe

that strong upwelling, which can occur on the equatorial side of the Mediterranean type sedimentary basins or the west coasts of continental margins, is the predominant source of phosphorus in most major phosphorite deposits (McKelvey, et al, 1953; Sheldon, 1964a; Cook and McElhinny, 1979).

Most of the major phosphorite deposits appear to have formed on stable shelves or platforms at several hundred metres below sea level in area of low palaeolatitudes and arid climatic conditions (Sheldon, 1964b; Cook and McElhinny, 1979). They typically display condensed sequences of phosphatic and carbonaceous shales, clays, cherts and limestones and are notably deficient of terrigenous sediments. The recognition of this characteristic 'phosphate facies' has led to the discovery of several economic phosphorite deposits (Sheldon, 1964b).

The P-Si-C biophile-element trinity of the phosphate - chert or porcellanite - organic matter association of the 'phosphate facies' suggests that the main step in the two million fold concentration of phosphorus from sea water to francolite is biochemical rather than inorganic (Bentor, 1980). This association is found today in oceanic upwelling regions (Bremner, 1980) and it was hoped that their discovery might lead to a general theory for the formational mechanism of most if not all major phosphorite deposits. Unfortunately these hopes have been disappointed. Seafloor phosphorites are difficult to study in situ and also to collect, for they occur on continental shelves, and rises, commonly at depths of over 50 m (Kolodny, 1981). Progress in understanding modern phosphogenic systems therefore has been slow and the origin of modern offshore Peru/Chile

phosphorite has been hotly debated (Burnett et al, 1980; McArthur, 1983). It has been found also that numerous differences exist between recent and ancient phosphorites (Bentor, 1979).

Recent phosphorites are commonly nodular (Baturin, 1971; Burnett, 1977; Price and Calvert, 1978; Bremner, 1980) but this is comparatively rare in older deposits, which have variable textures but are mostly pelletal and set in a fine grained phosphatic matrix (Bentor, 1979, 1980). Unlike Recent phosphorites, older phosphate deposits are often associated with carbonates (McKelvey et al, 1953; Bentor, 1980) and often formed in areas of slow deposition (Baird, 1978; Jarvis, 1980; Odin and Letolle, 1980). The finely laminated and oolitic textures of many of the large older deposits is often thought to indicate an origin above the sediment-water interface whereas modern phosphorites appear to be forming exclusively below the boundary (Sheldon, 1981). Finally the modern phosphorites are only tiny deposits in comparison to many ancient deposits. The modern offshore Peru/Chile phosphorite reserves for example only amount to 10^8 tons compared to the 16×10^9 tons of phosphorus of the Permian Phosphoria Formation of the USA (Cathcart and Gulbrandsen, 1973).

Despite these differences, the discovery of modern phosphorites has established the fact that francolite can form authigenically in organic rich muds (Baturin et al, 1970; Price and Calvert 1978; Bremner, 1980) and that bacteria may play a direct role in phosphogenesis in some instances (O'Brien and Veeh, 1981). These provide alternative phosphogenic mechanisms

to the well documented replacement of carbonate which has clearly occurred in many seafloor phosphorites (Summerhayes, 1970; Parker and Seisser, 1972; Birch, 1980; Cullen, 1980; Manheim et al, 1980).

Recently phosphorite researchers have turned to stable isotope geochemistry as a tool for unravelling the past environments of formation but very little work has been done so far. In the work published to date the isotopic composition of structural PO_4-O, CO_3-C+O, and SO_4-S has been considered (Longinelli and Nutti, 1968; Kolodny and Kaplan, 1970; Nathan and Nielson, 1980). Benmore et al, (1983; 1984) and McArthur et al, (1980) found that the isotopic composition of structural carbonate in francolite is particularly useful in discriminating between phosphatized carbonates (replacement francolite) and authigenic francolite and may be able to define diagenetic zones of francolite formation.

1.1 SCOPE OF THE PRESENT INVESTIGATION

Phosphate rock is widely but sporadically distributed in the United Kingdom principally in the form of phosphatic nodule beds and the phosphatized casts of fossils. These occur at numerous stratigraphical horizons starting from Precambrian (Aultbea Formation, Torridonian, N Scotland) up to the Pleistocene (Red Crag nodules, Suffolk). Among all these occurrences, the highest P_2O_5 contents are recorded from nodules present around the Berwyn Mountains of N Wales and these constitute the subject matter of the present work. The phosphate nodules are present in thin beds of uppermost Caradocian rocks.

Nodules embedded in calcareous cherty mudstones are the main form of phosphorite although phosphatized organic fragments and a few oolites are also present. An attempt has been made to characterize the phosphorite chemically, mineralogically and petrographically.

In brief the overall purpose of this investigation is to

1) establish the petrological and mineralogical details of these phosphorites with the help of X-ray diffraction, scanning electron microscopy and standard petrographic studies.
2) carry out analytical studies of major and trace elements using Inductively Coupled Plasma Source Spectrometer and Electron microprobe.
3) analyse the stable carbon and oxygen isotopes of structural carbonate in apatite to support the replacement/authigenic origin.
4) Unravel the origin of the phosphorite in Berwyn Mountains on the basis of the results from 1, 2 and 3.

CHAPTER II

GEOLOGY AND STRATIGRAPHY OF PHOSPHORITE DEPOSIT

2.1 PREVIOUS WORK

Caradocian rocks of N Wales form a fairly uniform and very thick sedimentary sequence which underlies the phosphorite bed. Although the phosphorite occurrences have been known since 1863, they were first reported by Voelcker in 1866. The first detailed succession of phosphorite beds was produced by Davies (1875). A phosphate deposit was discovered above the Bala Limestone in the west and Davies (1875) gave valuable descriptions of the limestone succession in the Cwmgwnen and Berwyn mine sections which are now mostly inaccessible. The geology and structure of some of the phosphorite occurrences have been described by Wade (1911), King (1923, 1928), Jehu (1926), Pugh (1923, 1928), Williams and Bulman (1931), Cayeux (1932) and King and Williams (1948). King (1928) described the phosphate bed in some detail stating that the section at Meifod is very similar to Pen-y-Garnedd section. No sign of fossils were detected in the phosphate bed, other than some traces of minute bryozoa visible in rock slices. Cave (1965) worked around Gwern-y-Brain (near Welshpool) and described the Pen-y-Garnedd Shale and Pen-y-Garnedd Phosphorite members of the Nod Glas Formation. Nod Glas is a group of black mainly argillaceous sediments having an outcrop in the Gwynedd, Clwyd and Powys counties of Wales. The name Nod Glas was first used by Pugh (1923) for black shales and pyritous mudstone around Corris and Aberllefenni. North of these areas, Nod Glas thins and around Bala it disappears. The thinning is apparently in

sympathy with the appearance within it of fine arenaceous, calcareous muddy siltstone and near the base, traces of phosphatic material. The Nod Glas exposed at Powys, further to the east,has been divided into an upper portion of shale or mudstone, known as the Pen-y-Garnedd Shale and a lower phosphorite bed which is usually with a phosphatic limestone (Cave, 1965). In terms of thickness, the proportion of shale to phosphorite varies from one area to another, the shale in some places being thin or even absent.

Detailed micro-palaeontological studies have been carried out on the phosphate bed of Pen-y-Garnedd area by Lewis (1940). He described mainly silicispongiae (Hexactinellida and Demospongiae) and Hystrichosphaeridium (belonging to the Chitinozoa?) a group of uncertain position. He also reported bryozoa and brachiopods in these sediments.

The age of the Nod Glas in the Berwyns is still undetermined in terms of the faunal stages of Costonian to Onnian. On Bancroft's classification (1945) the Pen-y-Garnedd Shale exposed near Welshpool belongs to the Onnian gracilis zone. Thus with the beds below the Nod Glas belonging to the Upper Longvillian substage, a period of time representing the stages Marshbrookian, Actonian and part of the Onnian is left to be represented by Pen-y-Garnedd Phosphorite only. Cave (1965) suggested that either the Pen-y-Garnedd Phosphorite represents continuous but slow precipitation spanning the whole of this period or the deposit was laid down in the late stages only of that time gap, leaving a non-sequence beneath it. He preferred the latter view suggesting that a large hiatus, between

Longvillian and Onnian, is present at the phosphorite horizon.

2.2 LOCAL GEOLOGY

Phosphorite occurrences of the Powys area are found in the lower portion of the Nod Glas Formation. At Welshpool this Formation is divided into two members (Cave, 1965).

(ii) Pen-y-Garnedd Shale

(i) Pen-y-Garnedd Phosphorite

(b) Nodular Bed

(a) Basal Limestone

Cave (op cit) avoided using the term Pen-y-Garnedd Limestone for the limestone present in the base of the Pen-y-Garnedd Phosphorite because Pen-y-Garnedd Limestone refers to beds of different age and which are in part equivalent of the Gelli Grin Group and Bala Limestone (Wedd et al., 1929). Cave's terminology has been followed in the present work.

Phosphorite crops out on both sides of the Central Wales Syncline and also along the south eastern limb of the Berwyn anticline (Fig. 2.1). The present studies were carried out on phosphorite samples collected from several old workings located on the eastern (Pwll-y-Wrack, Cwmgwnen and Pen-y-Garnedd areas) and western (Berwyn and Pennant (Nant-Achlas) sections) limbs of the Berwyn anticline. Four lithological sections present at Berwyn (Davies, 1875), Nant-Achlas (Brenchley, 1966) Pen-y-Garnedd (Taylor, unpublished) and Gwern-y-Brain (Cave, 1965) are compared (Fig 2.2) and described in the following pages:

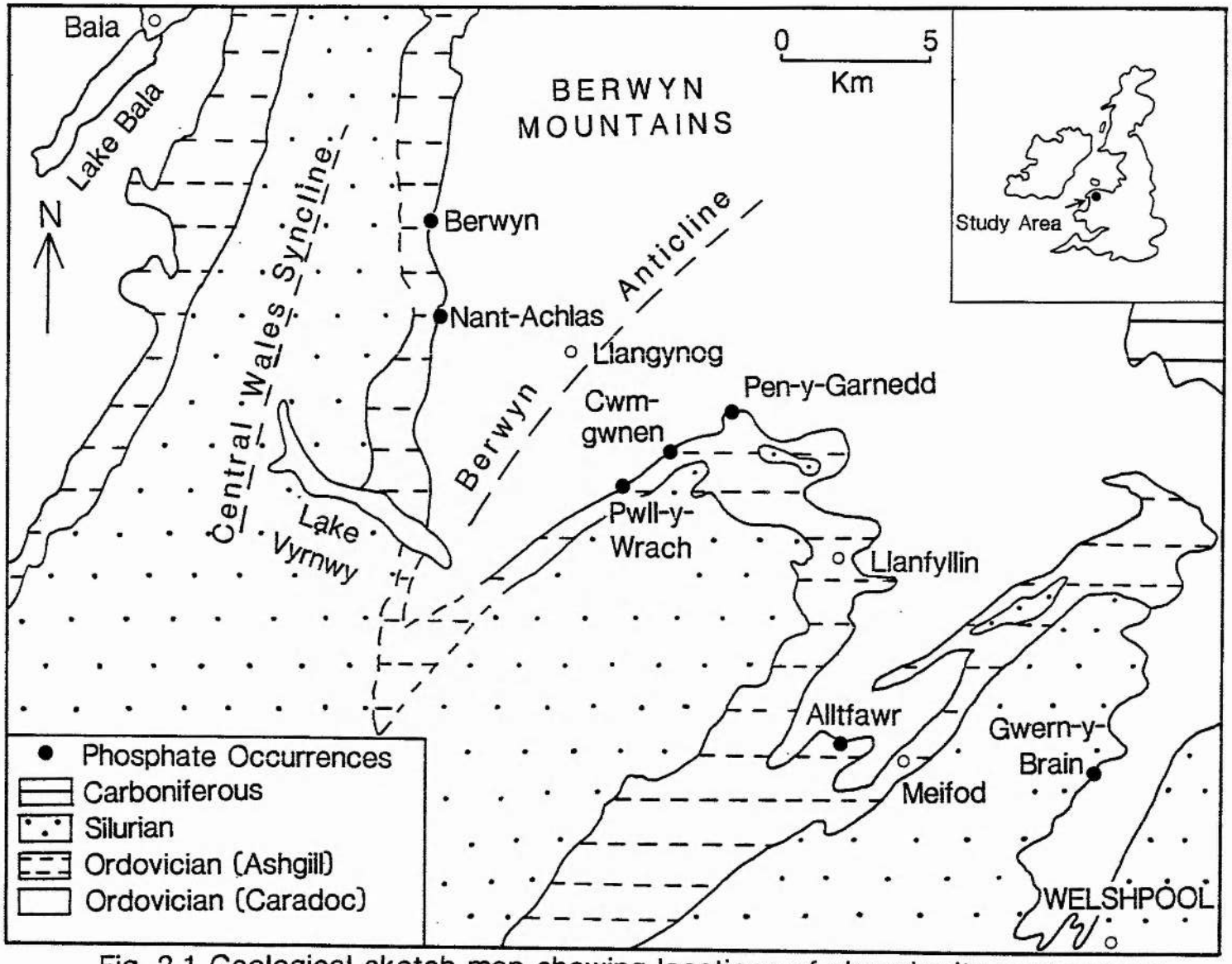

Fig. 2.1 Geological sketch map showing locations of phosphorite occurrences in N. Wales (Cave,1965).

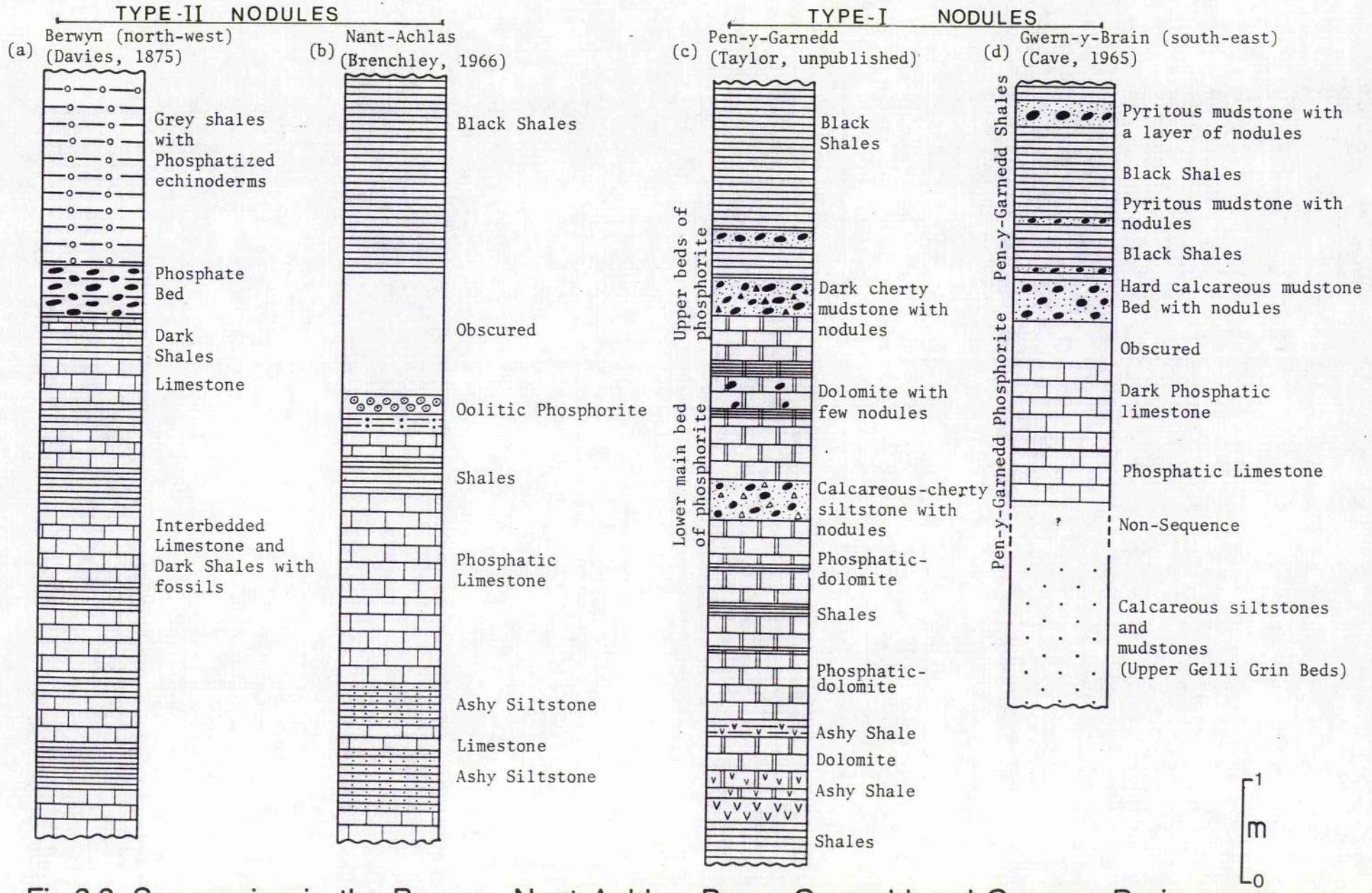

Fig.2.2. Succession in the Berwyn, Nant-Achlas ,Pen-y-Garnedd and Gwern-y-Brain areas.

(i) Pen-y-Garnedd Phosphorite

Eastern limb of Berwyn anticline

Former underground workings at Cwmgwnen and Pwll-y-Wrack are now inaccessible, but exposures of the phosphorite bed are still largely accessible at Pen-y-Garnedd area. At the base of the Pen-y-Garnedd section a thin ashy gritty shale and tuff band occurs succeeded by a 2 metre thick bed of dolomite interbedded with dark shales and mudstones. This is capped by 40 cms thick hard calcareous mudstone containing phosphatic nodules with visible white organic fragments (lower phosphorite bed). This phosphorite bed is overlain by a bed of dolomite interbedded with dark shales similar to the underlying bed. It is about 140 cms thick and at places contain a few nodules. This bed is succeeded by a thin dolomite bed (with baryte veins) and another phosphorite bed (Upper). This upper phosphorite bed which is about 40-45 cms thick and pyritized, is followed by dark shales belonging to the Pen-y-Garnedd Shale member with a thin layer of nodules towards the base (Fig 2.2c). In this layer nodules are very similar to the lower main bed of phosphorite although in size they are much smaller.

The nodules present in the phosphorite beds are numerous, ranging in size from 2 cms to 8 cms (in longest dimension), closely packed and even run into each other. The upper bed of phosphorite near its outcrop becomes oxidized and changes its black colour for a rusty appearance. The non-pyritized and calcareous lower bed of phosphorite is referred to subsequently as Lower main bed of phosphorite whereas the overlying pyritized beds (upper bed of phosphorite present in the Pen-y-Garnedd

Phosphorite member together with thin layers of phosphorite present in the Pen-y-Garnedd Shale members) shall further be referred as Upper beds of phosphorite (Fig 2.2c).

At Meifod, a few miles south east of Pen-y-Garnedd, the thickness of the Lower main bed of phosphorite is 1 ft (King, 1928). It contains ostracods and is underlain by about 1 ft of dark limestone. At Gwern-y-Brain (a few miles further east of Meifod) the Lower main bed of phosphorite is about 30-35 cms thick with 120-150 cms of basal limestone (Fig 2.2d) which is highly phosphatic (Cave, 1965). The nodules are numerous, hard and black and have a mean diameter between 2-4 cms. The overlying Pen-y-Garnedd Shale members also contain a few thin bands of phosphatic mudstone. Nodules show calcitic remains of sponge spicules, ostracod valves and bryozoa set in a dark brown homogeneous and amorphous matrix. In the mudstones enclosing the nodules, the remains of ostracods are abundant. The valves of these ostracods are flattened which suggest that mudstone has suffered considerable compaction which the nodules have resisted.

Western limb of Berwyn anticline

Former underground workings at Berwyn are now inaccessible. Davies (1875) described the phosphorite bed, at the Berwyn mine as one of the strongest development of the nodular phosphorite, 10-15 inches thick, overlain by beds containing echinoderms and underlain by 6 inches of crystalline phosphatic limestone (Fig 2.2a). The nodular bed was said to divide laterally producing two minor layers above the main horizon. He made no mention of

any black Pen-y-Garnedd Shales.

Almost the complete sequence of the Pen-y-Garnedd Limestone exposed in Nant-Achlas is described by Brenchley (1966). The phosphorite beds are here represented by dark grey limestone and oolitic beds (Fig 2.2b). The lowermost 30 feet in the Nant Achlas succession consisting of pebbly siltstones and calcareous tuffaceous siltstones is characterized by rich fauna. The overlying beds with thicker limestones are poor in fossils. The Pen-y-Garnedd Shales overlying the phosphorites are well exposed in Nant Achlas where an estimated thickness of about 50 feet are seen. Elsewhere in the west Berwyns the shales are apparently absent and the Ashgillian lies on top of the Pen-y-Garnedd Limstone. In Nant-Achlas the lowermost twelve feet of the Pen-y-Garnedd Shales are not exposed. The overlying junction of the Pen-y-Garnedd Shales with the Ashgillian is well exposed and is seen to be slightly irregular; the shales are somewhat weathered and lighter grey immediately below the junction. Brenchley (1966) noted phosphate nodules occurring in the top few inches of the shales and in the lowest few inches of the Ashgillian. He suggested that a hiatus in sedimentation, represented by the presence of phosphate at the junction although he could not prove an unconformity between Ashgillian and Caradoc.

Immediately underlying the Pen-y-Garnedd phosphorite, is a thick sequence of carbonate rocks, namely Pen-y-Garnedd Limestone, which are in part equivalent to the Gelli Grin Group and Bala Limestone (Wedd *et al*, 1929). These limestone beds are mainly bioclastic with a calcite cement which commonly encloses

silt grains. The shell material, consisting of fragmented brachiopods, bryozoa and echinoderms, suggests that the shell have encountered turbulent conditions sufficient to comminute the shells. The debris is commonly enclosed within silty mudstone and it seems likely that the shell material has been transported from a high energy environment into a quieter environment where mud was being deposited (Brenchley, 1966). The environment of deposition of the Pen-y-Garnedd Limestone appears to be one of relatively low energy with currents incapable of sorting out the coarser volcanic detritus. Much of the sediment in the form of broken shells (and some ooliths) may well have been supplied from a carbonate rich environment with much more vigorous current activity. It is clear from this discussion that Brenchley (1966) described the phosphorite bed and underlying basal limestone under the name of Pen-y-Garnedd Limestone Group. Basal crystalline limestone (or dolomite) (Cave, 1965) lying below phosphorite bed (or at times above the phosphorite bed as eg around the Pen-y-Garnedd area) shows great variation in the thickness. Generally the thickness decreases towards eastern part of the deposit (minimum around Gwern-y-Brain area). These limestones are similar to Pen-y-Garnedd Limestone beds except that they are phosphatic, interbedded with dark shales and a significant part of the bioclastic material has either been replaced by calcite or dolomite. Around Pen-y-Garnedd area, dolomite is the main carbonate mineral whereas around Berwyn, Nant-Achlas and Gwern-y-Brain, it is largely calcite. It is a crystalline mass of calcite/dolomite with brown opaque material dispersed between the crystals.

(ii) Pen-y-Garnedd Shales

Overlying the phosphorite bed is a succession of almost black shales estimated as 40 feet thick at Gwern-y-Brain (Cave, 1965) and 50 feet at Pen-y-Garnedd and Nant Achlas (Brenchley, 1966). Elsewhere in the Cwmgwnen and Berwyns the shales are apparently absent, and the Ashgillian lies on top of the Pen-y-Garnedd Limestone. At Cwmgwnen and Berwyns, Davies (1875) noted calcareous shales with echinoderms and brachiopods resting upon a phosphate bed 25-115 cms thick (Fig 2.2a).

Cave (1965) noted four thin beds of pyritous mudstone around Gwern-y-Brain area comparable in texture to that of Phosphorite bed. These beds also contain some phosphatic nodules of a size similar to those found in the main bed below. Similar thin beds are also present in Pen-y-Garnedd section containing pyritized nodules and the host rock which is mudstone. Other exposures in the area are too poor to indicate whether or not these higher phosphatic layers pass laterally into the main bed in a manner similar to that described as occurring in the Berwyn Mine, near Llangynog (Davies, 1875).

CHAPTER III

PETROGRAPHY

3.1 INRODUCTION

In this Chapter megascopic, optical microscopic and scanning electron microscopic features of phosphorites are examined. Nodules are the main form of phosphorite in the Welsh deposit although phosphatized organic fragments and oolitic grains are also present. On the basis of petrographic characteristics these nodules are grouped under two types:

Type I Nodules

Nodules with abundant organic material but with little clay (present around Pen-y-Garnedd).

Type II Nodules

Nodules with abundant clay minerals but with little organic material (present around Nant-Achlas and Berwyn mines).

This Chapter will be dealt in the following three sections:

Section - 1 - Megascopic and microscopic characters of phosphorites and their host rocks

Section - 2 - Scanning Electron Micoscopic studies of phosphorites

Section - 3 - Discussion on diagenesis and weathering of phosphorites

SECTION - 1

3.2 MEGASCOPIC CHARACTERS

3.2.1 Type I Nodules

This type occurs on the eastern limb of the Berwyn anticline around the Pen-y-Garnedd area. Nodules are generally dark grey to black in colour, hard and have a polished appearance. No internal zonation or structure is seen. They are rounded and ellipsoidal. At many places 2-3 nodules coalesce to form one elongated nodule (Figs 3.1 and 3.2). The mean diameter of nodules varies between one to 3 cms although examples as large as 10-15 cms have also been reported (Davies, 1875). These nodules contain abundant dolomitic organic fragments. Nodules present in the main bed of phosphorite are not pyritized whereas nodules in the upper beds are pyritized. The nodules in both the main bed and in the upper beds are embedded in muddy siltstone.

3.2.2 Type II Nodules

This type of nodule occurs on the western limb of the Berwyn anticline. They are dark grey to black in colour, not very hard but have a polished appearance. Similar to Type I nodules, they do not show any internal zonation or structure. Usually spherical, at times they are flattened. The mean diameter varies between 2-4 cms. In contrast to Type I nodules, Type II nodules do not contain any visible organic fragments but are mostly pyritized and embedded in shales (Fig 3.3).

3.2.3 Oolitic Phosphorites .

Ooliths are white in colour and embedded in dark grey dolomitic host rock. Sometimes a few scattered ooliths are also seen to be embedded in shales along with Type II nodules.

3.3 MICROSCOPIC CHARACTERS

3.3.1 Type I Nodules (Present in the main bed of phosphorite)

Apatite (62.9% average) occurs mainly as cement in nodules. It is also present to a limited extent as skeletal infillings. At places under high magnification individual apatite crystals can be seen (Fig 3.4) although at many places apatite crystals appear to have coalesced with one another. Other constituents present in the nodules are: 11.2% organic fragments (dolomitized), 0.2-2.7% detrital quartz and feldspar, up to 1% detrital clays, 4.2% pyrite and about 2-3% carbonaceous matter and opaques (Table 3.1).

Nodules contain abundant remains of organic fragments, including detached spicules of Hexactinellida and Demospongiae along with a few ostracod valves, bryozoa, echinoderm and Hystrichosphaeridium tests (belonging to the Chitinozoa, a group of uncertain systematic position but possibly flagellates). Spicules range in size from <1-3 mm in length but transverse diameters are usually less than 1 mm (Fig 3.5). A few spicules show their original siliceous material although most of them are replaced by dolomite. A large number of fragile spicules are unbroken. Axial canals in many spicules are filled wholly or partly by granular apatite. It is also noticeable that the siliceous spicules did not suffer any marked changes prior to the

phosphate formation as the axial canal remained open to admit the granular apatite. Hystrichosphaeridium tests are spherical and about 0.05-0.07 mm in diameter with short, broad based and sharply pointed spines (Fig. 3.6). The aggregates of crystals present inside the tests are probably haematite. Lewis (1940) suggested that most of the carbon present in this deposit is probably derived from these Hystrichosphaeridium tests.

Detrital quartz and feldspar are present only in minor amounts (0.2-2.7%). They are angular to subangular varying in size from fine to coarse silt. Detrital quartz grains present mostly show wavy extinction.

Dolomite constitutes about 20-25% of the total nodule. Most of the spicules present in the nodule are dolomitic. Dolomite also replaces apatite cement, detrital quartz and feldspar grains.

Muscovite hashes are scattered in these nodules. Total clay percentage is very low (up to 1.0%).

Several irregular cracks can be seen in these nodules. Most of them are restricted to the nodules whereas others cut through the host rock as well. Cracks restricted to the nodules are filled with well developed apatite crystals (Figs 3.7 and 3.8), chert and some dolomite. Cracks running through the nodules and the host rock are filled only with dolomite (Fig 3.9).

Pyrite cubes are rare and occur as scattered individuals. Rarely, under high magnification development of secondary phosphate can be seen as pyrite pseudomorphs.

3.3.2 Type - I Nodules (Present in the upper beds of phosphorite)

These nodules are very similar to the nodules present in the main bed of phosphorite except that they are pyritized and do not contain carbonates (Fig 3.10). Modal analysis shows 70% apatite, 12.8% pyrite, 8% detrital quartz, 2.2% spicules, 1.8% feldspar, 2% recrystallized apatite and about 2% opaques and carbonaceous matter (Table 3.1). Under high magnification apatite crystals can be seen although much is obscured by pyritization.

Detrital quartz and feldspar (fine sand to silt size) and organic fragments (0.4-3.5 mm) are scattered uniformly. A few spicules are siliceous. Most other spicules and organic fragments are filled with an aggregate of tiny colourless birefringent laths with straight extinction (Fig 3.11). This mineral has been identified as illite-smectite mainly by microprobe and SEM studies (Fig 3.37). Authigenic illite-smectite precipitated in the voids provided by the dissolution of some unstable material surrounding the axial canals. Axial canals are filled with apatite and pyrite. Apatite present in many spicules is recrystallized displaying centripetal growth of small hexagonal apatite crystals (Fig 3.12). Apatite forming colloform texture is also present at places (Fig 3.13). It is evident that colloform apatite is diagenetic in origin resulting from recrystallization of pre-existing phosphate matter, in voids created by dissolution of some unstable material (perhaps some organic fragments). This type of apatite recrystallization is common and reported from

several phosphorite occurrences (Lowell, 1952; Gulbrandsen, 1960; Sweet and Croder, 1982).

Pyrite occurs in many forms eg as scattered grains, in clusters or as fracture fillings. Fractures are also filled with secondary phosphate replacing pyrite at places. Pyrite pseudomorphs are also common and occupied by Fe-rich secondary phosphate (Fig 3.14).

3.3.3 Host Rock For Type I Nodules (main bed of phosphorite)

The host rock for Type I nodules is calcareous, cherty and muddy siltstone. At a few places, shale and silty laminae are quite distinct but mostly they are diffused. Shale bands contain abundant carbonaceous and ferruginous matter in contrast to silty bands. As a result silty bands are much lighter in colour in plane polarized light (Fig 3.15).

Modal analyses show an average calcareous muddy siltstone contains about 19.8% detrital quartz, 4% plagioclase, 3.6% organic fragments, 5% clays and 2.5% carbonaceous and ferruginous matter cemented together by chert (42.8%) and carbonate (16.9%) cements (Table 3.2).

Fine sand to coarse silt size quartz is subhedral to euhedral due to syntaxial overgrowths (Fig 3.16). Probably biogenic silica precipitated as overgrowth on quartz grains forming sharp crystal faces and also as the chert cement present in the rock. The large chert cementation perhaps suggests a rapid rate of nucleation.

Dolomite cement is present filling pore spaces as scattered rhombs (Fig 3.17) and at places replacing chert, quartz (Fig

3.18) and plagioclases (Fig.3.19). Dolomite rhombs are more common in the muddy matrix than in the silty material. At places rhombs are ferruginous and show dark brown margins. Dolomite is also present as fracture filling material. These fractures even run through the enclosed nodules suggesting their late origin (Fig 3.9).

Phosphatized organic fragments include echinoderms, bryozoa, ostracods and brachiopod valves varying in size from 0.03 to 1 mm. Most of them show a ragged outline due to dissolution at their margins. A few of them are partially to completely replaced by chert.

Plagioclase feldspars are mostly altering into clays. Many of them show replacement by dolomite as well (Fig 3.19). Muscovite flakes are scattered everywhere. Clay matrix has much less silty material in comparison to shale bands. Pyrite is present either as scattered grains or in clusters. A few organic fragments are partially to completely replaced by pyrite.

3.3.4 Host Rock For Type I nodules (upper beds of phosphorite)

Modal analyses of the host rock for the nodules present in the upper beds of phosphorites show an average of 17.2% detrital quartz, 5% organic fragments, 5.9% feldspar, 7.7% pyrite, 6.2% clays cemented together by 23.8% chert and 34% ferruginous material (Table 3.2). Carbonate cement is absent except a few scattered ferruginous rhombs. The host rock is cut by veinlets carrying either pyrite or yellow-orange to orange-red material with colloform texture. A few pyrite pseudomorphs are also present filled with secondary phsophorite minerals.

3.3.5 Type II Nodules

The nodules have buff brown groundmass with few organic and oolitic fragments but with abundant clay minerals. Under high magnification apatite grains can be seen although pyritization has obscured most of them.

Clay minerals comprising illite-smectite, chlorite and muscovite are abundant. Chlorite stacks are usually roughly ovate with high relief and blue birefringence colours. Muscovite sometimes occurs interfoliated with chlorite. Muscovite flakes are common and identified by high interference colours. Illite-smectite was identified mainly by X-ray diffraction studies. Organic fragments are mostly shell fragments of bryozoa, echinoderms and a few detached spicules (of Hexactinellida and Demospongiae) about 0.4-1 mm in size. Some of them are now partly empty, others are filled with an aggregate of fine grained material of low birefringence (authigenic illite-smectite). Some carbonate is present replacing organic fragments. A few broken oolitic fragments are also present.

Another organic feature identified during the present investigation is a funnel shaped assemblage of filaments in one of the thin sections of Type II nodules (Fig 3.20). This filamentous form could be primitive algal or fungal hyphae. Under high magnification cellular structure resembling algae can be seen. Detailed discussion of this feature is beyond the scope of the present work.

Subangular to angular silt size detrital quartz, subordinate plagioclase feldspar and a few volcanic fragments are

present in all nodules.

Nodules also contain cracks filled mostly with either pyrite or a secondary phosphate mineral and rarely with carbonates, gypsum and apatite. At places pyrite has been partially to completely dissolved and the cracks are occupied by a secondary phosphate mineral (Fig. 3.21). This secondary phosphate is a yellow-orange to orange-red birefringent mineral occasionally with colloform texture (Fig 3.22). It is some hydrated phosphate of Fe and Al (Strengite?). Chemically it shows a large variation in its composition with colour. The Yellow-orange variety contains less iron and more Al_2O_3 in comparison to the orange-red which contains a very high percentage of Fe and low Al_2O_3.

Nodules also show the presence of secondary Al-phosphate, wavellite in cracks. The wavellite crystals are in the form of spherulitic aggregates (with radiating crystals) (Fig 3.23). Radiating texture is due to the arrangement of individual blades about a nucleus of the same composition. Wavellite crystals are colourless with high relief and low order interference colours.

A few cracks present in nodules are filled with gypsum (the mineral with a high Ca and S content can most reasonably be interpreted as gypsum) along with dolomite, apatite and pyrite (Fig. 3.24). The presence of gypsum in these marine sediments is puzzling although similar occurrences have been described by Marshall and Cook (1980) from nodules present around the E Australian continental shelf and off S W Africa by Siesser and Rogers (1976), who concluded as did Criddle (1974) that the gypsum formed by the reaction of sulphate ions introduced during

pyrite formation with calcium carbonate from the sediment.

3.3.6 Host Rock for Type II Nodules

The host rock for Type II nodules is shales. It is composed of clay matrix containing chlorite intermixed with muscovite flakes and silt grade quartz. Many phosphatized organic fragments, a few detrital medium sand size quartz, feldspar and volcanic fragments are present in clusters throughout (Fig 3.25). The shaly matrix mostly wraps around the nodules. Chlorite stacks are roughly ovate with high relief and blue birefringence colours. Muscovite occurs interfoliated with chlorite and shows high order interference colours. Silt size detrital quartz is angular to subangular. Most of the feldspars present have altered to clays (Fig 3.26).

Phosphatized organic fragments include shell fragments of brachiopods, bryozoa, echinoderms and a very few ostracod valves are present in clusters in the shaly matrix. They vary in size greatly from 0.1 mm to 1.4 mm. These fragments tend to be ragged in outline presumably due to dissolution.

Pyrite is present either in clusters or as a vein filling material. Secondary phosphate minerals are commonly seen to be present as vein fillings and rarely as pyrite pseudomorphs. The residual pores formed by the dissolution of some unstable material (?organic fragment) are also filled with secondary phosphate minerals (Fig 3.27). It is believed that some of the pyrite from veins was first dissolved and combined with apatite. Some residual pyrite can still be seen at places along with the secondary phosphate mineral.

3.3.7 Oolitic Phosphorite

Ooliths range from 0.3 to 0.7 mm in diameter and usually consists of a core surrounded by brown or colourless concentric layers (Fig 3.28). The core of the ooliths may be round or angular. It may be small or apparently absent. In some ooliths the core is a volcanic grain, while in others it is quartz or some shell fragment. The ooliths are spherical, at times deformed into ovoids or may be disrupted so that only a part of the oolith is preserved. The brown laminae of oolites are highly phosphatic (as revealed by microprobe studies). In some ooliths phosphatic laminae alternate with quartz laminae. Most of the oolites and organic fragments have been partially or wholly pyritized (Fig 3.29). Pyrite is mostly present all along the concentric laminae of oolites and at times as scattered crystals.

The host rock for these oolites and shell fragments appears to be an intimate mixture of isotropic and anisotropic material. The groundmass contains irregular relict masses of carbonate which has been replaced by fine grained colourless strongly birefringent material resembling mica. Along with mica, crystalline quartz is also abundant, at places surroundng oolites. Feldspars and volcanic fragments showing alterations are also abundant.

The rock is cut by veinlets carrying secondary phosphate minerals. At places pyrite cubes are partially or wholly replaced by secondary phosphate (strengite?) (Fig 3.30). The rock is highly altered and it is difficult to tell the original nature.

SECTION - 2

3.4 SCANNING ELECTRON MICROSCOPIC STUDIES

Scanning electron microscopic (SEM) examination of phosphorites reveals that apatite occurs as well developed crystals cementing mainly organic fragments in Type I (Figs. 3.31 and 3.32) and clay minerals in Type II nodules (Figs 3.33 and 3.34). Apatite crystals are somewhat variable in size and generally are of the order of 4-5 μm along the c-axis although crystals as big as 10 μm are also present at places (Fig 3.35). The crystals are prismatic with hexagonal outline. Rooney and Kerr (1967) have also reported very similar but much smaller hexagonal apatite crystals from Miocene rocks in the coastal plain of North Carolina. At places apatite needles have also been observed in intercrystalline spaces. The needles represent apatite poor in carbonate content (Fig 3.36).

An interesting feature shown by Type I nodules is the presence of elongated rod like bodies composed of apatite crystals. These rods probably represent the relicts of axial canals of spicules and project into voids created by the dissolution of spicular material (Figs 3.37 and 3.38). Rims or walls of these voids also show similar growth of apatite crystals. The nodules present in the upper beds of phosphorites, however, show the authigenic smectite-illite clays in these voids (Figs 3.39 and 3.40). Many other organic fragments also show authigenic apatite precipitation on their surfaces (Figs 3.41 and

3.42).

Both types of nodules show the presence of irregular cracks. These cracks may have developed by contraction of sediments suggesting subaerial exposure (Fig 3.43). Very frequently Type II nodules show the presence of euhedral pyrite crystals with interlocking texture (Fig 3.44). Most of these pyrite cubes show very clear dissolution features (Fig 3.45).

SEM studies also show the presence of organic forms which could be bacterial, fungal and/or algal bodies. They are bean shaped and attached to solid surfaces. Generally they are present either as an individual cell or at times two or three attached to one another (Figs 3.46). The cellular structure is 5-7 μm in length and 1-1.5 μm in width, generally cylindrical with a tendency to be curved in the centre. O'Brien et al (1981) reported very similar structures in East Australian phosphorites and concluded that the phosporites originated through the slow bacterial assimilation of P from seawater in an area of restricted sedimentation. It is not known whether the phosphorites under present investigation were formed by the similar process or not but the occurrence of these unidentified organic forms do suggest some direct or indirect biological control.

In brief, these SEM studies are significant mainly because

1 there appears to have been direct precipitation of apatite.

2 the crystal habits are consistent with inorganic precipitation, though the possibility that microbial activity within the sediments could have influenced the physico-chemical conditions cannot be ignored,

3 there is a striking similarity between the Welsh phosphorites and those from Recent offshore phosphorites from Chile and Peru (Burnett, 1977) and nodules from East Australian continental shelf (Marshall and Cook, 1980). Morphological similarities amongst these deposits may suggest that similar chemical processes have been operative in all cases.

SECTION - 3

3.5 DISCUSSION

3.5.1 Apatite Precipitation and Formation of Nodules

The most striking sedimentological feature of the Type I nodular phosphorites is the scarcity of detrital sediments. Fine quartz sand is the most abundant detrital sediment but it is present only in a minor amount. The most part of the Type I nodules consists of chemical precipitate (apatite) and biogenic material. Type II nodules in contrast contain clays and a few detrital quartz, feldspar, volcanic fragments along with chemical precipitate (apatite). It suggests that the sedimentary environments were quite different at the eastern and western parts of the deposit. The absence of clays and presence of detrital quartz sand grains in Type I nodules indicates a moderately high energy environment. Western part of the deposit containing abundant clays was formed in a semiprotected low energy environment. The presence of a few quartz, feldspar, volcanic framgments and rarely organic fragments suggest periodic sediment influx.

The biogenic material present in Type I nodules is largely sponge spicules of Hexactinellida and Hyalospongia and rarely mollusks, crustaceans and Hystrichosphaeridium tests. The near absence of organic remains in the Type II nodular phosphorite may support the fact that the physico-chemical conditions were quite diferent during the formation of two types of nodular phosphorites. The presence of algae/fungi and bacteria-like bodies suggest the existence of some organic acitivity even in the western part of the basin. Another likely explanation is the presence of some toxic chemicals which did not allow luxuriant growth of organisms. It is well known that organisms play a major role in the formation of sedimentary phosphorites. They are an important biological phosphate machine which directly concentrates phosphorus and modified its distribution and its chemistry within the depositional environment (McConnell, 1963; 1973; Riggs, 1979; Doyle et al, 1978; Burnett, 1977). A few living inarticulate brachiopod build their shells out of carbonate fluorapatite. Crustaceans generally have a carapaces with a very high phosphorus content (Clarke and Wheeler, 1922). The role of bacteria is probably even more important but it is also more elusive. The relationship of bacteria-like cells to marine phosphorites has been fairly well established (Riggs, 1979; O'Brien et al, 1981).

The altered character of the western part of the phosphorite bed may be due to the abundance of marine vegetation, although the role of plants in the phosphogenic system is totally unknown at present. However, Azad and Borchardt (1970) have found that the permanent storage of inorganic phosphorus by algae

is a normal characteristic in an environment where there is an excess over and above what is necessary for continuing metabolic needs. This "luxury uptake of phosphorus" reaches levels of 10% PO_4 dry weight in several species of green algae. The role that algae might play in the processes of concentration and precipitation of inorganic phosphorus in the sediments is not known.

The chemical sedimentation was probably fairly slow as indicated by the condensed succession (Cave, 1965). The chemical precipitate in both types of nodular phosphorite was mainly apatite (francolite), phosphorus being liberated by decaying protoplasm of marine organisms in the eastern part and algae and probably marine vegetation in the western part of the deposit. Robertson (1966) and Pytkowicz and Kester (1967) have shown that the solubility of apatite in sea water is greatly affected by pH variations. At higher pH values, apatite is less soluble. Berner (1969) showed in a series of laboratory experiments that a rise in pH may be expected during the decomposition of organic matter because of the formation of NH_4+ and other nitrogenous bases from the breakdown of proteins and other biochemical compounds. The thermodynamic solubility product constants for carbonate fluorapatite calculated at two different temperatures by Kramer (1964) indicate that apatite is less soluble at higher temperatures. It is conceivable that for a given system which is close to equilibrium relative to apatite, temperature variation of only a few degrees could determine whether apatite will precipitate. It is noteworthy that the Welsh deposit formed in Caradocian times when the seas must have been warm as the British

Isles are believed to have lain 30° South of the equator (Lovell, 1977). Under these favourable conditions ie higher than normal concentration of P, high pH and warm climate, apatite precipitation is believed to have occurred, particularly around various organic fragments as favourable nucleation sites. The primary precipitation of phosphorite is envisaged as producing a layer on the sea-floor. Nodules must have formed from breakage of this layer during a period of high energy (?storms) into fragments which were rounded during reworking. The alternative of the formation of nodules directly without fragmentation and abrasion is considered less likely because of the contrast in the chemical and organic composition between the nodules and their host rock. Although the complexity of the diagenetic processes that have taken place makes it difficult to present an accurate ordering of the events during formation of the rocks containing phosphorite nodules, a tentative paragenetic sequence can be outlined as follows:-

3.5.2 Type I Nodular Phosphorite Bed

1 Formation of phorphorite nodules.
2 Deposition of detritals along with nodules and phosphatized organic fragments, quartz overgrowth and chert cementation.
3 Compaction causing fracturing of the nodules and the host rock.
4 Calcitization followed by dolomitization of spicules and other organic fragments. Formation of scattered dolomite rhombs replacing detrital grains.
5 Pyrite filling residual fissures and pore spaces.

6 Dissolution of pyrite and apatite and formation of secondary minerals of phosphorite in veins and as pyrite pseudomorphs mainly in the upper beds of phosphorites.

3.5.3 Type II Nodular Phosphorite Bed

1 Formation of nodules.
2 Deposition of clay matrix along with nodules and phosphatized organic fragments.
3 Burial and compaction and formation of chlorite and illite clay minerals.
4 Pyrite filling fissures and pore spaces.
5 Dissolution of pyrite, clays and apatite and formation of secondary phosphorites including wavellite and hydrated Fe-Al phosphate.

3.5.4 Oolitic Phosphorite

1 Formation of oolites - by apatite precipitation around organic and rock fragments.
2 Deposition of clay matrix within open spaces between oolites, shell fragments and volcanic fragments.
3 Silica cementation in available pores as chert and quartz.
4 Pyritization of oolites, shell fragments and cementing material. Pyritization is most intense on oolites and shell fragments, whereas matrix and cement show very little effect.
5 Compaction causing squeezing of clay matrix, fracturing and denting of oolites.
6 Patchy development of carbonate replacing cement and matrix.

7 Dissolution of pyrite, apatite and clays and formation of secondary phosphorite minerals.

Formation of nodules in Type I phosphorites was followed by their deposition along with detritals including quartz, feldspars and clays as matrix in nearby areas within the basin. The second stage of diagenesis involved quartz overgrowth and chert cementation. Most of the fissures present in the nodules were filled with chert (partially with apatite as well). Silica precipitated as quartz overgrowth and chert cement present in the rock. The excessive chert cementation perhaps suggest rapid rate of nucleation ie the environment was highly favourable for silica precipitation so that large numbers of nuclei were formed. Third stage of diagenesis involved burial and compaction causing fracturing of the rock.

The fourth stage of diagenesis involved the precipitation of calcite/dolomite in residual pores, compactional fractures and replacement of most of the detrital crystals. Spicules present in the nodules and detrital quartz and feldspar present in the host rock were affected the most by calcitization/dolomitization. It is not known whether the calcitization has followed by dolomitization or whether there was direct precipitation of dolomite because at present all the carbonate is dolomite. Pyrite was formed during the last stages of diagenesis. It occurs as scattered grains all over the rock.

Type I nodules present in the upper beds of phosphorites have very similar diagenetic history except that during the formation of nodules the siliceous material surrounding the axial

canal of spicules was dissolved and filled with authigenic smectite-illite clays. No dolomite was observed in these nodules except a few ferruginous rhombs. During the late stages of diagenesis nodules and the host rock were affected by pyritization. Most of organic fragments were pyritized and the ferruginous material precipitated as cementing material along with chert in the host rock. Cracks are all filled with pyrite. Diagenetic reactions seem to stop after pyritization as effects of weathering can be seen.

In Type II phosphorites, nodules were deposited along with organic fragments in a clay matrix. This was followed by burial and compaction of the rock with the formation of fractures. The absence of dolomite (present in Type I phosphorite) may be explained by the fact that nodules are embedded in shaly rocks which are impervious and it was not possible for carbonate solution to migrate through the sediments. In shales, stagnant environments are created resulting in high CO_2 content (which can not be released because of impervious layers of clays) and hence low pH. In these conditions even if Ca, Mg and CO_3 ions are present they cannot precipitate. During closing stages of diagenesis pyrite was introduced preciptating in fractures and other voids.

3.5.5 The weathering of phosphorite

The very first and foremost affect of weathering is reflected in an impoverishment in the structural CO_2 content of carbonate fluorapatite. This is followed by the dissolution of primary apatite and precipitation of secondary apatite during

meteoric weathering. The impoverishment can result either from a modification of the genetic conditions as proposed by Gulbrandsen (1970) or from a transformation of carbonate fluorapatite into fluorapatite by leaching. According to the constant composition hypothesis, upon formation, marine sedimentary carbonate fluorapatite contains about 8.4% CO_3 and during weathering it reduces to low levels (McArthur, 1978). In sedimentary environments, as a matter of fact, fluorapatite is never a primary mineral but always a weathering product (Lucas et al, 1980).

Type I nodular phosphorite containing very little structural CO_2 may indicate weathering effect. An appreciable amount of free carbonates, protects apatite from being dissolved and going further down than the fluorapatite stage. It is noteworthy that these carbonate-rich phosphorites do not contain any secondary phosphorite minerals.

Type I nodules present in the upper beds of phosphorite do not contain free carbonate minerals which could be due to one of the two reasons given below:

i) calcite/dolomite was not introduced during diagenesis.

ii) calcite/dolomite has been completely dissolved during leaching.

The occurrence of a few ferruginous rhombs may suggest the presence of some dolomite which was dissolved later on. However, impoverishment in the structural CO_2 and presence of Fe-rich secondary phosphate suggest that these rocks have undergone intense leaching. After leaching of the free carbonate fraction and decarbonation of apatite, dissolution of apatite and etching

of associated minerals occur. Then two pathways are possible (Altschuler, 1973), either direct fixing of phosphorus and calcium, released from apatite on other minerals or combination of both ions with the aluminium and the iron leached from the lattice of these minerals. In Type I nodular phosphorite present in the Upper beds, both these effects can be seen. Apatite is present as colloform bands in voids or surrounding some organic fragments. Secondary Fe-Al phosphate is also present in fractures replacing pyrite and/or as scattered pyrite pseudomorphs. As expected all these hydrated Fe-Al-phosphates are very rich in Fe and poor in Al because of the fact that these rocks are rich in pyrite and poor in clay minerals.

Apatite present in Type II phosphorite is highly susceptible to dissolution during leaching as free carbonates are absent to protect it. The decarbonation of these apatite and the presence of wavellite and hydrated Fe-Al phosphates suggest that these rocks have undergone strong leaching during weathering mainly along fractures.

The secondary Al-phosphate, wavellite, forms during intense leaching by percolating water which first dissolve apatite and then clays. Calcium phosphate can be dissolved in the presence of carbonated water and react with aluminium hydroxide with the formation of aluminium phosphates. The chemical composition of these phosphorites shows the absence of CaO, thus removing the possibility of crandallite being present as an intermediate mineral in the weathering series of carbonate fluorapatite - crandallite - wavelllite. It could be possible that crandallite, formed during early stages of leaching, was gradually replaced by

the more stable product, wavellite.

Figure 3.1 Type I nodules embedded in calcareous mudstone. Arrow shows white organic fragments in the nodule.

Figure 3.2 Elongated Type I nodules. Arrow shows coalescing of two separate nodules. Note white organic fragments embedded in the nodule.

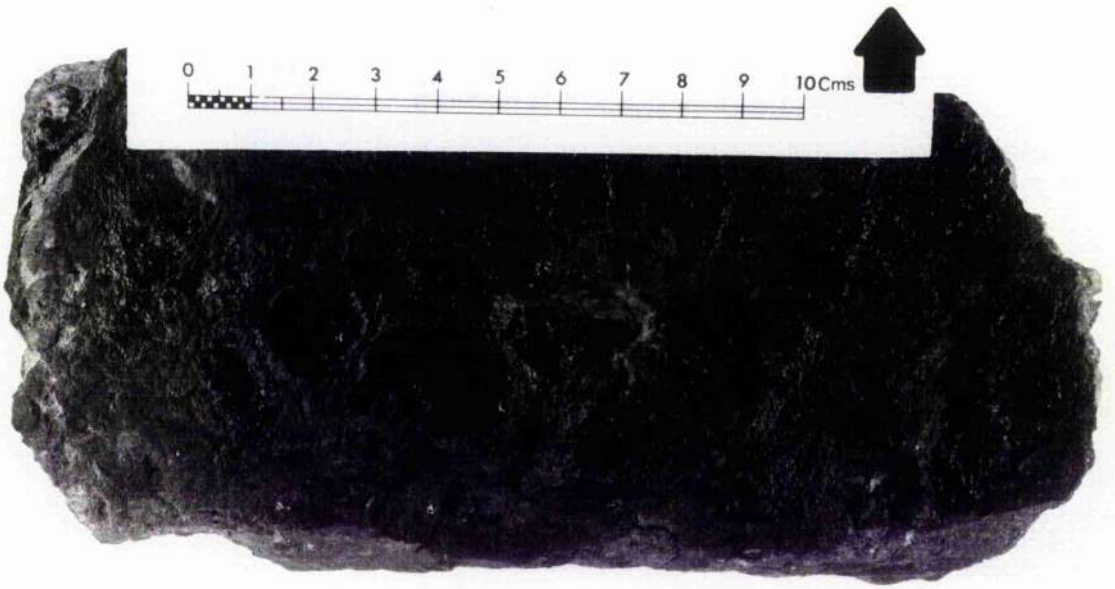
0 1 2 3 4 5 6 7 8 9 10Cms


2 cm

Figure 3.3 Highly fractured Type II nodule embedded in shale. Most of the fractures are filled with pyrite and/or secondary phosphorite minerals.

Figure 3.4 Photomicrograph showing prismatic apatite crystals present in Type I nodules (Lower main bed of phosphorite) of the Pen-y-Garnedd area. Note coalescing of crystals in bottom right and top left corners. Plane polarized light. Scale bar equals 10 μm.


1 cm

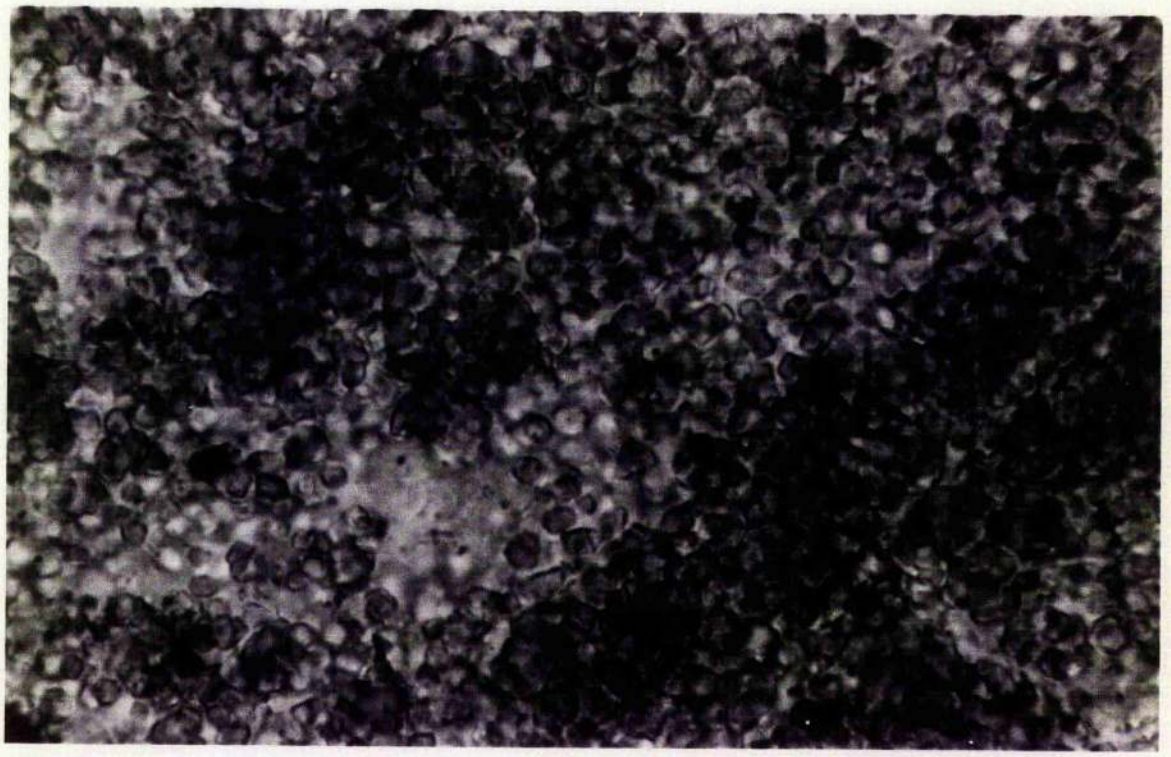

Figure 3.5 Photomicrograph of a spicule-bearing Type I phosphorite nodule from Pen-y-Garnedd area. Arrow shows axial canal of a detached spicule filled with apatite. X-nicols. Scale bar equals 250 μm.

Figure 3.6 Photomicrograph showing spherical Hystrichosphaeridium test, with short, broad based and sharply pointed spines. The aggregate of crystals present inside the test are probably haematite. Plane polarized light. Scale bar equals 10 μm.

Figure 3.7 Photomicrograph showing cracks, present in the nodule, are filled with apatite, chert and sometimes dolomite (D). X-nicols. Scale bar equals 100 μm.

Figure 3.8 Photomicrograph showing a close up of the crack in the nodule filled with apatite crystals (arrow), chert (Ch) and some dolomite (D). Plane polarized light. Scale bar equals 10 μm.

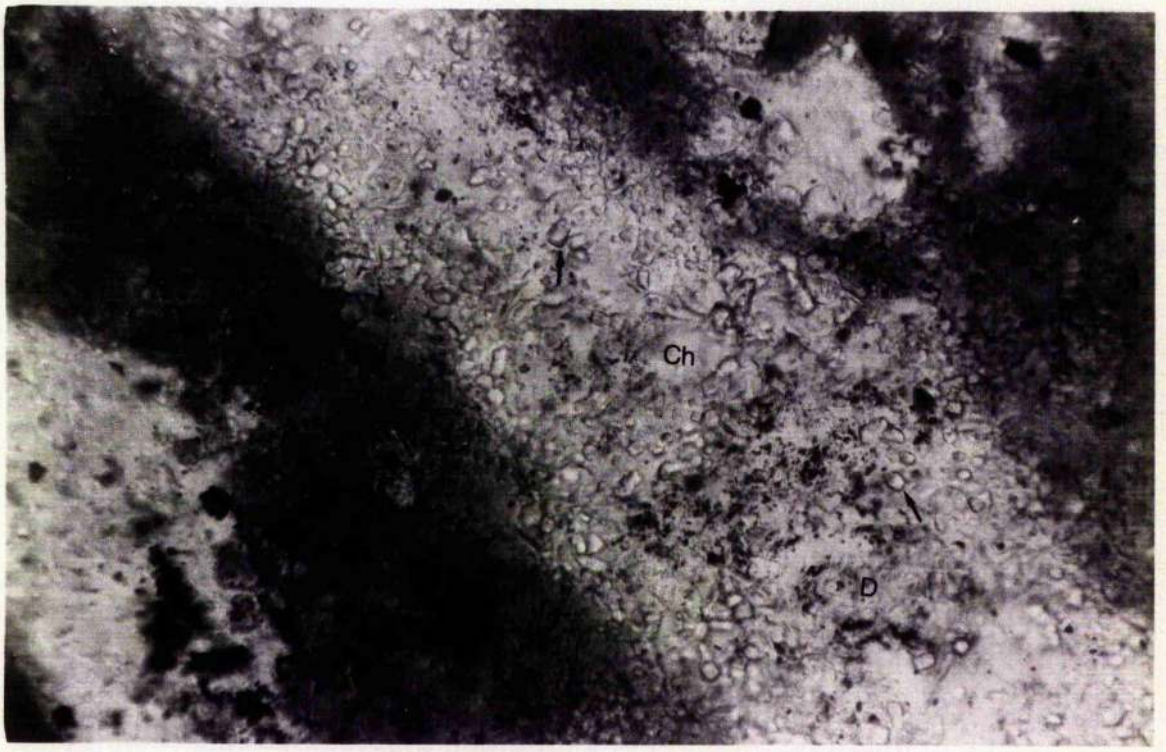
Ch
D

Figure 3.9 Photomicrograph showing irregular cracks running through the nodule (right) and the host rock (left). Cracks are filled with dolomite. X-nicols. Scale bar equals 200 μm.

Figure 3.10 Photomicrograph showing pyritized spicules and Hystrichosphaeridium test present in Type I nodules (Upper beds of phosphorite). Plane polarized light. Scale bar equals 200 μm.

Figure 3.11 Photomicrograph showing spicules and other organic fragments filled with authigenic clays. Note phosphorite is replacing these clays. (Type I nodules present in the Upper beds of phosphorite). Plane polarized light. Scale bar equals 100 μm.

Figure 3.12 Photomicrograph showing recrystallized apatite displaying centripetal growth of small hexagonal apatite crystals, present in a spicule (Type-I nodules present in the Upper beds of phosphorite). Plane polarized light. Scale bar equals 100 μm.

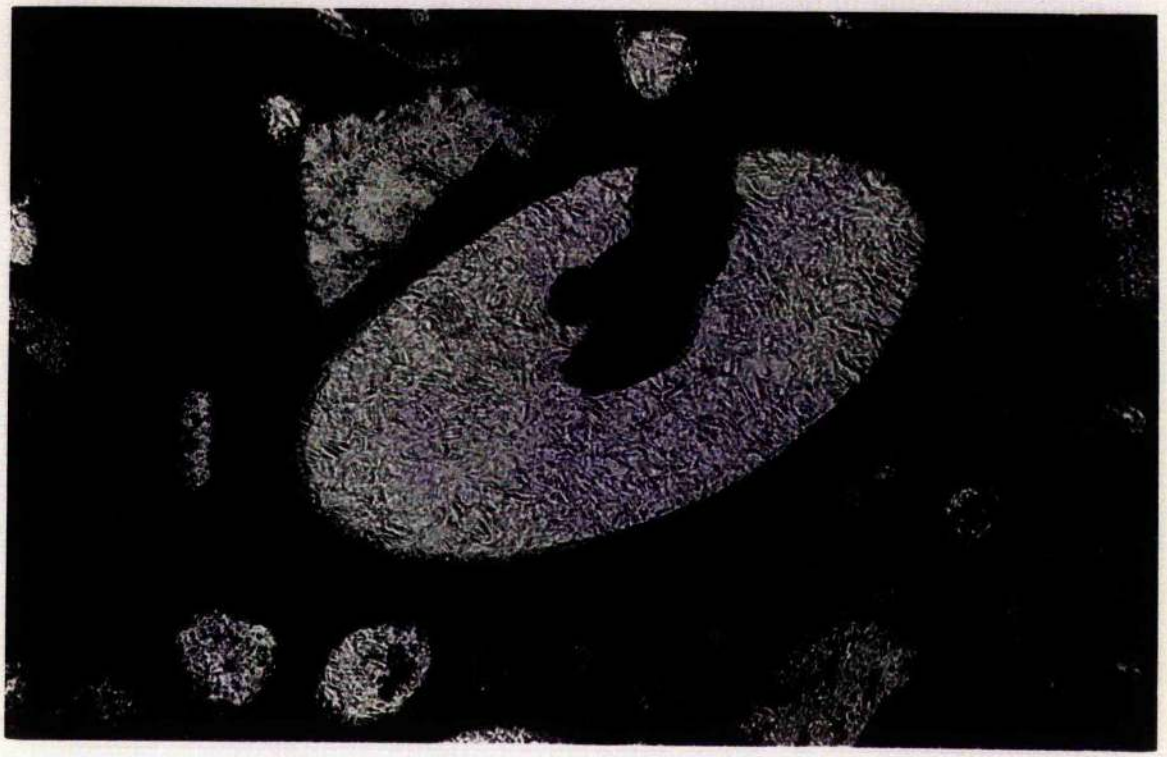

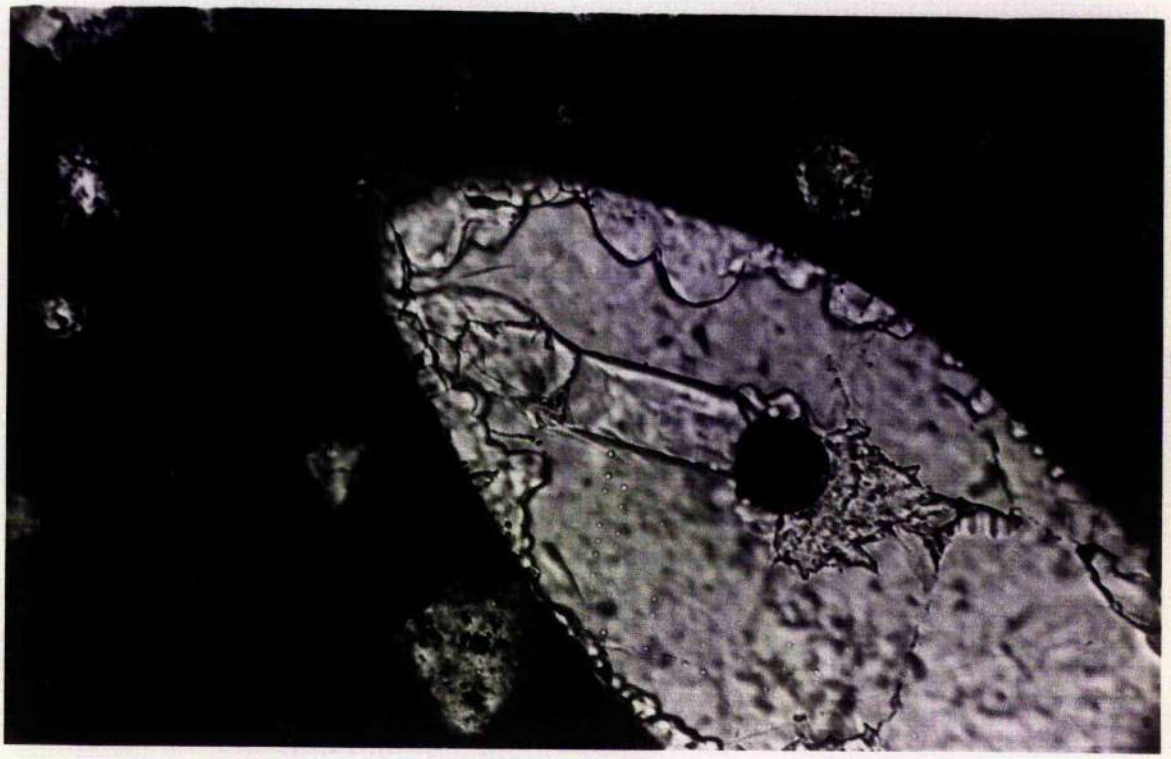

Figure 3.13 Photomicrograph showing apatite forming colloform texture in Type I nodules present in Upper beds of phosphorite. The central white area is a void formed by the dissolution of some unstable material. Plane polarized light. Scale bar equals 200 μm.

Figure 3.14 Photomicrograph showing secondary phosphorite minerals present as fracture fillings and as concentric rings around pyrite (arrow). Note that pyrite present initially in the fracture has been completely dissoled (white band). Plane polarized light. Scale bar equals 100 μm.

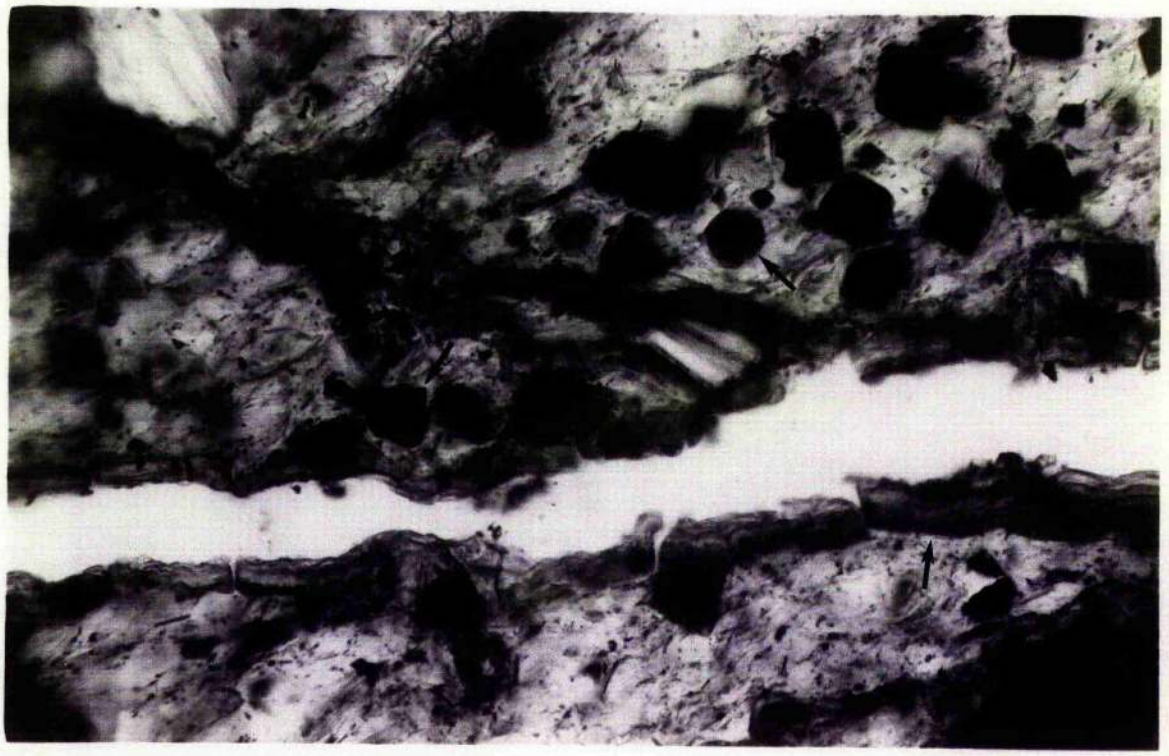

Figure 3.15 Photomicrograph showing the host rock for Type I nodules. Shale band contain carbonaceous and ferruginous matter (dark band in the right) in contrast to silty band (light coloured area in the left). Plane polarized light. Scale bar equals 1 mm.

Figure 3.16 Photomicrograph showing subhedral to euhedral quartz grains with syntaxial overgrowth (arrow). X-nicols. Scale bar equals 200 μm.

Figure 3.17 Photomicrograph showing scattered dolomite rhombs in the silty band (host rock for Type I nodules). X-nicols. Scale bar equals 200 μm.

Figure 3.18 Photomicrograph showing dolomite (D) replacing euhedral quartz grain (Q). Note dust line in the quartz grain (arrow). X-nicols. Scale bar equals 100 μm.


D
Q

Figure 3.19 Photomicrograph showing dolomite (D) replacing plagioclase feldspars in the host rock for Type I nodules. X-nicols. Scale bar equals 200 μm.

Figure 3.20 Photomicrograph showing funnel shaped assemblage as algal/fungal filaments present in Type II nodules. Plane polarized light. Scale bar equals 200 μm.


D
D

Figure 3.21 Photomicrograph showing secondary phosphorite minerals present in cracks and also as pyrite pseudomorphs. It is noticeable that pyrite cubes are partially to completely replaced by secondary phosphorite. Arrow shows a completely replaced pyrite cube. Plane polarized light. Scale bar equals 100 μm.

Figure 3.22 Photomicrograph showing secondary phosphorite with colloform texture present in a fracture. The central dark area is red in colour (higher iron content) surrounded by orange coloured mineral (with lower iron content), (see Chapter V). Plane polarized light. Scale bar equals 250 μm.

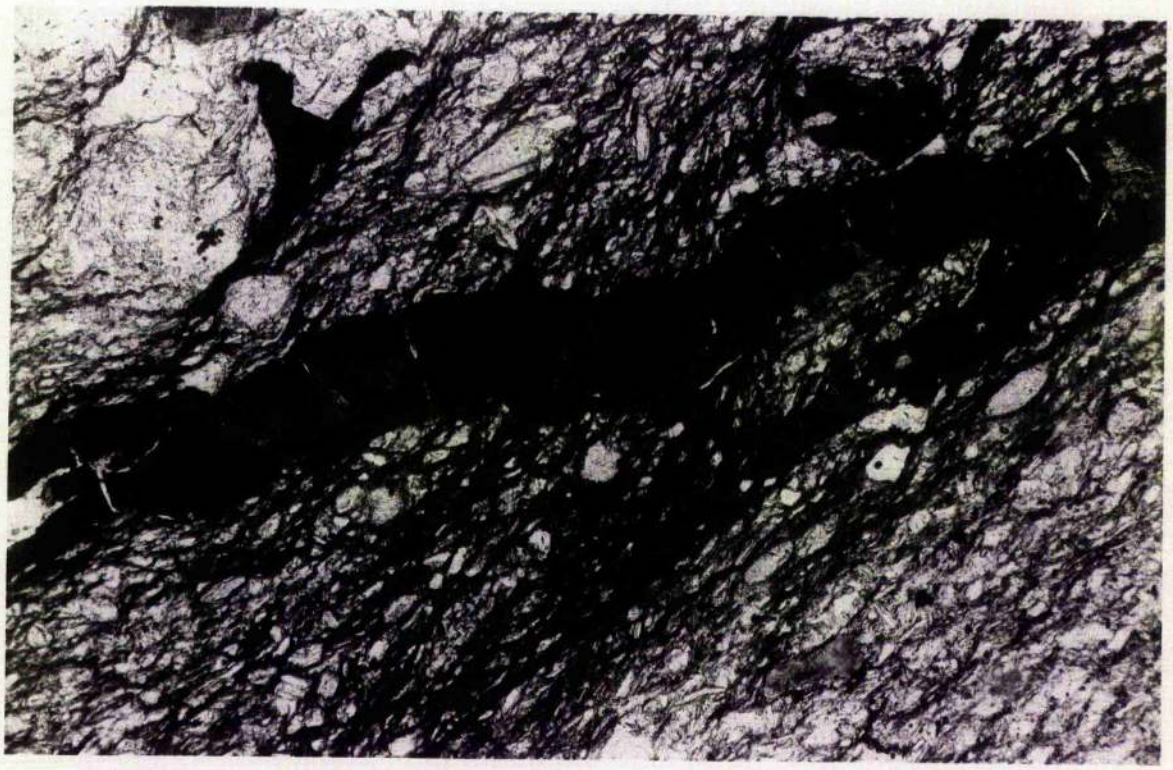

Figure 3.23 Photomicrograph showing the presence of secondary aluminium phosphate mineral wavellite in a crack. The wavellite crystals are in the form of spherulitic aggregates with radiating crystals (arrow). Plane polarized light. Scale bar equals 200 μm.

Figure 3.24 Photomicrograph showing a crack in the Type II nodule filled with pyrite, apatite (A), gypsum (G) and calcite (C). Plane polarized light. Scale bar equals 1 mm.

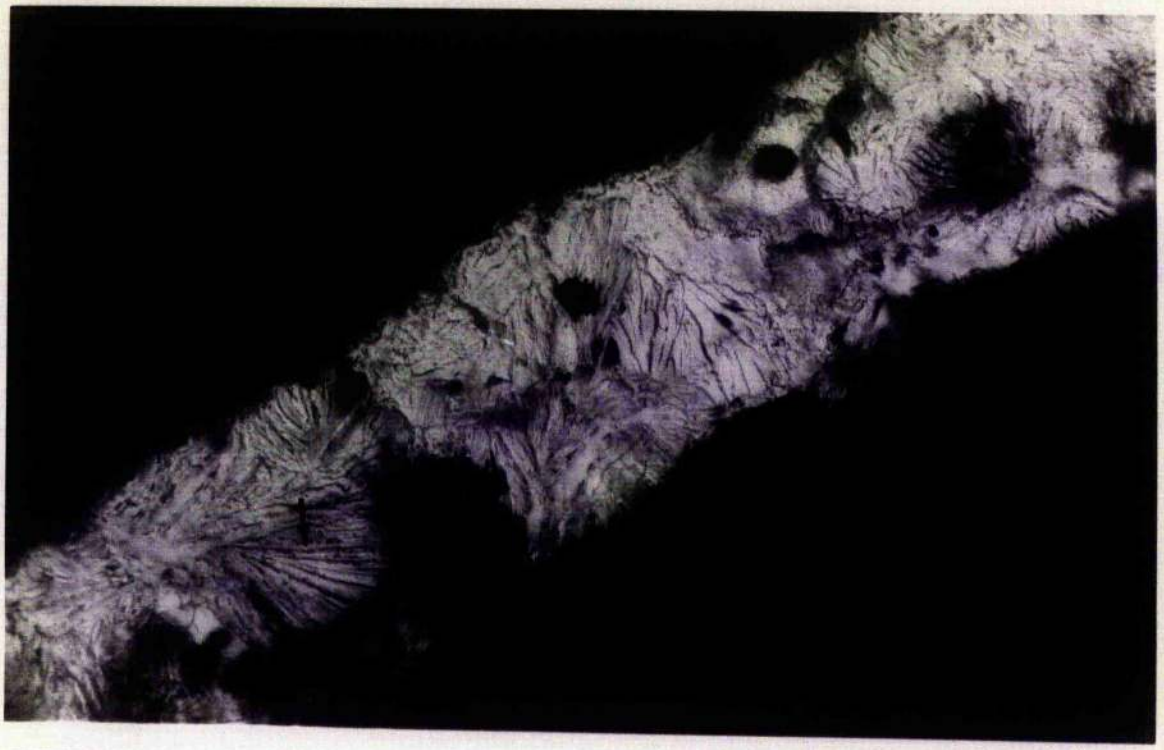


C

Figure 3.25 Photomicrograph, showing phosphatized organic fragments, detrital quartz and feldspar present in clusters in the shaly host rock for Type II nodules. Plane polarized light. Scale bar equals 2 mm.

Figure 3.26 Photomicrograph showing feldspars altering into clays (arrow). X-nicols. Scale bar equals 200 μm.

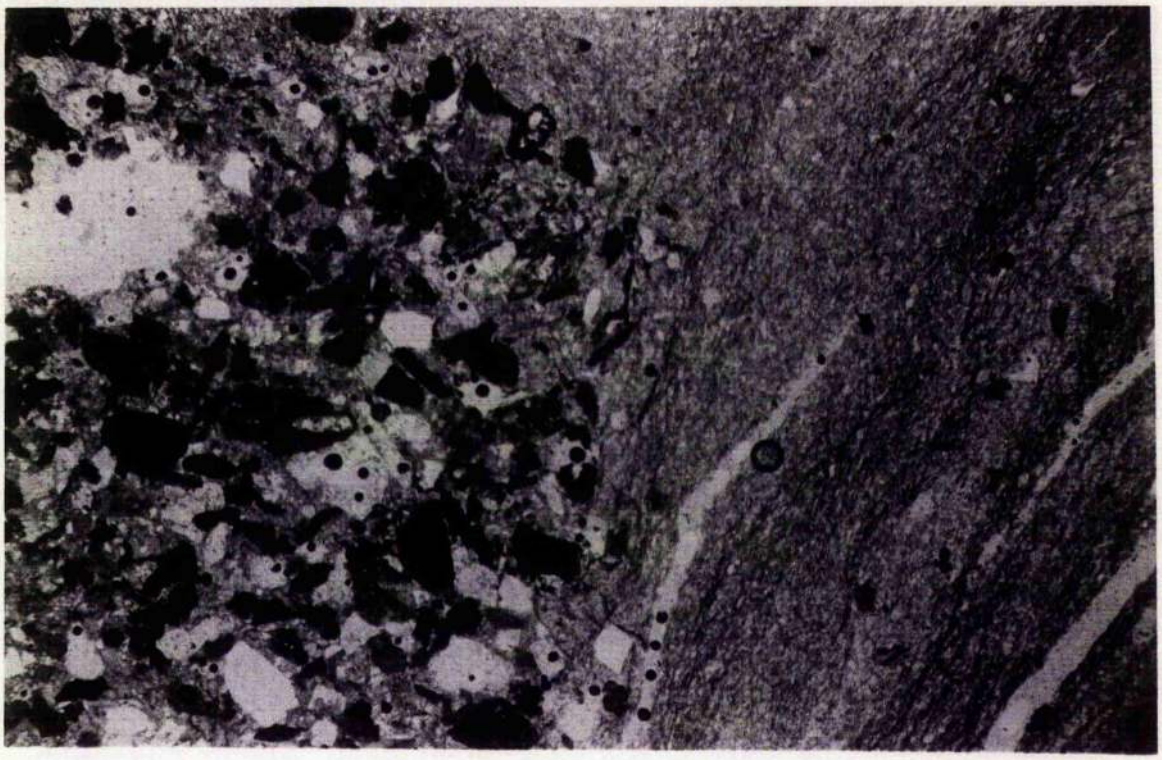

Figure 3.27 Photomicrograph showing voids formed by the dissolution of some unstable material (probably organic) filled with secondary phosphorite. Plane polarized light. Scale bar equals 200 μm.

Figure 3.28 Photomicrograph showing oolites. Note large variations in the shapes of oolith cores. X-nicols. Scale bar equals 2 mm.

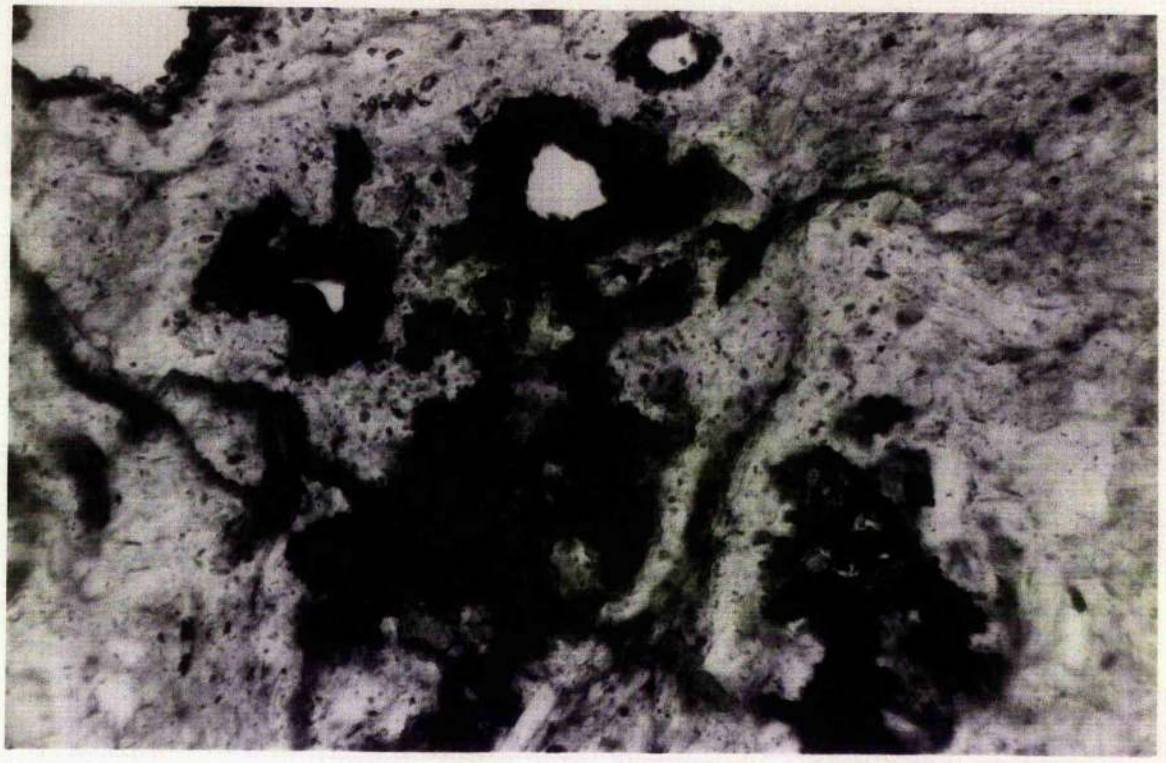

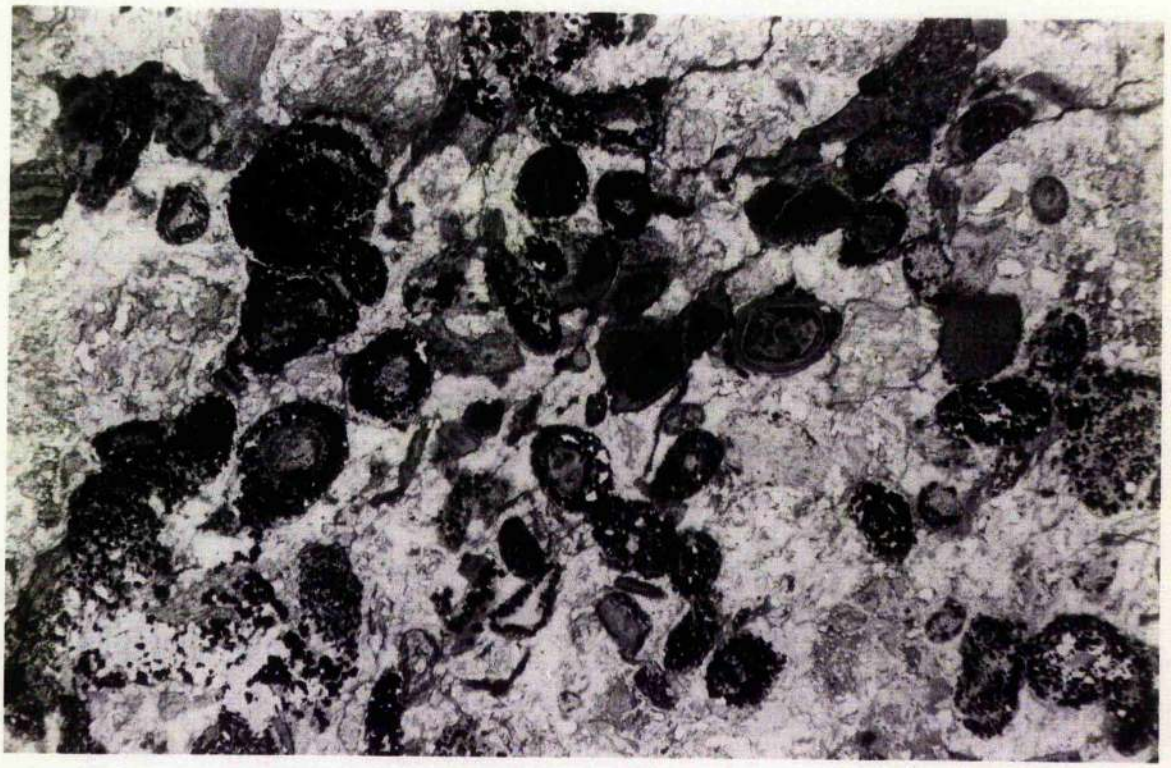

Figure 3.29 Photomicrograph showing partially to completely pyritized oolite. Pyrite grains are mostly euhedral. X-nicols. Scale bar equals 200 μm.

Figure 3.30 Photomicrograph showing pyrite cubes with concentric rings of secondary phosphorite mineral in oolitic phosphorites. Plane polarized light. Scale bar equals 100 μm.

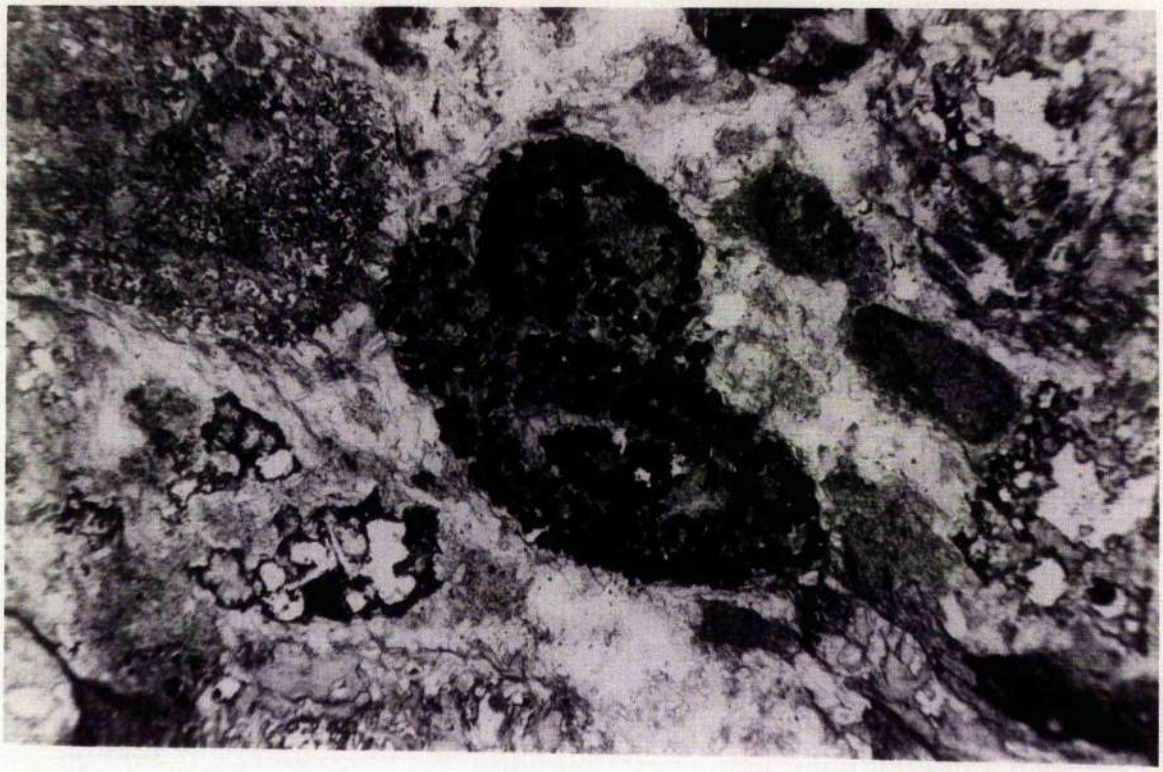

Figure 3.31 SEM photograph showing spicules embedded in Type I nodule. Note axial canal in the middle of the spicule marked with an arrow. Scale bar equals 400 μm.

Figure 3.32 SEM photograph showing well developed apatite crystals (arrow) forming interlocking texture. Scale bar equals 5 μm.

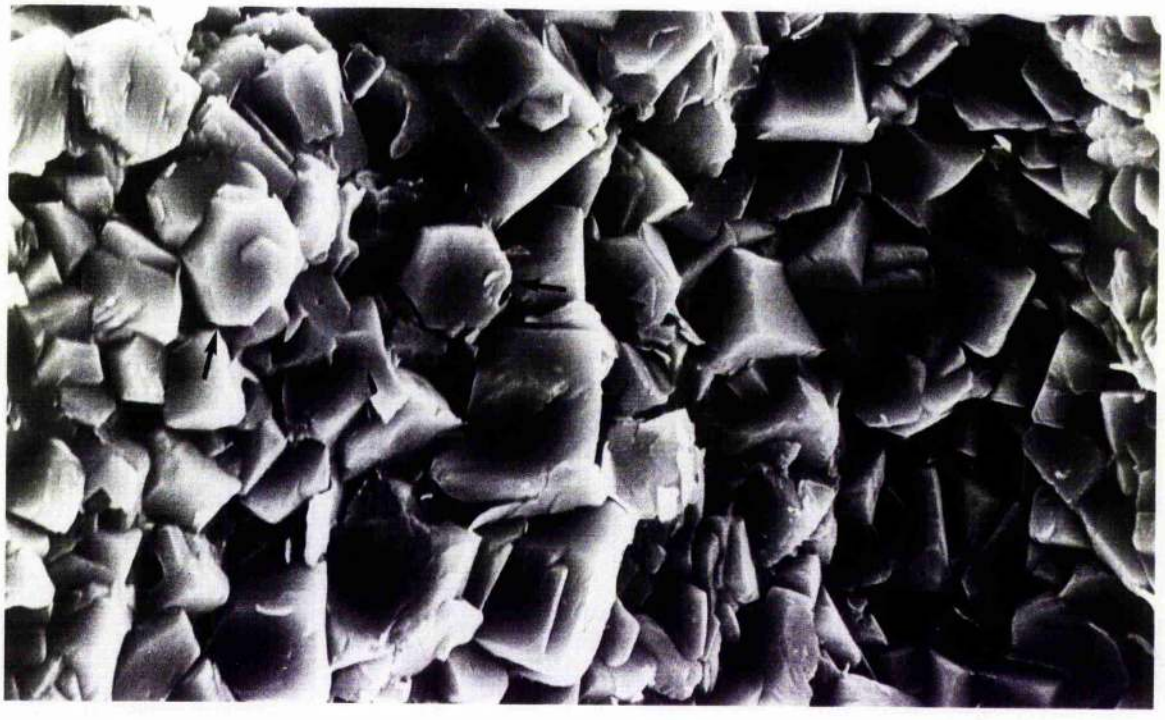

Figure 3.33 SEM photograph of Type II nodule showing detrital clays and well developed hexagonal apatite crystals (bottom central area). Scale bar equals 10 μm.

Figure 3.34 SEM photograph showing well developed hexagonal crystals with detrital clays in Type II nodules. Scale bar equals 5 μm.

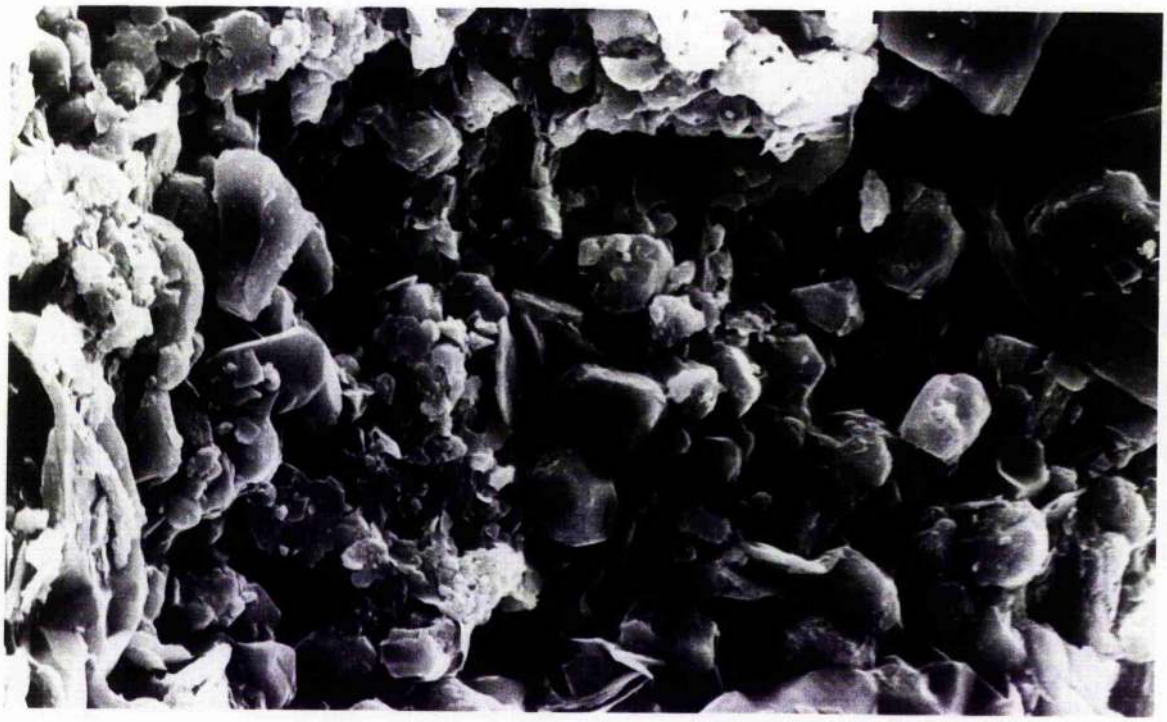

Figure 3.35 SEM photograph showing hexagonal prismatic apatite crystals present in Type II nodules. Scale bar equals 5 μm.

Figure 3.36 SEM photograph showing acicular crystals of apatite in the intergranular spaces. Scale bar equals 2 μm.

Figure 3.37 SEM photograph showing relict of axial canal of a spicule sticking into a void created by the dissolution of spicular material (Type I nodules from Pen-y-Garnedd area). Scale bar equals 100 μm.

Figure 3.38 Close-up of Fig 3.37 showing apatite crystals growing on axial canal as well as on the walls of the void . SEM photograph. Scale bar equals 20 μm.

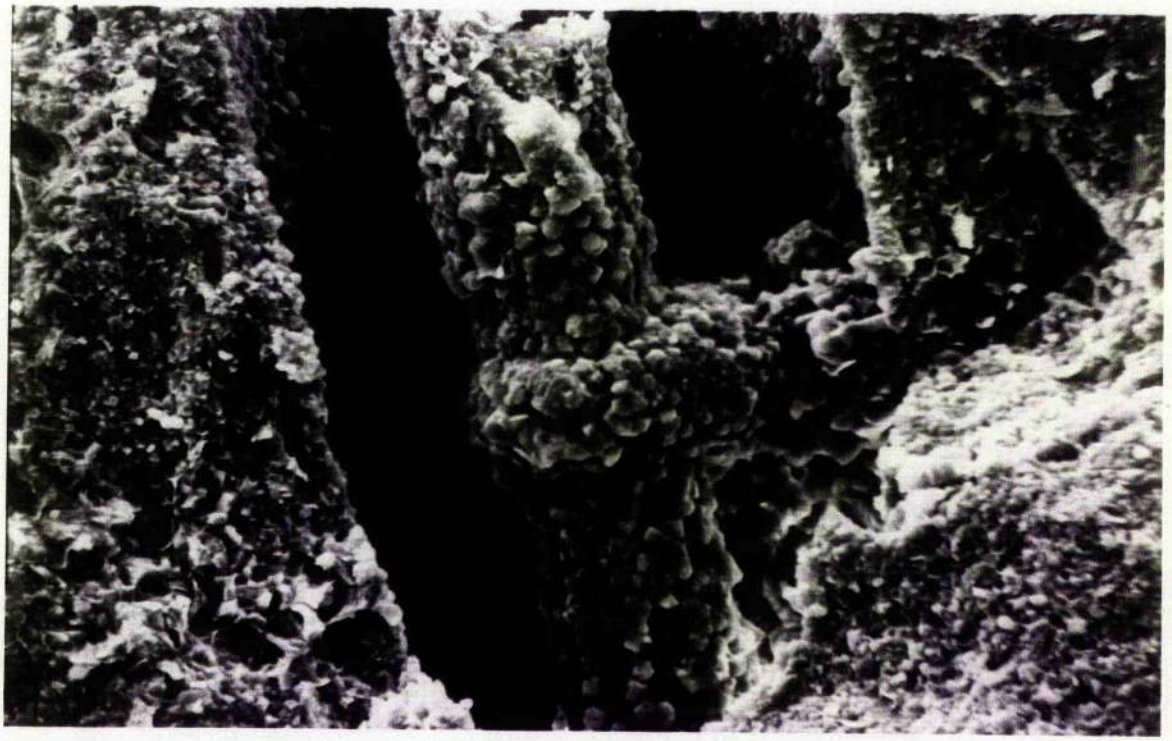

Figure 3.39 Spicule (present in the nodules of the upper beds of phosphorites) showing authigenic clays in area surrounding axial canal. Axial canal is filled with apatite. SEM photograph. Scale bar equals 200 μm.

Figure 3.40 SEM photograph showing authigenic clays occurring around axial canal as seen in Fig. 3.39. Microprobe analyses suggest mixed layer smectite-illite composition (Chapter V). Scale bar equals 10 μm.

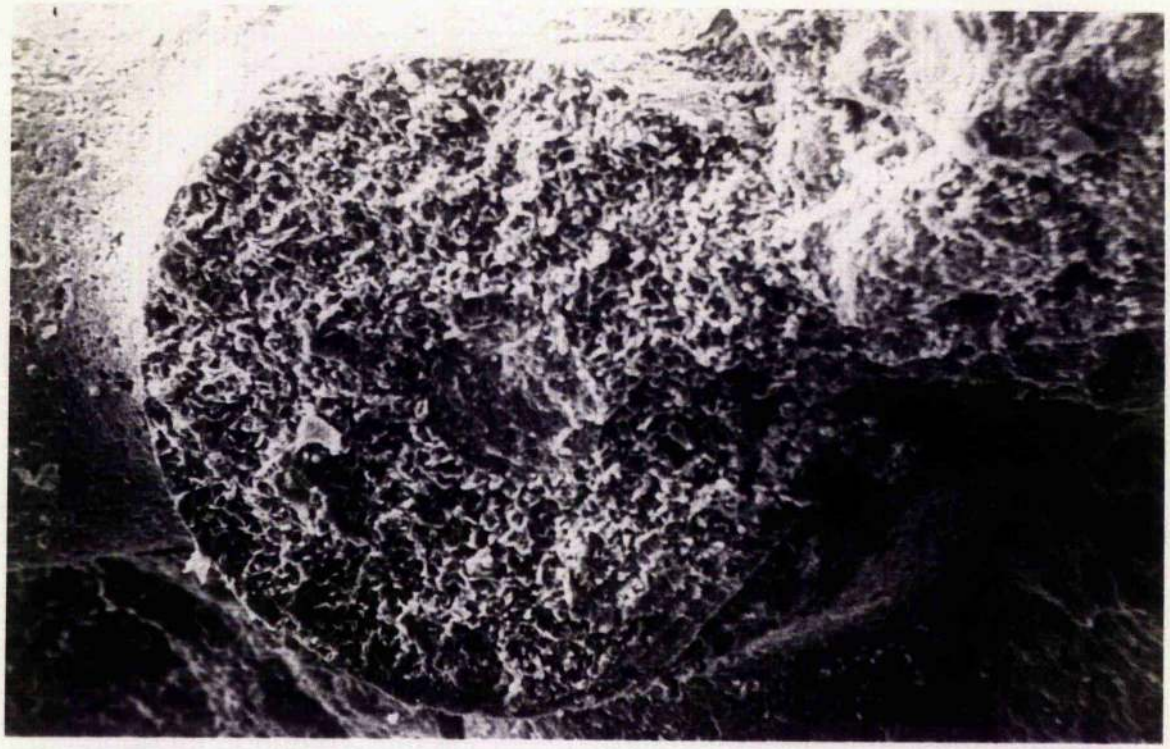

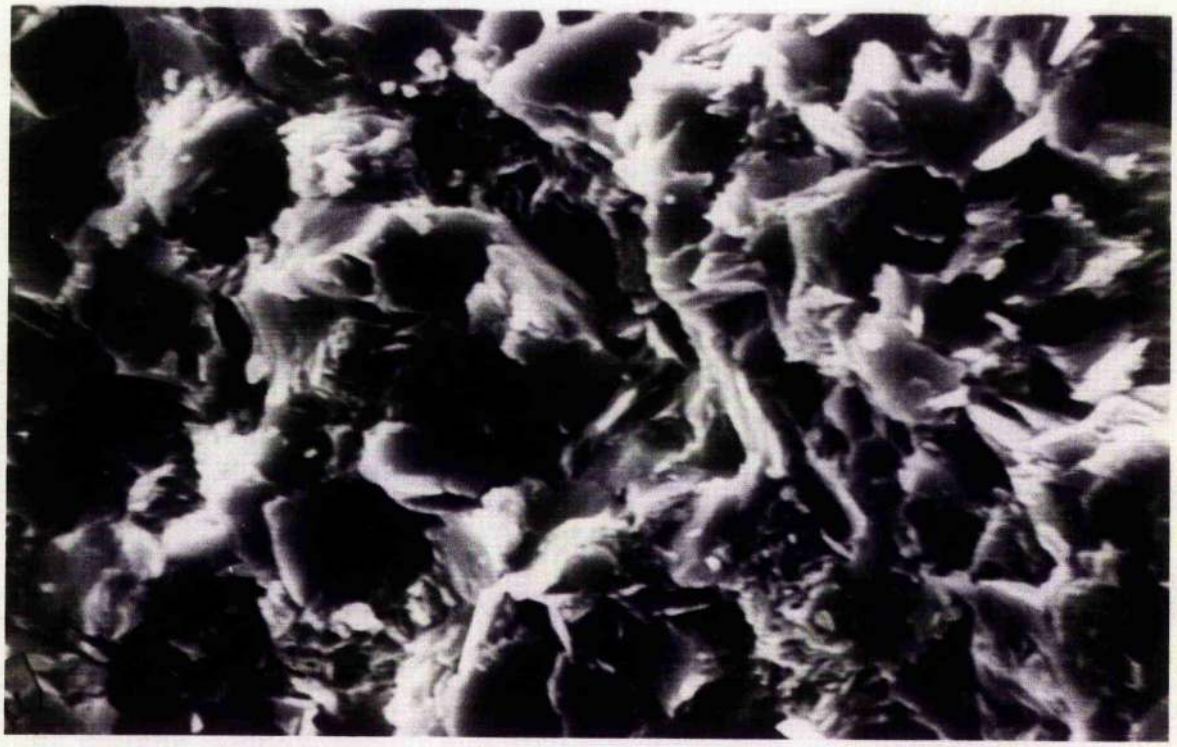

Figure 3.41 SEM photograph showing mold formed by the dissolution of some organic fragment embedded in Type I nodular phosphorite. Scale bar equals 200 μm.

Figure 3.42 Well developed interlocking hexagonal apatite crytals filling the mold shown earlier in Fig 3.41. SEM photograph. Scale bar equals 4μm.

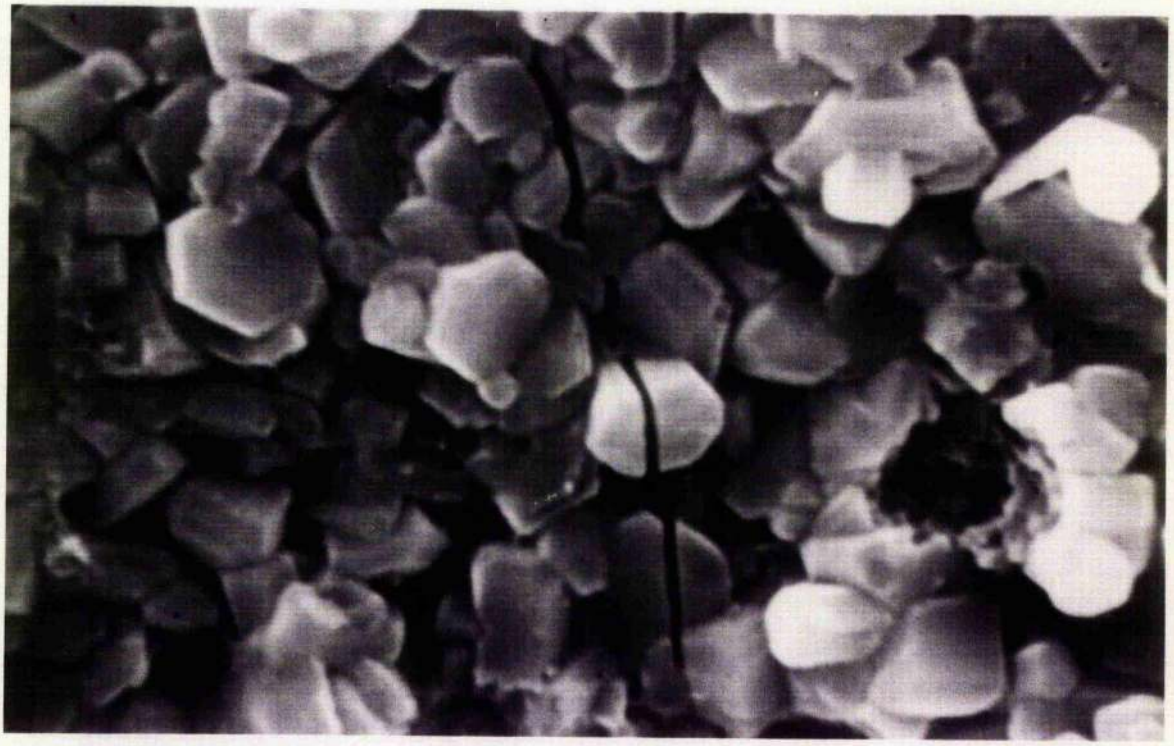

Figure 3.43 SEM photograph showing irregular polygonal cracks in phosphorite nodules. Scale bar equals 40 μm.

Figure 3.44 SEM photograph showing euhedral pyrite crystals forming interlocking texture. Scale bar equals 20 μm.

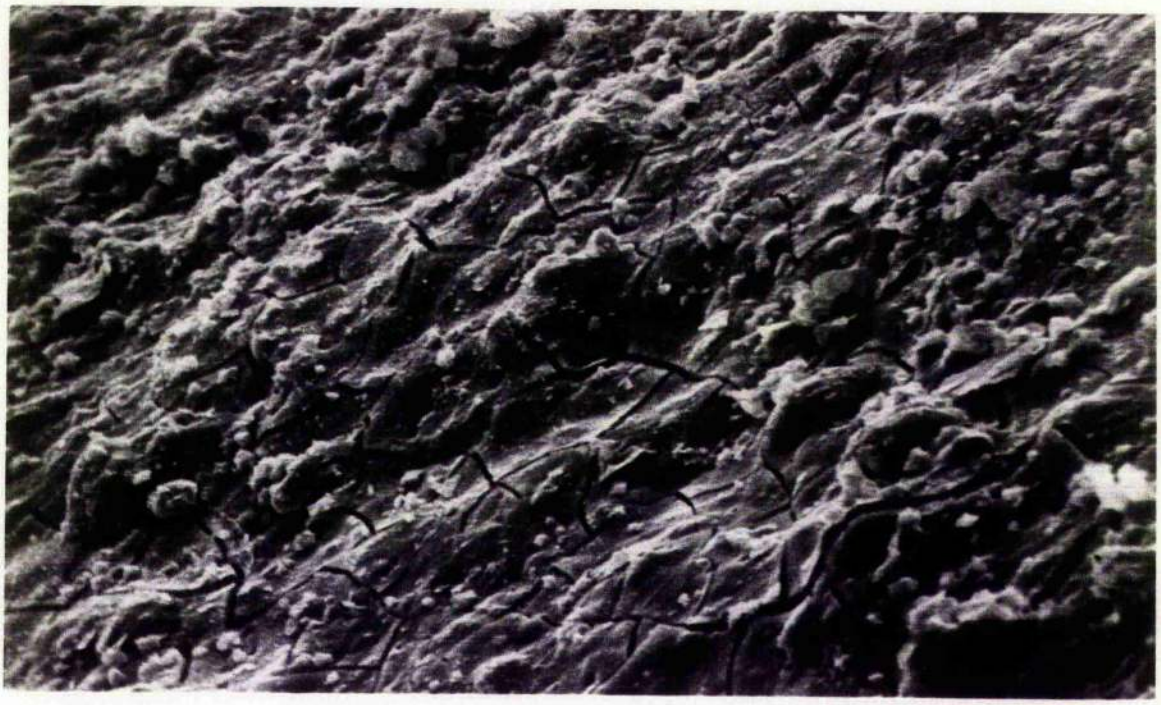

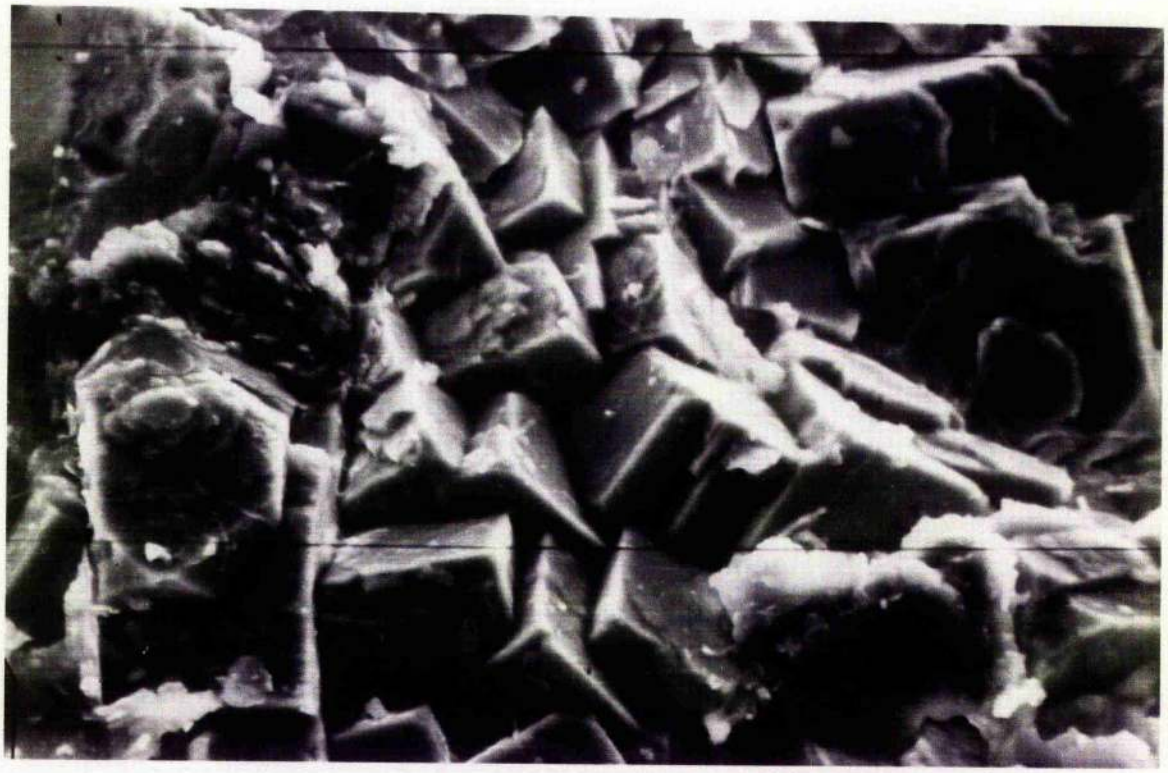

Figure 3.45 SEM photograph showing dissolution of pyrite cube present in Type II nodules. Scale bar equals 10 μm.

Figure 3.46 SEM photograph showing curved bean shaped organic forms. Scale bar equals 10 μm.

Table 3.1 Average mineralogical composition of Type I nodular phosphorite (Vol %)

Sample No	Apatite	Dolomite	Organic Fragments	Pyrite	Quartz	Feldspar	Clays	Chert Cement
(i) Ph-5	58	19	15	4	2	-	-	2
(i) Ph-6	60	17	13	5	3	-	-	2
(i) Ph-10	65	16	10	2	2	-	2	3
(ii) Ph-12	65	15	10	4	3	-	1	2
(ii) Ph-15	55	19	15	5	4	-	-	3
(ii) NS-1	65	18	10	6	1	-	<1	-
(i) NS-3	71	9	7	6	3	-	<1	4
(ii) NS-8	71	10	10	3	3	-	-	3
(i) Ph-31	57	18	11	5	2	1	2	4
(ii) Ph-57	62	15	12	2	4	1	3	1
(ii) PG-1	71	2	3	11	7	2	3	1
(ii) PG-2	73	1	2	12	8	1	2	1
(ii) PG-3	65	1	3	15	11	3	2	-
(ii) Ph-46	70	-	6	15	7	1	1	-
(ii) Ph-48	68	-	7	11	7	2	3	2
(ii) Ph-49	70	1	6	10	6	3	2	2
(ii) Ph-51	66	-	3	16	8	2	3	2
Average (i)	62.9	15.6	11.2	4.2	2.7	0.2	1	2.4
Average (ii)	69.4	0.8	4.2	12.8	8	1.8	2.2	0.8

i = Nodules present in the Lower main bed of phosphorite
ii = Nodules present in the Upper beds of the phosphorite

Table 3.2 Average mineralogical compositon of host rock for Type I nodular phosphorite (Vol %)

Sample No	Quartz	Feldspar	Organic Fragments	Pyrite	Clays	Chert Cement	Dolomite Cement	Ferruginous+ carbonaceous matter
(i) Ph-5	21	4	3	4	5	45	15	3
(i) Ph-6	19	4	5	6	6	40	15	4
(i) Ph-10	22	3	2	4	4	45	18	2
(i) Ph-12	22	5	4	5	4	39	20	1
(i) Ph-15	16	3	3	7	5	47	16	3
(i) NS-1	23	4	3	4	3	46	15	2
(i) NS-3	15	5	2	6	7	45	18	2
(i) NS-8	17	4	3	5	5	39	22	5
(i) Ph-31	21	5	6	4	6	40	17	1
(i) Ph-57	19	3	5	6	5	47	13	2
(ii) PG-1	16	6	6	8	7	22	-	35
(ii) PG-2	18	4	5	7	6	26	-	34
(ii) PG-3	17	5	6	6	5	26	-	35
(ii) Ph-46	19	8	5	9	7	24	-	28
(ii) Ph-48	16	7	4	10	5	22	-	36
(ii) Ph-49	17	6	5	6	6	25	-	35
(ii) Ph-51	18	5	4	8	8	22		35
Aver- (i)	8	4	3.6	5.1	5	42.8	16.9	2.5
age (ii)	17.2	5.9	5	7.7	6.2	23.8	-	34

(i) Lower main bed of phosphorite
(ii) Upper beds of phosphorite

CHAPTER IV

MINERALOGY

4.1 Introduction

Thin section studies are considered inadequate for a complete mineralogical evaluation of marine phosphorites mainly because of their microcrystalline nature and difficulty in measuring the optical properties. Hence, to distinguish various mineral species of apatite in the Welsh deposit, a number of powdered phosphorite samples were subjected to X-ray diffraction analysis. In addition, X-ray diffraction determine the structural CO_2 contents and unit cell dimensions of apatite as discussed in the following pages.

Phosphate minerals identified by X-ray diffraction are grouped as carbonate apatites and noncarbonate apatites on the basic of CO_2 content (Rooney and Kerr, 1967). Both these groups are known to have variable concentrations of F, Cl and (OH) ions. McConnell (1938) believed that the carbonate apatites are the dominant component of marine sedimentary apatites and that they are mineralogically either dahllite with <1 percent fluorine or francolite with >1 percent fluorine. McClellan and Lehr (1969) are of the opinion that most sedimentary apatites are a carbonate-substituted variety of francolite.

4.2 Mineralogy of the phosphorite

The major constituent of Type I and Type II phosphorites, is the mineral francolite, a fluorine-rich (>1%F) carbonate fluorapatite (Table 4.3). The three characteristic peaks of this

apatite occur at 2.790Å(211), 2.769Å(112) and 2.692Å(300) (Figs 4.1, 4.2 and 4.3). There is, however, a general prevalence of carbonate-poor francolite, often approaching the composition of pure fluorapatite. Besides francolite, various secondary phosphate minerals have also been identified. Due to the paucity of these secondary phosphorites, they could not be subjected to X-ray diffraction analysis. One of the Type II nodular phosphorite samples from Nant-Achlas shows intensity reversal of the (300) and (211) peaks of carbonate fluorapatite (fig. 4.4). In common phosphorites with carbonate fluorapatite composition these two peaks are always either nearly equal or (211) peak is slightly bigger than (300) peak. The same sample after being subjected to heating process, however, shows normal intensities of (300) and (211) (fig. 4.4, heated sample). These intensity reversals may be due to the differential substitution in the structure of apatite or due to the presence of certain trace elements as adsorbed ions on the surface of apatite. Another probable cause of such intensity variations could be the presence of carbonate ion in unusual position in apatite lattice, which get more or less completely removed during the heating process. According to McClellan (pers. comm.) there are at least 2 possible causes for this intensity reversal: i) the presence of manganogoethite in the rock can increase the apparent intensity of the (300) peak of apatite. ii) the presence of small amounts of Sr, Ba or Mn substituted for Ca.

The major gangue components of the Type I nodules present in the main bed of phosphorite are quartz and dolomite (Fig 4.1) whereas nodules present in upper beds contain quartz and pyrite

(Fig 4.2). Type II nodular phosphorite contain clays along with pyrite and quartz (Fig 4.3). It is evident that Type I nodules are devoid of clay minerals in contrast to Type II nodules which contain abundant illite-smectite and chlorite. Different techniques used for kaolinite/chlorite identification are described in the Appendix 4.3. The quartz peaks were used as an internal standard, to correct peak positions. Modifications of peaks present in the untreated samples show the following results:-

(i) Acid-digestion: It shows complete removal of chlorite peaks as chlorite is soluble in hot HCl while kaolinite, quartz and mica are all resistant (Fig 4.5b).

(ii) Heating to 600 °C: Kaolinite loses water at 550 °C and its peaks disappear from the diffractogram if it is present. Our samples do not show any variation in the intensities of chlorite/kaolinite peaks which suggest the presence of chlorite (Fig 4.5c).

(iii) Treatment with dimethyl sulphoxide (DMSO): By this treatment the (001) reflection at 7.15 Å is expanded to 11.18 Å and the (002) peak at 3.56 Å to 7.15 Å. Another peak appears at 3.63 Å whilst 3.56 Å peak remains unaffected. None of these changes were seen in samples which confirm that kaolinite is absent (Fig 4.5d)

Table 4.1 gives the X-ray diffraction data for representative phosphorite samples and Table 4.2 includes their

structural CO_2 contents and unit cell dimensions.

4.3 CO_2 contents

CO_2 contents of carbonate fluorapatite were determined by semi-quantitative X-ray method of Gulbrandsen (1970) (Appendix 4.4). This method was used because the determination is unaffected by the presence of other carbonate bearing minerals as well as other impurities so long as the X-ray peaks are defined well enough for accurate measurement.

Although the overall CO_2 content is very low, as expected Type I nodules present in the main bed of phosphorite (least weathered) contain the highest amount (1.58%) and nodules present in the upper beds contain the lowest (0.95%). Type II nodules contain an average of 1.40% of structural CO_2 (Table 4.2).

4.4 Unit Cell Dimensions

Unit cell dimensions of apatite were calculated using the method described in the Appendix 4.5. The a°-values are more significant in the distinction of apatite species: they vary from 9.30 to 9.36 Å. References in the literature are sometimes contradictory:

- Altshuler et al, (1953) give 9.413 Å for hydroxi-apatite, 9.386 Å for fluorapatite and 9.344 Å for carbonate fluorapatite.
- For other authors (in: Deer, et al, 1963) the average values are 9.41 Å for hydroxi-apatite, 9.34 Å for carbonate fluorapatite and only 9.35 Å for fluorapatite.
- The francolite of McConnell (1938) has 9.34 Å. The Welsh phosphorites show small but significant variations in unit cell

dimensions in different types of nodular phosphorites. Type I nodules containing the highest amounts of CO_2 have lowest a^o (a^o = 9.345 Å; c^o = 6.880 Å) and nodules present in upper beds containing the lowest amount of CO_2 have highest a^o values (a^o = 9.355 Å; c^o = 6.886 Å). Type II nodules containing intermediate amounts of CO_2 have a = 935 Å and c^o = 6.879 Å. It follows that on the basis of a^o values, these apatites could equally well be classified as fluorapatite (Type I nodules present in the upper beds of phosphorite and Type II nodules) or as carbonate fluorapatite (mainly Type I nodules present in the main bed of phosphorite).

The variation in the a^o cell dimensions also suggest that all these nodular phosphorites were affected by differential substitutions of $(CO_3)^{2-}$ for $(PO_4)^{3-}$ and/or uneven removal of (CO_3) by post depositional alterations. CO_2 contents plotted against a^o-cell dimension show an overall inverse relationship inspite of some scatterring of points. Whatever the manner of drawing the regression line relationship is antagonistic suggesting the location of CO_2 in the apatite lattice (Fig 4.6).

4.5 Calcination

Many of the phosphorite samples were heated to 1000 °C for an hour in an open platinum crucible and the cooled powder when subjected to X-ray diffraction, showed ommission of certain peaks. Some of the apatite peaks became sharper whereas the other peaks became stunted (Figs. 4.2 and 4.3). In addition the heated samples showed complete removal of CO_2 with an increase in a^o cell dimensions (Table 4.2). This supports the earlier drawn

conclusion that CO_2 is located within the apatite lattice.

4.6 Structural formula of apatite

The structural formulae were deduced on the basis of calculation method of Manheim and Gulbrandsen (1979). Only the apatite constitents are reported in the analyses. All the samples reported are averages of about 10 or 11 spot analyses. The CO_2 content determined by X-ray peak pair method was used for the calculations. Average structural formulae for nodular phosphorites are as follow (Table - 4.3):

Type I phosphorite - $Ca_{9.95}Mg_{.02}Na_{.02}/(PO_4)_{5.66}(Co_3)_{.34}/F_{1.77}$

Type II phosphorite - $CA_{9.81}Mg_{.12}Na_{.08}/(PO_4)_{5.70}(CO_3)_{.31}F_{.05}/F_2$

These formulae show meagre amounts of substituent element. However, Type II nodules contain comparatively more substitutent element than Type I nodules. SO_4 contents were found in samples ranging from 0.01 to 0.015 moles, amounts considered to be too low generally to be of significance.

The balance of compensating substitutions (Na moles + Excess F moles = CO_3) moles in these apaties can be determined from their structual formulas; for example Type I nodules show 0.02 moles of Na, no excess fluorine and 0.34 moles of CO_3, an imbalance of 0.32 moles. In fact Type I nodules have F deficiency (1.77 moles) as fluorapatite structure itself requires 2 moles of F. However, Type II nodules contain slightly more fluorine than required for fluorapatite structure. Inspite of excess fluorine these apatites show an imbalance of 0.18 moles. Consistent deficiency of negative charges (Table - 4.3)

is difficult to explain. It could possibly be either due to the substitution of $(SiO_4)^{-4}$ for $(PO_4)^{-3}$ or $(OH)^{-1}$ for F although so far these substitutions have not been proved by mineralogists.

4.7 DISCUSSION

The X-ray diffraction patterns for most Welsh phosphorites show sharp, well defined diffraction lines, suggesting a high degree of crystallinity for these apatites. The primary phosphorite mineral is francolite (a F-rich carbonate fluorapatite) with a tendency to be poorer in carbonates, often approaching the composition of pure fluorapatite. Phosphate minerals are characteristically carbonate fluorapatite with more carbonate substitutions in Type-I nodules, than, in the nodules present in upper beds of phosphorite and Type II nodules. Besides these primary apatite minerals, various secondary phosphorite minerals have also been identified (by electron microprobe studies).

The variation in unit cell dimensions of apatite are small but significant. Type-I nodular phosphorite show lower a^{o} values (consistent with higher CO_2 contents) than nodules present in the upper beds and Type-II nodules which show higher a^{o}-values (consistent with lower CO_2). Whether this variation is dependent on the depositional environment is not certain and difficult to prove. However, results of calcination of phosphorite samples could be used to interpret the post-depositional alteration of a deposit as suggested by McArthur (1978) and McClellan (1980). In nature CO_2 could be removed as a result of a variety of geological processes such as weathering, metamorphism and

diagenesis. In brief, impoverishment of CO_2 in these phosphorites may suggest 2 possibilities.

i) these phosphorites originated in carbonate-poor environment as a result of authigenic precipitation and/or

ii) CO_2 has been removed during post depositional alterations.

An original deficiency of carbonte seems more likely especially in Type-I nodules (present in the main bed of phosphorite) containing free dolomite. As long as this free carbonate is present it will protect the phorphorite from being dissolved. In addition, no other secondary phosphorite minerals were observed negating the second possibility of post depositional alteration. In other words this may suggest that these apatites have been formed authigenically in carbonate poor environment rather than by replacing carbonates. Similar examples of authigenically derived phosphatic rocks are Saldanha Bay and the South African shelf containing an average of 2.6 percent and 1.8 percent CO_2 respectively (Birch, 1980). These values are markedly different from the CO_2 content of the apatite phase in phosphatic rocks of the replacement type which has been determined by both Parker (1971) and Birch (1975) to be 5.5%. It appears from these figures that the highest CO_2 values are associated with phosphorites formed by replacement of calcareous sediments, whereas low CO_2 values are related to authigenic varieties which originate in carbonate poor sediments. However, high CO_2 values reported for other authigenic material from SW Africa by Rogers (1977) (5.5%) and Baturin (1969) (6.3%) render any relationship between the CO_2 content of phosphorite and

genesis or depositional environment extremely doubtful.

However, impoverishment of CO_2 in Type-I nodules present in upper beds of phosphorite and in Type II nodules, support the second possibility because the first effect of leaching is the decarbonation of phosphorite followed by the formation of secondary phorphorite minerals. Both of these effects have been observed in Type-I (upper beds) and Type II nodular phosphorite suggesting post depositional leaching.

Structural formulae of Type I and Type II phosphorite indicate that these apatites are pure carbonate fluoroapatite with meagre amounts of other substituents. Another important feature of these structural formulae is the variation of F. Type-I nodules show characteristic deficiency in F in contrast to Type-II nodules containing higher amounts than required for the fluorapatite structure. It has been suggested that decarbonation of apatite is followed by the removal of Ca and F (Prevot et al, 1979; Lucas et al, 1980). Fluorine is lost first before calcium (Gusev et al, 1976) during the weathering. Hence, variations in F concentrations in these nodules may occur due to

i) Original deficiency/higher than normal contents of F in the depositional environment

ii) Uneven removal during leaching.

An original deficiency of F in the depositional environment seems more likely during the formation of Type I nodules because of the fact that these phosphorites contain abundant free carbonate and some structural carbonate as well inhibiting leaching. Hence it is difficult to imagine removal of F without affecting any other associated minerals/elements.

Higher than normal amounts of F in Type-II nodular phosphorites, inspite of visible leaching effects (including decarbonation of phosphorite, low contents of Ca and presence of secondary phosphorite minerals) are probably due to abnormally high concentrations of F in the depositional envionment. This is why even after leaching F content is higher than normal. These contrasting features indicate different geochemical/depositional environment for Type I and Type II nodules rather than denoting post-depositional alterations.

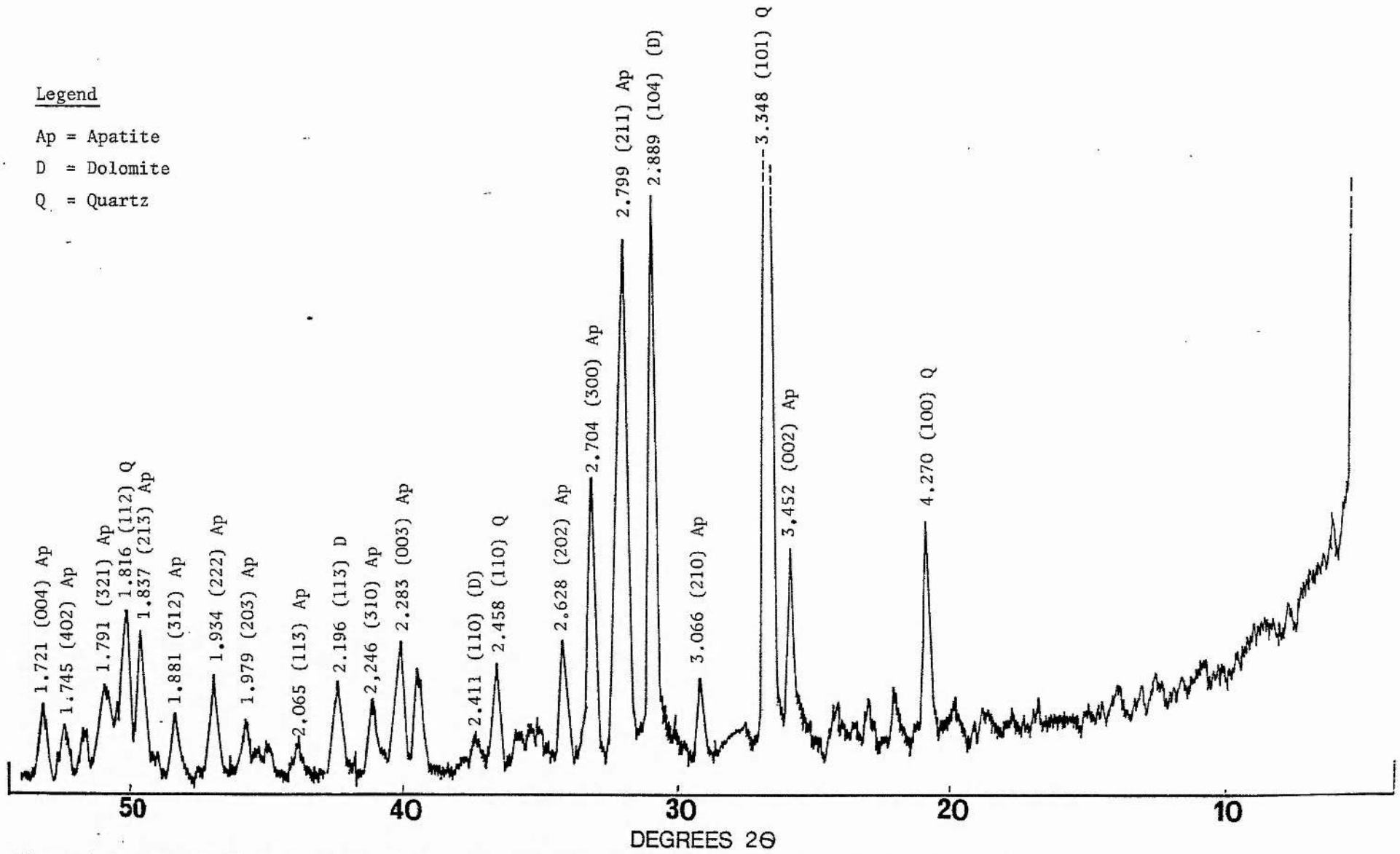

Figure 4.1 X-Ray Diffraction pattern of sample No Ph-5, Type I nodular phosphorite present in the lower main bed of phosphorite (Pen-y-Garnedd), N. Wales.

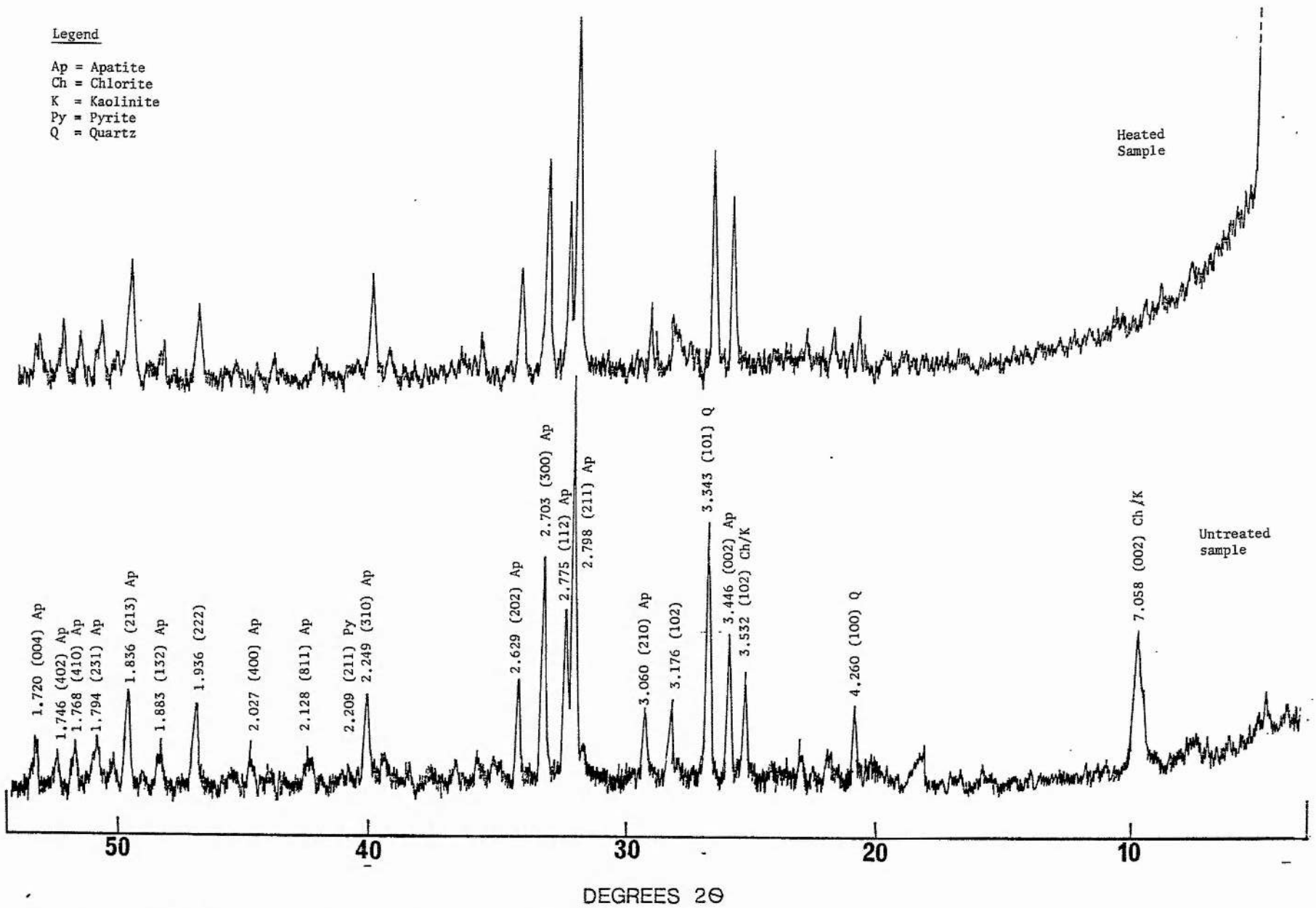

Fig 4.2 X-Ray Diffraction patterns of sample No Ph-49 Type I nodular phosphorite present in the upper beds of

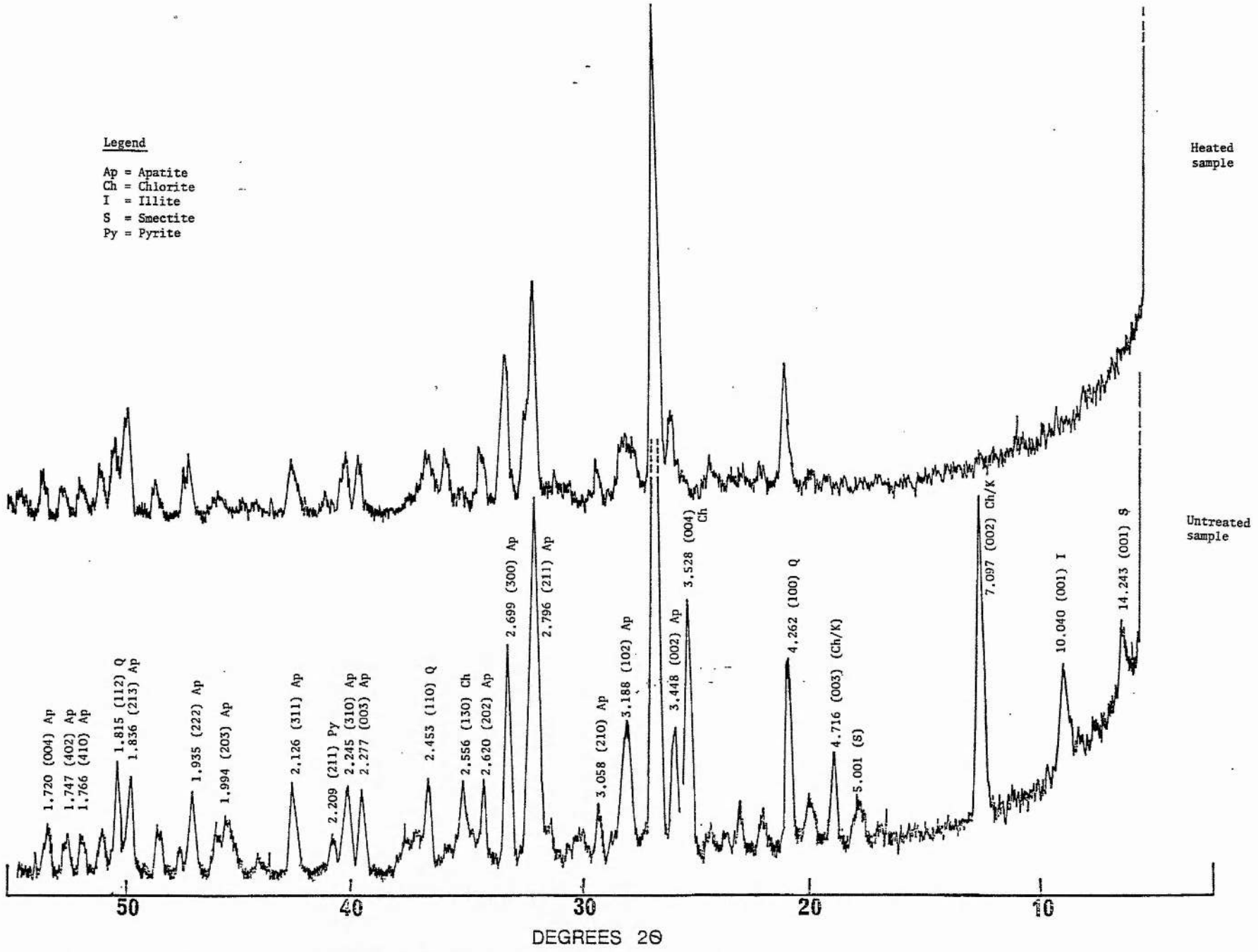

Figure 4.3 X-Ray Diffraction patterns of sample No Ph-39, Type II nodular phosphorite, Nant Achlas, N Wales.

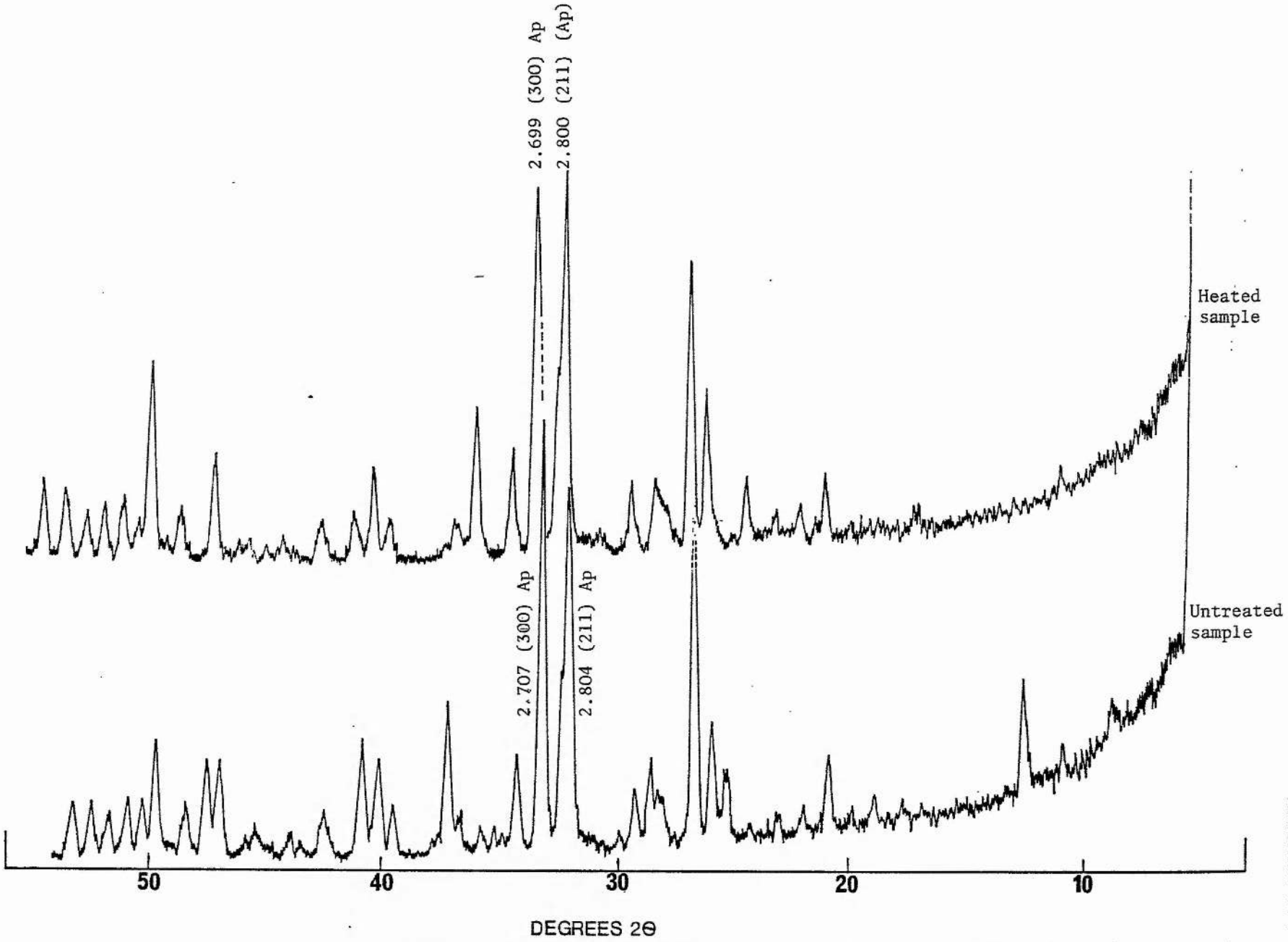

Figure 4.4 X-Ray Diffraction patterns of sample No Ph-35 (N)-1 (Type II nodular phosphorite) showing intensity reversal of the (300) and (211) peaks, Nant Achlas area, N Wales.

Legend:-

CH = Chlorite
K = Kaolinite
I = Illite
Q = Quartz
S = Smectite

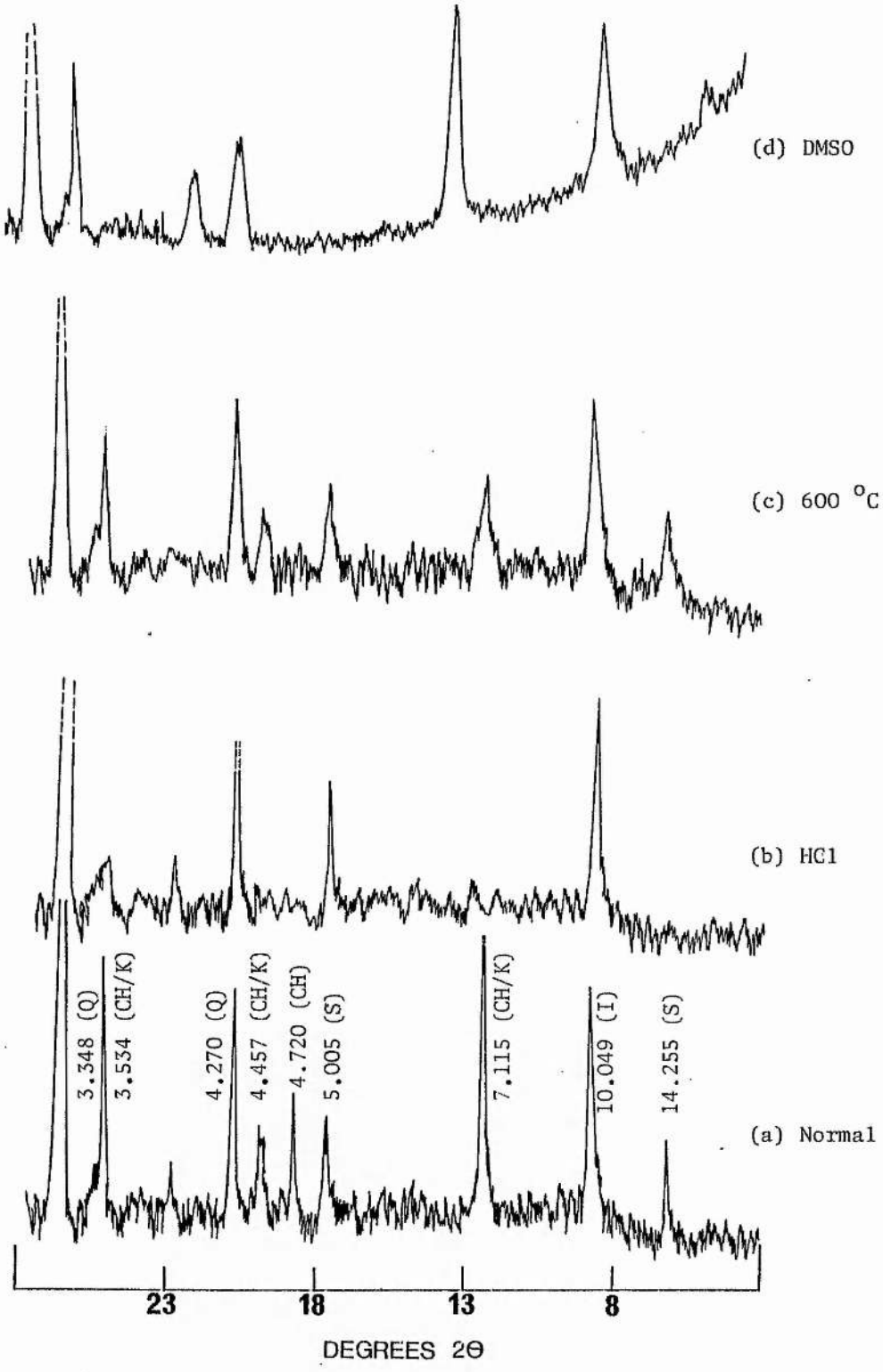

Fig 4.5 X-Ray Diffraction scans showing effects of different treatments on clay minerals

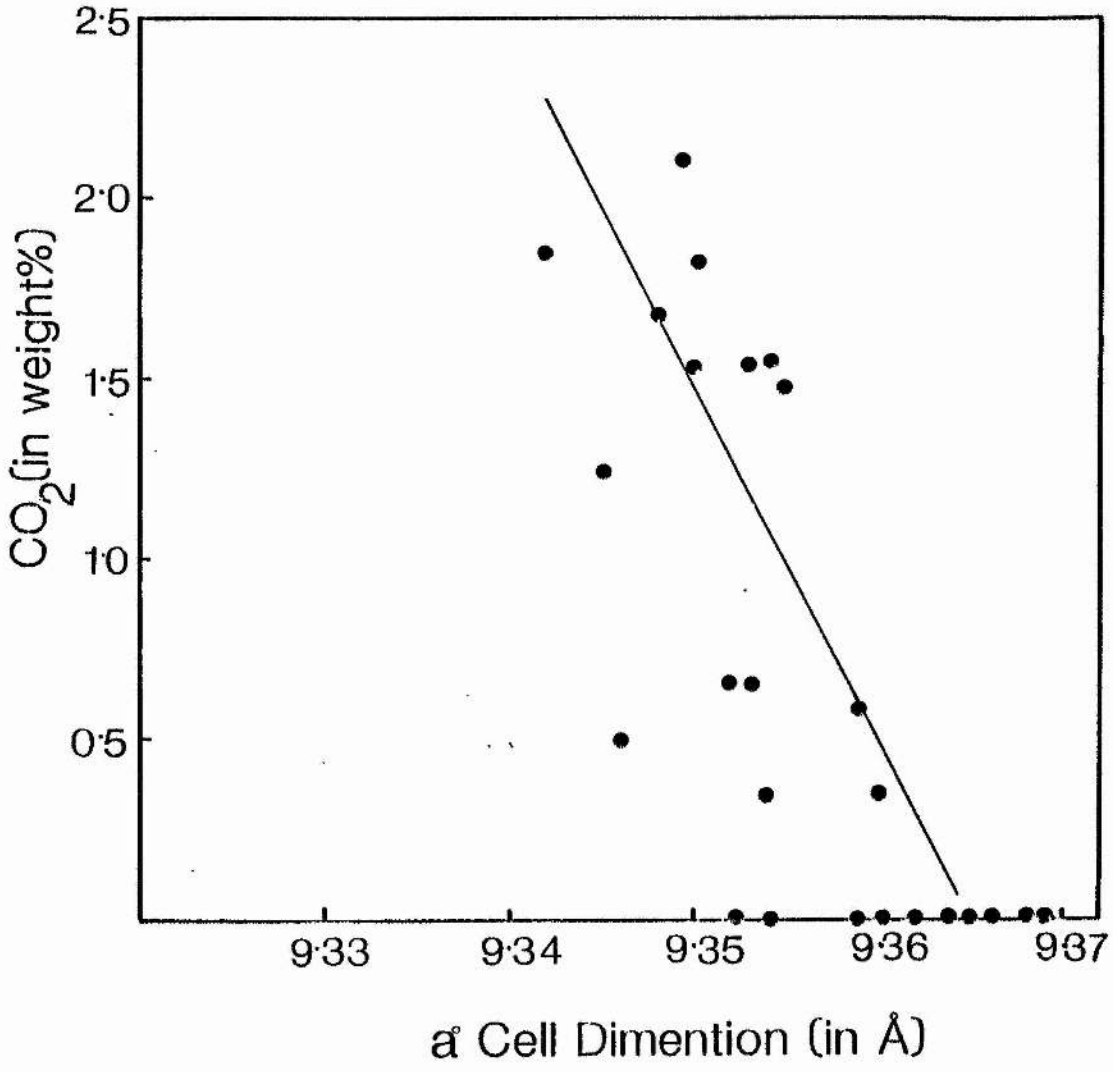

Fig 4.6 Plotting of Structural CO_2 content present in apatite lattice versus a°-cell dimension.

Table 4.1 X-Ray diffraction data of Type I and Type II nodular phosphorites

TYPE-I Nodular Phosphorite

Mineral Phase	hkl	Ph-5 Untreated		Heated at 1000 °C		Ph-10 Untreated		Heated at 1000 °C		Ph-49 Untreated		Heated at 1000 °C		Ph-57 Untreated		Heated at 1000 °C	
		dÅ	I	dÅ	I	dÅ	I	dÅ	I	dÅ	I	dÅ	I	dÅ	I	dÅ	I
Ap	100	8.184	6	8.184	6	8.184	6	-		-		-		8.184	8	S	
Ch/K	002	7.132	8	-		-		-		7.058		-		-		-	
Ch	003	4.731	15	4.717	6	4.717	6	-		-		-		4.721	10	S	
Q	100	4.270	49	4.262	19	4.262	19	4.260	22	4.260	28	4.270	27	4.266	21	4.270	35
Ap	200	4.038	20	-		4.049	12	4.036	15	4.058	19	4.076	24	4.040	16	4.065	25
Ap	111	3.890	16	3.889	17	3.873	11	3.876	13	3.870	22	3.880	24	3.881	12	3.873	23
Ch/K	102	3.677	16	S		-		-		3.532	25	-		3.532	30	S	
Ap	002	3.452	31	3.442	33	3.446	40	3.437	43	3.446	43	3.450	56	3.447	41	3.450	53
Q	101	3.348	H	3.346	H	3.343	69	3.373	85	3.343	68	3.351	68	3.343	100	3.351	98
?	?	3.220	H	S		-		-		-		-		-		-	
Ap	210	3.066	20	3.063	22	3.062	18	3.059	20	3.068	28	3.076	30	3.061	21	3.076	29
D	104	2.889	18	S		-		-		-		-		-		-	
Ap	211	2.799	100	2.798	100	2.801	100	2.799	100	2.798	100	2.802	100	2.801	100	2.808	100
"	112	2.779	66	2.778	68	2.780	55	2.772	79	2.775	49	2.776	55	2.777	50	2.778	50
"	300	2.704	56	2.705	60	2.702	58	2.704	61	2.703	61	2.709	66	2.704	62	2.712	62
"	302	2.628	28	2.618	28	2.624	28	2.619	27	2.629	34	2.626	38	2.625	29	2.633	38
Ch	130	2.558	14	S		-		-		2.562	17	S		2.557	10	S	
Q	110	2.458	24	2.459	25	2.455	9	S		2.461	16	2.460	19	2.453	14	2.465	22
D	110	2.411	11	-		-		-		-		-		-		-	
Ap	003	2.283	23	2.284	24	2.282	11	2.285	12	2.291	18	2.292	19	2.283	15	2.288	23
"	310	2.246	28	2.278	29	2.245	24	2.249	24	2.249	31	2.254	35	2.248	27	2.254	30
D, Py	113	2.196	18			-		-		2.215	15	S		-		-	
Ap	311	2.130	20	2.131	21	2.128	10	2.131	10	2.128	20	2.150	18	2.128	13	2.132	18
"	113	2.065	10	2.061	12	2.057	8	2.055	7	2.027	16	2.061	17	2.057	7	S	
D	2.02	2.013	10	-		-		-						-		2.031	35
Ap	2.03	1.981	13	S		1.996	8	S		1.997	15	S		1.996	9	S	
"	222	1.937	21	1.933	22	1.932	25	1.936	27	1.936	28	1.937	29	1.933	23	1.937	33
"	312	1.881	15	1.882	16	1.880	14	1.882	15	1.883	20	1.884	21	1.880	13	1.884	20
"	213	1.837	30	1.838	34	1.835	34	1.835	37	1.836	31	1.839	40	1.835	28	1.838	40
Q	112	1.816	40	1.817	41	1.814	11	1.818	12	1.820	17	1.821	18	1.816	11	1.823	22
Ap	231	1.795	19	1.797	21	1.794	16	1.794	17	1.794	21	1.797	25	1.794	15	1.798	25
"	410	1.765	12	1.768	14	1.767	14	1.769	15	1.768	20	1.773	22	1.769	14	1.774	22
"	402	1.745	12	1.747	14	1.744	14	1.747	13	1.746	18	1.751	25	1.746	13	1.746	21
"	004	1.721	16	1.722	17	1.720	17	1.719	17	1.720	21	1.722	22	1.723	15	1.722	22
Py	311	-		-		-		-		1.633	10	1.633	12	1.633	9	1.633	10

Note:- Ap = Apatite
Ch = Chlorite
D = Dolomite
I = Illite
Py = Pyrite
Q = Quartz
H = High Intensity
S = Suppressed

Table 4.1 Continued

TYPE-II NODULAR PHOSPHORITE

Mineral Phase		Ph-35				Ph-39				Ph-42			
		Untreated		Heated at 1000 °C		Untreated		Heated at 1000 °C		Untreated		Heated at 1000 °C	
	hkl	d Å	I	d Å	I	d Å	I	d Å	I	d Å	I	d Å	I
S	001	14.107	7	S		14.243	21	S		14.243	14	S	
I	001	10.155	9	S		10.040	30	S		10.063	8	S	
Ap	100	8.184	9	8.109	8	-		-		8.036	7	S	
Ch/K		7.086	21	S		7.097	90	S		7.063	43	S	
Ap	100	-		5.269	8	-		-		5.275	6	S	
Ch/K	003	4.713	18	S		4.716	26	S		4.711	11	S	
Ch	020	-		-		4.453	15	S		4.442	10	S	
Q		4.275	27	4.256	25	4.262	44	4.246	67	4.254	28	4.250	35
Ap	200	4.064	15	4.060	18	4.051	21	4.031	29	4.036	15	4.054	33
"	111	3.853	14	3.885	17	3.880	24	3.895	26	3.863	17	3.870	33
Ch	004	3.520	23	-		3.528	74	S		3.522	36	-	
Ap	002	3.447	34	3.439	46	3.449	43	3.429	48	3.431	45	3.429	51
Q	101	3.343	88	3.343	78	3.338	H	3.343	H	3.343	>100	3.348	74
Ap	102	3.166	19	3.171	24	3.188	44	3.197	38	3.168	24	3.186	35
"	210	3.061	19	3.067	24	3.057	24	3.056	29	3.057	24	3.064	33
"	211	2.804	93	2.800	100	2.796	100	2.793	100			2.802	100
"	112	2.787	48	2.773	51	2.780	54	2.774	50	2.775	54	2.788	58
"	300	2.707	100	2.699	96	2.699	62	2.695	69	2.696	71	2.708	63
"	202	2.627	27	2.626	31	2.620	29	2.618	33	2.621	31	2.623	37
Ch	130	2.558	10	S		2.555	28	S		2.555	11	S	
Ap	301	2.516	11	2.508	41	-		2.506	33	2.506	10	2.519	37
Q	110	2.463	17	2.455	13	2.453	28	2.452	33	2.449	17	-	
Ap	003	2.285	15	2.287	13	2.277	26	2.283	29	2.281	17	2.280	31
"	310	2.248	26	2.247	27	2.247	27	2.245	31	2.242	31	2.249	37
Py	211	2.214	30	-		2.209	15	2.201	14	2.209	13	-	
Ap	311	2.130	14	2.145	13	2.126	27	2.127	29	2.130	15	2.130	28
Ch	205	2.063	8	2.057	9	2.056	10	S		2.061	9	S	
Ap	400	-		2.028	6	-		-		-		-	
Ch	203	1.997	10	1.998	8	1.994	19	S		1.996	12	S	
Q	201	-		1.979	7	1.979	18	1.988	17	1.979	8	S	
Ap	222	1.937	25	1.937	30	1.935	25	1.934	31	1.937	26	1.937	35
"	132	1.884	15	1.882	16	1.879	16	1.883	19	1.879	17	1.884	28
"	210	1.838	30	1.837	52	1.836	29	1.836	50	1.836	35	1.837	39
Q	112	1.818	16	1.820	13	1.815	34	1.819	38	1.815	15	-	
Ap	231	1.797	16	1.797	19	1.793	16	1.795	26	1.795	17	1.797	30
"	410	1.769	13	1.772	17	1.766	15	1.769	21	1.766	17	1.768	28
"	402	1.746	13	1.746	21	1.747	15	1.746	19	1.744	17	1.750	30
"	004	1.723	15	1.722	22	1.720	18	1.719	21	1.720	18	1.724	28
Py	311	1.633	9	1.633	10					1.633	15	1.633	17

Table 4.2 CO_2 contents (in weight percent) and unit-cell dimensions of Type-I and Type-II nodular phosphorites.

Sample No	a^{o} (Å)	c^{o} (Å)	CO_2* (weight%)
Ph-5	9.350	6.894	1.82
Ph-5 (H)	9.360	6.888	A
Ph-6	9.354	6.890	1.54
Ph-6 (H)	9.365	6.879	A
Ph-31	9.355	6.888	1.49
Ph-31 (H)	9.360	6.878	A
Ph-57	9.350	6.893	1.52
PH-57 (H)	9.369	6.880	A
PG-1	9.353	6.886	0.65
PG-1 (H)	9.354	6.876	A
PG-2	9.345	6.878	1.24
PG-2 (H)	9.355	6.875	A
Ph-48	9.359	6.888	0.58
Ph-48 (H)	9.365	6.879	A
Ph-49	9.352	6.886	0.65
Ph-49 (H)	9.369	6.880	A
B-1	9.354	6.885	0.35
B-1 (H)	9.360	6.877	A
B-2	9.349	6.888	2.11
B-2 (H)	9.362	6.878	A
Ph-28	9.358	6.889	1.65
Ph-28 (H)	9.364	6.879	A
Ph-35	9.355	6.889	2.11
Ph-35 (H)	9.366	6.875	A
Ph-36	9.353	6.887	1.53
Ph-36 (H)	9.351	6.877	A
Ph-37	9.346	6.880	0.50
Ph-37 (H)	9.350	6.878	A
Ph-39	9.342	6.888	1.82
Ph-39 (H)	9.352	6.867	A
Ph-42	9.348	6.871	1.68
Ph-42 (H)	9.360	6.889	0.35

Note:- * = By Peak-Pair method
A = Absent
H = Heated at 1000 ^{o}C for two hours

Table 4.3 Chemical constituents and the Recalculated Mole Percentages of Average apatite in Type-I and Type-II phosphorites.

		COMPOSITION (in weight %)						RECALCULATED MOLES						STRUCTURAL FORMULAE	Charges	
	SAMPLE No	CaO	MgO	Na_2O	P_2O_5	CO_2*	F	Ca^{2+}	Mg^{2+}	Na^{1+}	$(PO_4)^{-3}$	$(CO_3)^{-2}$	F^{-1}		Cations	Anions
TYPE-I	Ph-5	49.25	0.12	0.06	36.31	1.82	3.14	9.95	0.03	0.02	5.55	0.45	1.79	$Ca_{9.95}Mg_{.03}Na_{.02}/(PO_4)_{5.55}(CO_3)_{0.45}/F_{1.79}$	+19.98	-19.33
	Ph-6	48.00	0.11	0.05	35.62	1.54	2.99	9.95	0.03	0.02	5.62	0.38	1.76	$Ca_{9.95}Mg_{.03}Na_{.02}/(PO_4)_{5.62}(CO_3)_{.38}/F_{1.76}$	+19.98	-19.38
	Ph-22	50.86	0.04	0.07	37.88	1.52	3.19	9.97	0.01	0.02	5.64	0.36	1.77	$Ca_{9.97}Mg_{.01}Na_{.02}/(PO_4)_{5.64}(CO_3)_{.36}/F_{1.77}$	+19.98	-19.41
	PG-1	51.69	0.04	0.04	38.22	0.65	3.11	9.98	0.01	0.01	5.84	0.16	I.77	$Ca_{9.98}Mg_{.01}Na_{.01}/(PO_4)_{5.84}(CO_3)_{.16}/F_{1.77}$	+19.99	-18.61
	Ph-49	43.76	0.25	0.08	33.40	0.65	2.97	9.89	0.08	0.03	5.82	0.18	1.93	$Ca_{9.89}Mg_{.08}Na_{.03}/(PO_4)_{5.82}(CO_3)_{.18}/F_{1.93}$	+19.97	-18.75
TYPE-II	Ph-33	49.55	0.08	0.24	36.80	0.35	3.39	9.89	0.02	0.09	5.91	0.09	2.15	$Ca_{9.89}Mg_{.02}Na_{.09}/(PO_4)_{5.91}(CO_3)_{.09}/F_{2.15}$	+19.91	-20.06
	Ph-35	43.08	0.46	0.18	32.20	2.11	2.90	9.79	0.14	0.07	5.43	0.57	1.94	$Ca_{9.79}Mg_{.14}Na_{.07}/(PO_4)_{5.43}(CO_3)_{.57}/F_{1.94}$	+19.93	-19.38
	Ph-36	44.18	0.15	0.23	33.32	1.53	3.00	9.86	0.05	0.09	5.59	0.41	1.92	$Ca_{9.86}Mg_{.05}Na_{.09}/(PO_4)_{5.59}(CO_3)_{.41}/F_{1.92}$	+19.91	-19.52
	Ph-37	41.39	0.78	0.14	31.18	0.50	3.10	9.69	0.25	0.06	5.85	0.15	2.18	$Ca_{9.69}Mg_{.25}Na_{.06}/(PO_4)_{5.85}(CO_3)_{.15}/F_{2.18}$	+19.94	-20.03

Note:- * By X-ray peak pair method

CHAPTER V

GEOCHEMISTRY

In this chapter the geochemistry of phosphorites is examined in order to:

1) establish possible differences in substitution which might occur amongst different types of phosphorites

2) examine whether such differences, if they occur, are related to the environment of deposition of phosphorites and

3) assess the effects of weathering on the substitutions. This factor severely limits the value of any conclusions drawn regarding the original major and trace element assemblage.

5.1 Analytical methods

A total of 60 samples were analysed for 30 major and trace elements. All except F were measured at the Department of Geology, Kings's College, University of London, using Inductively Coupled Plasma Source Spectrometer (ICPS - Spect.). Sample solutions were prepared by a routine method (Walsh and Howie, 1980) (described in Appendix 5.1) and calibrated with KCl1, USGS-22, USGS-47 and University College London laboratory phosphate rock standards P(cal)-1, P(Fe)-1, P(Fe)-2 and P(GL)-1. F was determined at the Department of Geology, St. Andrews University using SP6-3x 50 Spectrophotometer (Appendix 5.2). Polished thin sections were also analysed at the Grant Institute of Geology, Edinburgh, using electron microprobe for spot analyses of primary and secondary apatite. Technical details and procedures are given in Appendix 5.3.

5.2 Interpretive Techniques

Data are listed in Tables 5.1 and 5.2, grouped according to petrographic classification, namely Type I nodules and Type II nodules and their host rocks respectively. Data for oolitic phosphorite were insufficient (only two analyses) hence not subjected to statistical analyses.

Major and trace element data were analyzed statistically utilizing the Statistical Package for the Social Sciences (SPSS) on twin processor digital Vax - II/780 computer (St. Andrews Vax "A" (SAVA) and St. Andrews Vax "B" (SAVB). Factor analysis reduces complex relationships amongst a large number of variables to a small number of relationships which explain most of the variance in the original data. This method, previously used in phosphorite geochemistry (Reeves and Saadi, 1971; Summerhays, 1972; Jarvis, 1980) was found to be most significant in terms of data reduction. Variables are grouped on the basis of their intercorrelation into factors which are associations of highly correlated variables. These factors are statistically the dominant features of the data variation. Any variable may appear in one or more groups or factors and its coherence to a particular factor is expressed as a factor loading. In this study the Principal Factor matrix was rotated to produce a Varimax orthogonal solution in which each factor represents a single dimension in the data. The most significant results were obtained when factor analysis was applied to Type I nodules, Type II nodules and their host rocks respectively.

Although factor analysis is very useful in grouping numerous

variables in one factor, it does not give inter-element relation e.g. it may combine all the variables, in one factor, needed for making one particular mineral species but it may not tell what relations they have with one another. Hence Pearson correlation coefficient was calculated for each element in phosphorites. Regression lines were plotted for significant correlations, using Least square Method.

This Chapter is divided into four sections as follow:

Section 5.3 Major Elements (Bulk analyses)

Sectron 5.4 Electron Microprobe Analyses

Section 5.5 Trace Elements

Section 5.6 Discussion

5.3 Major element variations in phosphorite

Major elements analysed and expressed as oxides include SiO_2, TiO_2, Al_2O_3, Fe_2O_3, Na_2O, K_2O, P_2O_5, CaO, F, C and CO_2. Chemically the phosphorites may be described in terms of CaO, P_2O_5, F, CO_2 and Na_2O. Numerous substitutions are possible in an apatite lattice without causing major disruption in its structure. The elemental variations found in Type I and Type II nodules and their host rocks is discussed below:

Type-I Nodules

Type I nodules contain an average of 23.33% SiO_2, 6.04% Al_2O_3, 0.23% $TiO2$, 1.59% MgO, 0.45% Na_2O, 0.97% K_2O, 1.92% F, 33.56% CaO and 23.61% P_2O_5 (Table 5.1). The nodules present in the Upper Beds are very similar except that they contain higher amounts of Fe_2O_3 (3.55%), and F (2.46%) and lower amounts of MgO

(0.82%).

An average CaO/P_2O_5 ratio for Type I nodules is 1.48 which is higher than that expected for a pure carbonate fluorapatite phase (1.33). The reason for this higher ratio is the presence of a free dolomite phase. The CaO/P_2O_5 ratio for nodules present in upper beds is 1.36 which is similar to the pure carbonate apatite phase. All the CaO present is assigned to the apatite phase in view of the fact that no other mineral is present which contains CaO. Since no other phosphate mineral is present, it is assumed that all the P_2O_5 is contained within the apatite. The F/P_2O_5 ratio is more reliable as an indication of the composition of the apatite because the amounts of F-bearing accessory minerals are insignificant in many sedimentary rocks. It has been shown that F/P_2O_5 ratio rises from 0.089 in fluorapatite to 0.148 in a highly substituted francolite (McClellan, 1980). F/P_2O_5 ratio for Type I nodules varies considerably from 0.073 to 0.179 (Av. 0.089). Lower ratios of F/P_2O_5 suggest that there is a F-deficiency in these phosphorites.

The host rocks in contrast to nodules contain very high amounts of silica (63-75%), alumina (7-20%) and MgO (3-6%). Iron content is lower in the main bed of phosphorite (1.83-2.55%) than the upper beds (2-7%). Upper beds are also deficient in MgO content (0.80%) (Table 5.1).

Type II nodules

Type II nodules contain an average of 27% SiO_2, 8.4% Al_2O_3, 6.5% Fe_2O_3, 0.43% TiO_2, 0.79% MgO, 0.54% Na_2O, 1.43% K_2O, 27.98% CaO, 20.04% P_2O_5 and 1.97% F (Table 5.2).

The CaO/P_2O_5 ratio of these nodules varies considerably with mean value 1.396 which is slightly higher than expected for a pure carbonate fluorapatite phase. Mean F/P_2O_5 ratio in these nodules is 0.101 suggesting considerable substitutions in francolite.

The host rock in contrast to nodules, show large variation in SiO_2 content (39-62%). The other oxides present in higher amounts than nodular phosphorite are Al_2O_3 (14-23%), Fe_2O_3 (3-6%) and K_2O (2-5%) (Table 5.2).

The average major element composition for Welsh Phosphorites, together with average for phosphorites from other areas in the world is reported in Table 5.3. It is clear from this Table that chemically, Welsh Phosphorites are more similar to Peru-Chile and Namibia (SW Africa) and Phosphoria Formation of western United States than to the phosphatized limestones of the Agulhas Bank (S. Africa). The relationship is reflected in the average CaO/P_2O_5 ratio. The higher ratios (2.35) in the Agulhas Bank deposits are a consequence of the phosphatization of limestone and not the direct precipitation of apatite.

5.3.1 Statistical treatment

Factor Analyses, Regression Lines and Correlation Coefficients

Four factors representing more than 90% of the total variance of the data were extracted (Table 5.4A). It is evident that the bulk of the variance (more than 60%) is explained by only two factors. Minor loadings (<3) have been removed from these factors. It could be reasonably anticipated from the regression lines drawn in between important pairs of elements that a positive correlation exists between P_2O_5 and elements

located within the apatite lattice, whereas a negative or random correlation will be apparent between P_2O_5 and elements located outside the lattice. However, despite the fact that some of the regression lines are of very doubtful validity due to the wide scatter of the points and the relative paucity of data, there are undoubtedly marked differences in the major element distribution in phosphorites and their host rocks respectively.

Factor 1

Statistically this is the most dominant factor accounting for more than 40% of the variations in Type I and Type II nodules. This factor also accounts for more than 55% and 40% variation in their host rocks respectively.

As expected very high loadings in Type I nodules are shown by CaO and P_2O_5 (and comparatively low loading for F) is due to their geochemical coherence in sedimentary apatite. Mineralogically the factor must be attributed to the only phosphorus bearing mineral present - francolite. Antipathy of this association to SiO_2 and MgO reflects their association with some other minerals. Scarcity of clays in Type I nodules and their insignificant correlation suggest that they are independent variables. Type I nodules contain silica as chert cement and a few detrital grains. MgO is related to secondary dolomite present in these nodules.

In the host rocks, Factor 1 shows high loadings for many elements (Table 5.4B) which is clearly due to the effects of mineralogical controls not present in the nodular phosphorite. The high positive loading for Al_2O_3, Fe_2O_3, and K_2O is due to

some clay present in the host rock. Negative moderate loadings for CaO and P_2O_5 is due to the fact that apatite associated elements, although present in the host rocks, are not geochemically related to clay minerals.

In Type II nodules, Factor 1 shows high coherence for SiO_2, Al_2O_3, Na_2O and K_2O. The close relationship amongst these oxides has been recognized in many sediments including phosphorites (Gulbrandsen, 1966; Jarvis, 1980) and has been interpreted as aluminosilicate control or the clay mineral factor. This factor also shows high loadings for francolite related elements CaO, P_2O_5, and F. Their antipathetic relation to clays, suggest that francolite and clays are not related to one another geochemically, hence these two associations are independent.

The high coherence for SiO_2, Al_2O_3 and K_2O in the host rock for Type II nodules, is interpreted as an illite factor (Table 5.4B). Very high loading for SiO_2 and high silica/alumina ratio (3 to 5) suggest that some free silica is also present and this might have been released from montmorillonitic minerals during the formation of illite. This supports the mineralogical determination where X.R.D. studies show that host rock is rich in quartz and mixed layer minerals.

Looking first at the elements found predominantly within the apatite lattice (and in factor 1), a CaO - P_2O_5 plot shows the anticipated straight line relationships with only a small separation of the Type I and Type II regression lines (Fig. 5.1). The fit of the F - P_2O_5 regression lines are undoubtedly poor, but whatever the manner of drawing the lines, the correlation is always positive (Fig. 5.2). F - P_2O_5 show better

correlation in Type II nodules (0.66) than Type I nodules (0.40). P_2O_5-CO_2 plot shows a large scattering of points indicating differential leaching during weathering (Fig. 5.3).

Other elements showing significant correlations are SiO_2, MgO, Al_2O_3, K_2O and Fe_2O_3. The regression lines show an inverse relation with P_2O_5 (Figs. 5.4 to 5.8) sugesting that these elements are present outside the apatite lattice. MgO - P_2O_5 show an anticipated inverse correlation, as Mg is known to inhibit the precipitation of apatite (Fig. 5.5).

The significant correlations of SiO_2 - Al_2O_3 (0.87), SiO_2 - K_2O (0.95) and Al_2O_3 - K_2O (0.98) in Type II nodules evidenced by the generally excellent fit of the regression lines (Figs. 5.9 to 5.11) indicate that clays and silica are present in a constant proportion in Type II nodules in contrast to Type I nodules in which these oxides show either insignificant correlations or an inverse relationships.

Factor 2

This factor accounts for 17.6% and 23.4% of variance in Type I and Type II nodules respectively and 24.0% and 32.7% in the host rocks respectively.

Type I nodules comprise significant positively loaded Al_2O_3 and TiO_2 and very low loadings for Fe_2O_3. Very low negative loading is present for silica as well. The geochemically well known correlation between Ti and Al shows a correlation coefficient of 0.77 (Fig. 5.12) and the Al/Ti ratio is claimed to indicate the provenance (Bostrom, 1970). A high ratio (near 20) suggests a terrigenous source while weathering products of

average oceanic material should have low Al/Ti ratio of around 5. Al/Ti ratios of Type I nodules is around 6-7. The strong correlation of Ti and Al and K, (Fig. 5.13), however, favours its association with mixed layer clays rather than denoting significant concentrations from oceanic material or a terrigenous source.

Very high negative loadings are present for SiO_2 in the host rocks for Type I nodules with moderate positive loadings for CaO and P_2O_5. It is noteworthy that low negative loadings are also present in Type I nodules for SiO_2. It is possible that the depositional environment favoured large amounts of silica (biogenic chert?) in the sediments. Low negative loadings for SiO_2 and positive loadings for P_2O_5 and CaO in Type I nodules perhaps suggest that phosphorite protected the nodules from silicification. However, chert precipitated simultaneously, as filling the cracks and fissures in these nodules and as cementing material for the host rock.

In Type II nodules, Factor 2 has high positive loadings for only one element Fe and low negative loadings for CaO and P_2O_5. Similarly, the host rock for Type II nodules, show very high positive loading for Fe_2O_3 and Ti as well. As described in Chapter III, pyrite was introduced in these sediments during late stage diagenesis. It seems pyrite has affected the nodules and the host rock in a similar manner and separates out as an independent factor.

Factor 3

This factor accounts for 15.6% and 10.9% of variance in Type

I and Type II nodules respectively. Their host rocks show 10.9% and 15.1% of variance respectively.

Factor 3 has high positive loading for iron and Ti in Type I nodules. Geochemically Ti follows Fe in sediments, hence the association. The isolation of this element Fe as a separate factor is due to its large variation in nodules. Upper beds at Pen-y-Garnedd area contain high amounts of Fe but the nodules present in the main bed do not contain much pyrite.

Host rocks for the Type I nodules show high positive loading for only one element Na_2O, but the reason for this is not clear.

Type II nodules show high loadings for MgO, Na_2O and lower loading for Al_2O_3. This association perhaps suggest a chlorite association, as these nodules also contain this mineral. MgO - Al_2O_3 (0.84) and MgO - SiO_2 (0.83) correlations are highly significant and confirm their association with chloritic minerals (Figs. 5.14 and 5.15). The host rock for Type II nodules shows moderate positive loadings for Al_2O_3 and K_2O and very low loadings for silica and this might suggest, some K-feldspar control. The high negative loading for MgO and moderate loading for CaO, are difficult to understand as dolomite is absent in these sediments.

Factor 4

This factor accounts for 9.4% of variance in Type I and 8.9% in Type II nodules. Their host rocks show 5% and 3.3% of variance respectively.

Type I nodules show high positive loading for K_2O and moderate negative loading for SiO_2. As shown earlier, K_2O shows

positive correlation with P_2O_5 (Fig. 5.7), suggesting that a part of K_2O is present inside the apatite lattice. Isolation of this element as a separate factor is not entirely understood at this stage.

Host rocks for Type I nodules show high loadings for MgO and low loadings for CaO, suggesting dolomite association. Low loadings for CaO indicate that CaO is mainly involved in making apatite and only a little part of it has combined with MgO in making dolomites.

Type II nodules show high positive loading for F and low negative loading for TiO_2. Isolation of F as a separate factor is not understood.

5.4 Microprobe analyses of major elements

More than 10 spot analyses for each polished thin section of nodular phosphorites were performed in 15 samples. The average analyses of francolite, shell fragments and secondary phosphorites are reported in Tables 5.7, 5.8 and 5.9 respectively.

Several important differences may be noted between this data and the bulk chemical analyses reported earlier. As expected, the SiO_2, Al_2O_3 and FeO contents are lower than those reported for the bulk composition, because, these elements are mainly contained within the allogenic components, which are largely excluded by this method of analysis. The elemental ratios CaO/P_2O_5 are slightly lower than the bulk analysis mainly because CaO - contributing dolomite are largely excluded by this method in Type I nodules. Type II nodules, however show similar

variation in CaO/P_2O_5 ratio. F/P_2O_5 ratios are essentially the same as those reported earlier for the bulk analyses. These ratios are consistent with those reported for pure carbonate fluorapatite phase (Deer et al, 1966; Gulbrandsen, 1969; Burnett, 1977).

Various phosphatized shell fragments present in the host rocks for Type I and Type II nodules were also analysed (Table 5.8). The only appreciable difference found is in F/P_2O_5 and Na_2O/P_2O_5 ratios which are higher in shell fragments present in Type II host rock. These results are consistent with the probe analysis of nodules. The presence of higher (excess) F + Na ($=CO_3$) content in Type II nodules would suggest higher carbonate substitution in these nodules. On the other hand CO_2 contents are quite low which indicates that weathering has removed a considerable amount of CO_2 from these phosphorites.

5.4.1 Secondary phosphorites

Various secondary Fe-Al phosphates have been identified mainly in Type II nodules and occasionally in Type I nodules present in the upper beds. Their overall scarcity in Type I nodules present in the main bed of Phosphorite is firstly due to the paucity of clay and ferruginous minerals and secondly due to the presence of dolomite which is protecting francolite from being altered.

As the concentration of these secondary phosphorites is very low even in Type II nodules and the host rock, their chemical composition was determined by electron microprobe only. Type II nodules and their host rocks, being rich in clay and ferruginous

minerals are more affected by weathering processes. The wavellite (Al-phosphate) present in these nodules shows a large variation in chemical composition. It contains 23-35% Al_2O_3, 28-38% P_2O_5, 1-4% Fe and 2-5% SO_4. Ca, Mg and Na concentrations are too low to be of any significance. Higher concentrations, than usually present, of Fe and S are due to the fact that these nodules are rich in pyrite. Wavellite was precipitated during or immediately after the dissolution of pyrite as it is present in veins and fissures, previously occupied by pyrite. Dissolution features are commonly shown by these pyrite crystals (Fig. 3.45).

It appears that more and more pyrite was dissolved and reacted with apatite to from strengite ? (as it is known that Al-phosphates are followed by the formation of Fe-phosphates). During these conditions the pyrite present as cubes and in cracks was dissolved and at places completely replaced by strengite (?). Often it is possible to see the residual pyrite in the centre surrounded by strengite (?) (Fig. 3.14). Chemically this mineral shows a large variation with its colour. Red strengite (?) is richer in FeO (51-59%) and poorer in Al (2-8%) and P_2O_5 (11-15%) than the orange strengite (?). The orange strengite contains 35-37% FeO, 9-15% Al_2O_3 and 19-24% P_2O_5. Red strengite (?) always occurs in the centre surrounded by orange strengite (?). It seems that the formation of secondary Fe-phosphate started with more Fe and less P followed by less Fe and more P.

5.5 Trace element variations in phosphorites

It is well known that apatites readily act as hosts for

numerous trace elements (Gulbrandsen, 1966; Tooms et al, 1969; Cook, 1972; Altschuler, 1967, 1973; Prevot and Lucas, 1980). Data on trace elements (average concentrations) analysed during the present investigation are compared with the average concentrations found in sea water and the average shale (Table 5.10). Enrichment or depletion of trace elements similar to that of sea water would suggest the elements are derived from that source and not from crustal material. Type I nodules are enriched in Ag, Ce, Cr, La, Sr and Y and Type II nodules are also enriched in all these elements in addition to Mo relative to shales (Table 5.10). The elements found to be depleted in Type I nodules are Ba, Cu, Li, Mn, Mo, Ni, V and Zr whereas Type II nodules show depletion in only a few elements such as Co, Mn, V and Zr. Most of the elements depleted in Type I nodules eg Ba, Cu, Mn, Ni and V are also found to be impoverished in sea water (Tooms et al, 1969) which may suggest precipitation of apatite from sea water. That Li and Zr, though enriched in sea water are depleted in these nodules could be explained by the fact that the ionic radii of these two elements are too large to be accomodated in the apatite structure. The appreciable enrichment (eg 7 to 9-fold Y and 3-fold Sr and La) of various elements in these nodules with respect to marine shales may reflect their characteristic marine depositional environment. Another striking feature of these phosphorites is the 3-fold enrichment of Ce. Marine apatites are usually depleted in Ce as sea water is notably deficient in it (Goldberg, et al, 1963; Hogdahl, 1967). It is not known at this stage whether higher concentration of Ce is present in the apatite lattice or apatite has cerium bearing

impurities/ present in detrital minerals.

5.5.1 Statistical treatment

Factor Analyses, Regression Lines and Correlation Coefficients

Four factors representing more than 75% of the total variance of the data were extracted (Table 5.11 A and B). Minor loadings have been removed from these factors (<3). It is evident that the bulk of the variance is explained in merely two factors.

Factor 1

Statistically this is the most dominant factor accounting for more than 30% of the variance in Type I nodules and 40% in Type II nodules (Table 5.11A). Host rocks show more than 60% and 35% of the variation respectively (Table 5.11B).

Type I nodules show very high positive loadings for Ba, Sr, Zn and moderate loadings for CO and V. Low negative loadings are also present for Mn and Cr. These two associations reflect two different controls - apatitic and dolomitic. It has been shown earlier that whatever the composition of phosphorites Sr always correlates positively with P_2O_5, rarely with carbonates and never with Al_2O_3 (Prevot and Lucas, 1980). Hence, the association with Sr is thought to follow apatite. In addition Sr-P_2O_5 correlation is high positive (Fig. 5.16). Since these nodules contain dolomite, it could be argued that Sr might be related to these carbonates, but Sr-MgO correlation is very insignificant. Hence, all the Sr is thought to be present in the apatite lattice replacing Ca. Ba, also behaves similarly to Sr in phosphorites

and in the associated carbonates but is systematically more abundant in the former. P_2O_5-Ba correlation is insignificant and hence shows a large scattering of points (Fig. 5.17) but Ba-Sr relation is highly significant (0.82) (Fig. 5.18). The close relationship between phosphates and vanadates is well known. V substitutes for P, in some deposits, reaching sometimes commercial concentrations. Though more abundant in phosphorites, V does not show a marked regular positive correlation with any mineral of the phosphorites; yet its attraction for apatite is as clear as its affinity with the clay minerals. P_2O_5-V plot shows low positive correlation (0.50) (Fig. 5.19).

MgO-Mn show high positive correlation (0.82) but MgO-Cr show very insignificant correlation. Inspite of this insignificant correlation Cr is associated with dolomite, Mn-Cr relation is low positive hence the association.

Host rocks for Type I nodules show high loadings for various trace elements usually associated with clay minerals and organic material. Very high positive loadings are present for Ba, Co, Cr, Cu, Li, Nb, Ni, Sc, V and Zn. This is a result of many mineralogical controls present in the host rock data and hence there is no clear association with a particular mineral phase.

Factor 1 in Type II nodules shows high positive loadings for Ag, Sr, and moderate loadings for Ce, La and Sc. Negative high loadings are present for Mo, Nb, Li and Zr. These two associations are clearly due to two controlling mineral phases present in the nodules. Because the positively loaded association contains Sr, which closely follows apatite, the phosphorites are considered the main control for this

association. In addition P_2O_5-Sr (0.83), P_2O_5-Ce (0.89), P_2O_5-La (0.80) interelement correlations are highly significant (Figs. 5.16, 5.20, 5.21) This clearly suggests that these elements are present in the apatite lattice and were substituted during the formation of francolite. Sc does not show any significant relation with any of these elements. Its presence in this association is difficult to explain. Li and Zr are largely expelled by apatite lattice because of their bigger ionic radii. Hence, these elements get absorbed on clay minerals. Mo is almost absent in these nodules but shows very significant correlation with Al_2O_3 (0.80). Hence, it is appropriate to assign this association to clay minerals.

Host rock for Type II nodules also show high loadings for elements associated with apatite. These are Ce, Cr, La, Sr and Sc. Moderate to low loadings are present for Co, Ni, Y and Zn.

Factor 2

This factor accounts for 18.3% and 23.8% of variance in Type I and Type II nodules respectively (Table 5.11A). Host rock data shows 15.3% and 27% of variance respectively (Table 5.11B). This factor in Type I nodules show high loading for Ce and La and moderate to low loadings for Cr, Li, Ni, V and Zn. This association does not show any relation with apatite or clay-mineral related elements. Even their interelement correlations are insignificant except V-Zn (0.77) (Fig. 5.28). Similar association is also present in Factor 2 of Type II nodules. Elements with high positive loadings present are Ba, Co, Cr, Cu, Ni, and Zn. Few of the interelement correlations are

significant e.g. Zn-Ni=0.74; Zn-Co=0.76; Ni-Co=0.99 (Figs. 5.29, 5.30 and 5.31). These elements present in Type II nodules also do not show any dominant trend other than belonging to the group V, Ni, Cr and Zn. It has been shown that this association is related to the organic matter which commonly accompanies phosphorites (Krauskopf, 1955; Gulbrandsen, 1966; Cook, 1972; Prevot and Lucas, 1980). The known association of such elements with organic matter together with the abundant signs of biological activity of macro- as well as micro- organisms (Fauconnier, 1977; Doubinger, 1979) indicates that organisms, especially plankton, played an important role in the genesis of phosphorites.

Factor 2 in the host rock data for Type I nodules show high negative loadings for elements usually associated with apatite. These elements are Ce, La, Y and Sr. Low loadings are also present for various elements such as Ba, Cr, Li, Nb, Zn and Zr, usually associated with clays. Type II host rocks show high loadings for CO, and Cu and moderate to low loadings are present for Sc and Zn.

Factor 3

Statistically this is a minor factor accounting for 15.2% and 18.4% of variance in Type I and Type II nodules respectively. Host rock data shows 6.2% and 18.8% of variance respectively.

This factor in Type I nodules has high loading for only two elements Ag and Li. Ag-Li interelement correlation is highly significant (0.83), hence the association. As discussed earlier

Li, being excluded by apatite lattice, may get adsorbed onto clays present in the environment. Li-Al_2O_3 regression line confirms its association with clays (Fig. 5.32).

Host rock data show very high positive loading for only one element Ag. Very low loadings are present for Co and Mn.

Factor 3, in Type II nodules, shows very high negative loadings for Ce and La and moderate loading for Y. These rare earths also show very high inter-element correlation eg Ce-La=0.97 (Fig. 5.26); Ce-Y=0.78 (Fig. 5.27). Very high loadings present in this factor for these rare earths may suggest a part of these elements is associated with some phase other than apatite (because apatite-rare earth association has already been discussed in Factor 1). Their highly negative relations (except Y) with Al_2O_3 exclude any possibility of their association with aluminosilicate minerals. (Figs. 5.23, 5.24 and 5.25). One of the possibilities is, their association with secondary phosphorites as they are readily leached during weathering.

Factor 4

Factor 4 is also a minor factor accounting for 10.6% and 6.6% of total variance in Type I and Type II nodules respectively. Host rocks show 4.9% and 6.9% of the total variance respectively.

This factor has high positive loading for only two elements, Ni and Sc in Type I nodules. Geochemically these two elements are coherent and follow each other. Their inter-element correlation is also highly significant (0.74).

The host rock data for Type I nodules show high negative

loading for only one trace element Mn which is difficult to interpret. Although Mn is found to be related to dolomite in the nodular portions and hence it could be possible that this is due to the late stage introduction of dolomite along with Mn.

Factor 4 in Type II nodules has high negative loading for Sc and V and high positive loading for Y and low loading for Zr. This association is not understood. The host rock for Type II nodules show high positive loading for Ag and low loading for Ni. Geochemically Ag always concentrate in phases rich in Ni, hence the asscciation.

5.6 DISCUSSION

Factor analysis and regression plots show that there are two major groups of elements: those which are located predominantly within the apatite lattice (CaO, P_2O_5, F) and those located outside the lattice in minerals of detrital origin or introduced during diagenesis and/or weathering (SiO_2, Al_2O_3, K_2O, Na_2O). Both types of nodules show signifcant impoverishment of "lattice elements" and enrichment of "non-lattice elements". Large variations of CaO/P_2O_5 ratio in Type I nodules is due mainly to the presence of accessory dolomite. Whereas significant variations of this ratio (1.32 to 1.46) in Type II nodules is probably brought about by differential weathering processes. The CaO in francolite-type apatites remains nearly constant (in non-weathered apatites) while the P_2O_5 varies with substitution of carbonate and fluorine which raises the CaO/P_2O_5 ratio from 1.317 in fluorapatite to 1.620 in a highly substituted francolite. Contrary to this, the amount of CaO present in Type

I nodules show a large variation. This is mainly because of the presence of variable amounts of dolomite as well as weathering which mainly dissolves Ca, hence decreasing the CaO/P_2O_5 ratios. Carbonate substitution for PO4, also increases the CaO/P_2O_5 ratios. This substitution creates an imbalance of charges, a negative charge is lost. Balance is restored by substitution of F in the apatite lattice. Type I nodules show F deficiency in contrast to Type II nodules which show normal to, at times, excess F. Deficiency of F in Type I nodules could be due to two reasons:

i) Original deficiency of F in apatite precipitating solutions and/or

ii) Removal of F during weathering

An original deficiency of F seems more likely as these nodules contain significant amounts of accessory dolomite which protects them from dissolution. However, decarbonation of structural carbonates does suggest that these nodules have undergone some weathering. Another factor in favour of original F deficiency in the depositional environments, is the presence of abundant organic remains in these nodules. F-deficiency indicates a relatively non-toxic environment during phosphate formation which would allow luxuriant growth of organisms (Riggs, 1979). Burnett (1977) has shown that low F/P_2O_5 ratios are associated with Holocene diatomaceous oozes along the sea floor off the coast of Chile and Peru. The silica in these deposits acts as a nucleation site for precipitation of phosphate. It is probable that the F associated with the phosphate forms complexes with available silica, calcium, aluminium and iron and the

solubility of these complexes is pH dependent so that F precipitates while phosphate remains in solution. This would lower the F content below that required for the stoichiometry of the apatites resulting in fluorine deficient apatite. Inspite of the fact that Type II nodules are more weathered, they contain significantly higher amounts of fluorine (F/P_2O_5 = 0.101). This is important as these nodules also show an absence of any organic remains indicating toxic environment.

Microprobe data shows clearly that apatites of Type II nodules contain higher amounts of alkalies. They contain an average of 3-4 times higher Na_2O and MgO and 2 times higher K_2O contents than Type I nodules. (The bulk analyses are not compared because Type II nodules contain appreciable amounts of accessory clay minerals rich in these elements). Higher content of these alkalies suggests the following possibilities:

(a) Higher salinity conditions during the formation of Type II phosphorite indicating supratidal conditions.

(b) Higher substitution in the apatite lattice to balance the charge imbalance created by CO_3 substitution.

(c) Presence of clays and feldspar minerals.

The strong possibility is that, (as these nodules are more affected by weathering) these elements, being more mobile, have diffused into apatite lattice from clay minerals.

Silica content of Type I and Type II nodules is within a narrow range of variability, although its presence in both types is due to different factors. Petrographic studies show that silica in Type I nodules is not associated with clays or feldspars. It is thought that silica has been biogenically

precipitated by organisms like sponges of the class Hyalospongia and Demospongia since the saturation of sea water with silica is very unlikely. The majority of the silica in Type I nodules is either biogenically precipitated or detrital. The incorporation of detrital quartz and presence of the fragments of Hyalo and Demospongia, both suggest the formation of these nodules in shallow environment. Higher contents of silica in Type II nodules is mainly due to the presence of clays. Free silica which is present might have been released from the smectitie during the formation of illite.

Most of the trace elements also show contrasting behaviour in Type I and Type II nodules. Ba shows low positive correlation with P_2O_5 in Type I nodules in contrast to Type II nodules which do not show any correlation. Ba occurs mainly as adsorbed ions on the surface of apatite (it cannot easily be accomodated in the Ca-postions (1.06A) because of its bigger ionic size (1.43A)). Hence with the ageing of the deposits its amount decreases (Nathan, 1980). Ba is mainly incorporated with the host rock of Type II nodules (Table 5.2)

Sr is the one element present in the apatite lattice and shows significantly positive relations with P_2O_5. Its substitution in the apatite structure requires no balancing of charges. Hence it is freer to enter or leave the structure compared to Na, CO_3 or SO_4 which require coupled substitutions, to maintain charge balance. This would also suggest that Sr may be affected both by weathering and secondary enrichment processes. McArthur (1978) emphasized that the behaviour of Sr is such that it is relatively mobile in relation to the apatite

structure and is most affected by the weathering. He also suggested that upon formation all marine sedimentary carbonate fluorapatites contain a constant amount of Sr (0.24%). During weathering its concentration is reduced in a systematic manner to low concentrations. Sr-P_2O_5 correlation is significant in both types of nodules. But Sr/P_2O_5 ratios are very low in Type I (0.0043) and Type II (0.0040) nodules which may suggest two possibilities:

(a) Sr concentrations were low in the depositional environment and/or

(b) Weathering has removed considerable amounts of Sr from these apatites.

Low concentrations of Sr in the depositional environment is difficult to imagine at least during the formation of Type I nodules because they contain abundant organic remains and it is well known that phosphorus concentrates in soft parts of microorganisms and in bones of macroorganisms and Sr in tests and shells which can contain upto 1 percent Sr (Kulp et al, 1952). It seems both types of nodules have lost Sr during weathering. Normalized values of Sr were calculated (because it is present in the apatite lattice hence would show systematic variation with apatite weathering) which show 1645 ppm (Type I) and 1605 ppm (Type II) of Sr in the depositional environments. Slightly higher concentrations, as expected, are present in Type I in comparision to Type II nodules. The low ratios of Sr/P_2O_5 in Type II nodules are normal considering the effects of weathering. But the low values in Type I nodules, inspite of the insignificant weathering effects might support the conclusion

drawn by McArthur (1978) that Sr is more mobile than P_2O_5.

It has been shown that Ce, La and Y are enriched in these nodules in comparison to marine shales (Table 5.10). The enrichment of Y in apatite is to be expected as sea water is also enriched in Y. This enrichment is likewise a reflection of precipitation or fixation of apatite from a seawater source, as the rare earth distribution patterns for seawater show a marked enrichment of yttrium (Hogdahl, 1967). However, Y-P_2O_5 correlation is low positive for Type II nodules but is insignificant for Type I nodules. In addition Y-Al_2O_3 show high positive relations in both types of nodules. It has been thought that, Y being very light and mobile, has leached out of the apatite lattice and fixed with clays present in the environment.

Another striking feature of these nodules is the Ce/La ratio which is higher than 1, paralleling that of crustal abaundence (Goldberg, et al, 1963). Type I nodules show significant positive interelement correlation in between Ce-Al_2O_3 and La-Al_2O_3 implying their association with detrital clays. In spite of the higher ratio, P_2O_5-Ce and P_2O_5-La regression lines show high positive correlations especially in Type II nodules suggesting their presence in apatite lattice. Their significantly negative relations with Al_2O_3 also support their association with P_2O_5. This suggests a significant part of these rare earths is present in the apatite lattice of Type II nodules. Significant enrichment of Ce might represent significant differences from normal marine depostional environment which may create pronounced variations in solubility and fixation of the individual rare earths. This is particularly

applicable to the highly reduced organic and pyrite rich bone beds such as those of the Maikop sediments (USSR) which were deposited in a hyposaline, euxinic basin (Blokh and Kochenov, 1964; Kholodov, 1963). These beds are rich in Sc and Ce group elements. Type II nodules although deficient in organic remains, do show higher salinity conditions.

It is clear from this foregoing discussion that the chemistry of the depositional sites for these two types of nodules was significantly different. Each basin has its own subtle variants which influences the ultimate composition of the phosphorite formed.

5.6.1 Effects of weathering

One of the first results of weathering in phosphorites is a loss of CO_2 from the lattice and concomitant increase of the lattice constant in the apatite. The decarbonation and the increase of lattice constant are associated with the removal of many elements. The apatite lattice becomes depleted in Ca and F and also in Na and Sr. As long as free carbonates are present in the rock, they protect the associated apatite, stopping the evolution from going further than the fluorapatite stage. Type I nodules, containing considerable amounts of dolomite is protecting apatite from dissolving further down than the fluorapatite stage.

The intense weathering of marine phosphorites leads, after leaching of the free carbonate fraction and decarbonation of apatite, to the appearance and growth of aluminous and ferruginous phosphates. Type I nodules present in the upper beds

are a typical example of this. Most of their free carbonates has been leached and apatite shows decarbonation and appearance of Fe-phosphate (Strengite?). Here Al-phosphates are absent because of the scarcity of clay minerals. Type II nodules are more effected by weathering processes as they do not contain free carbonates. Here, the environment depleted in Ca^{++}, becomes more acid, so that the calcium is removed from apatite. Low values of CO_2/P_2O_5, CaO/P_2O_5 and Sr/P_2O_5 all indicate dissolution of apatite. As the environment is rich in clays and pyrite, dissolved apatite combines with Al and Fe and a chain of Al-phosphates and Fe-phosphates develops. During the development of these secondary apatites, the distribution and location of the trace elements change. Sr is very mobile and Sr/P_2O_5 ratios are significantly low (0.004) implying that these nodules have undergone considerable alteration. Very low concentrations of Na, also indicate the same process.

Wavellite present in Type II nodules has a high concentration of SO_4 (2-4%) and Fe (1.7-3.9%) and very insignificant content of Ca, Mg, Na and K. As the cracks, in which wavellite is now present, were earlier filled with pyrite, it may have consumed some Fe and PO4 from those pyrite crystals.

Fig 5.1

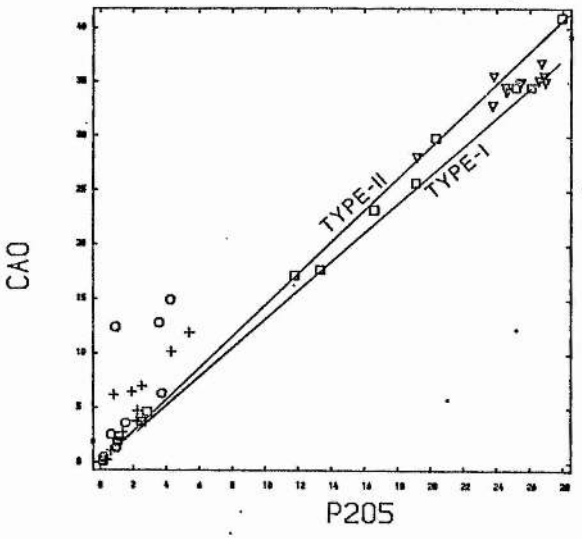

Fig 5.2

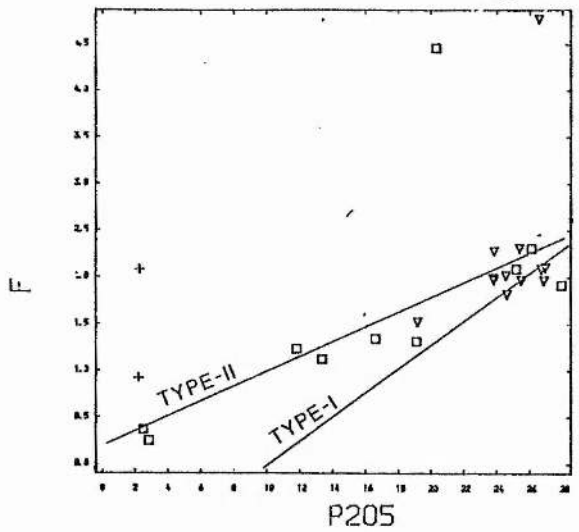

Fig 5.3

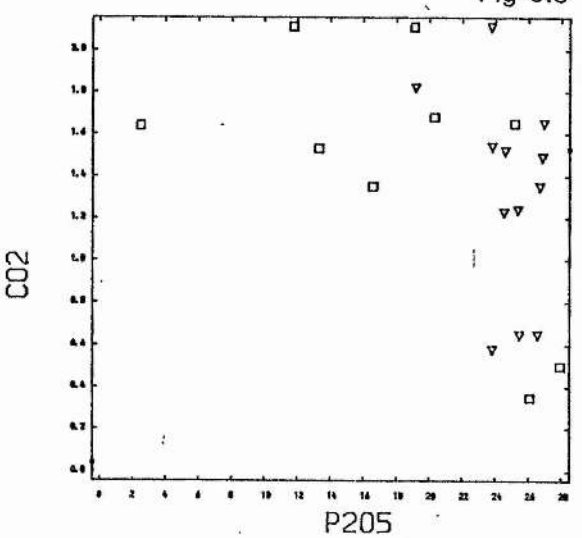

Fig 5.4

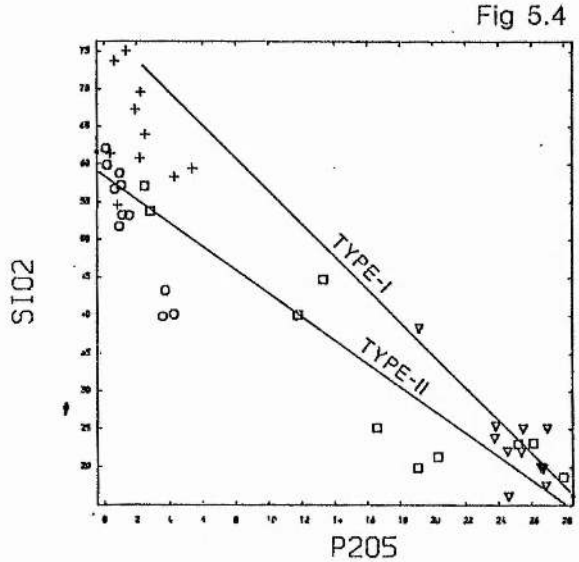

Fig 5.5.

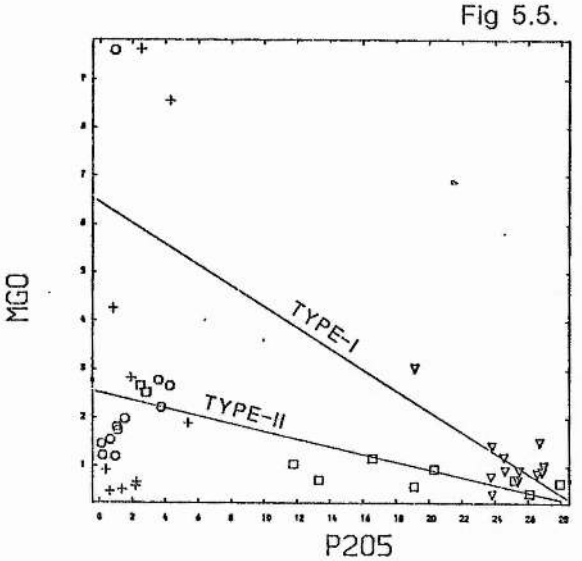

Fig 5.6

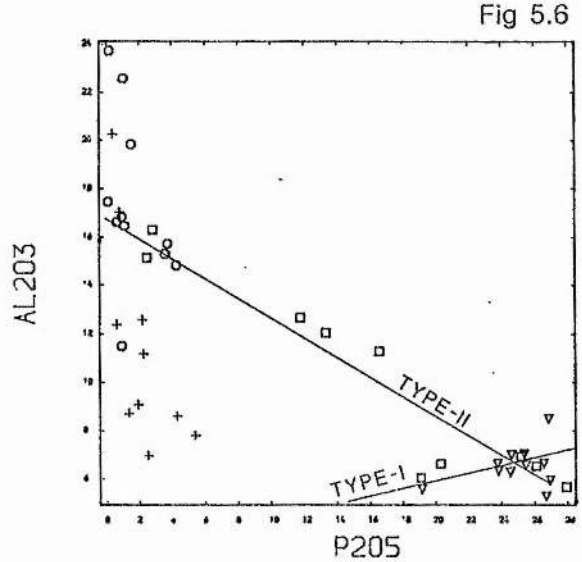

INDEX

▽ TYPE-I NODULES □ TYPE-II NODULES

\+ TYPE-I HOST ROCK o TYPE-II HOST ROCK

Fig 5.7

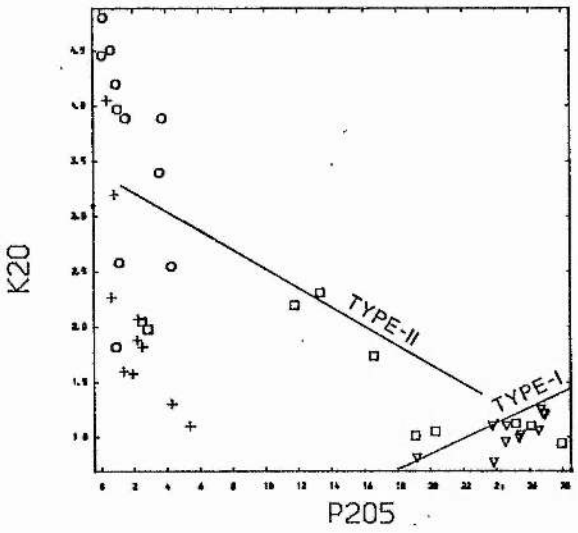

Fig 5.8

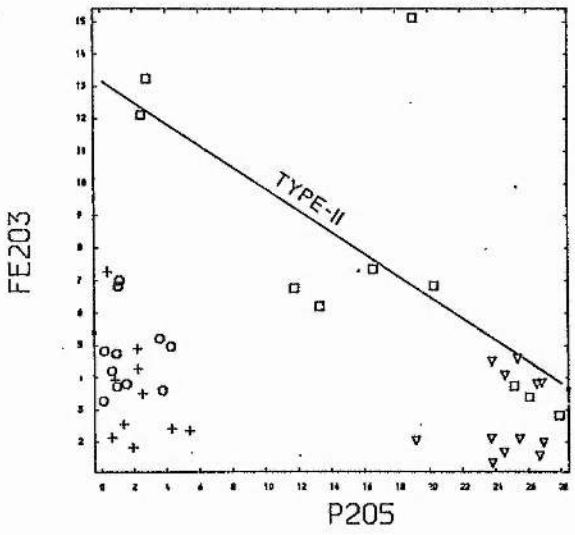

Fig 5.9

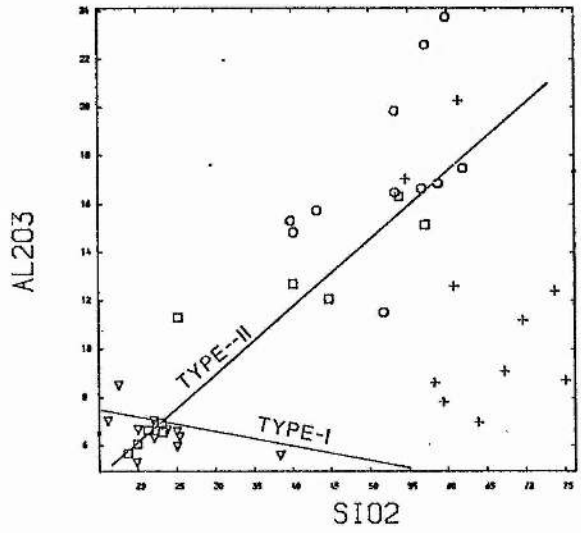

Fig 5.10

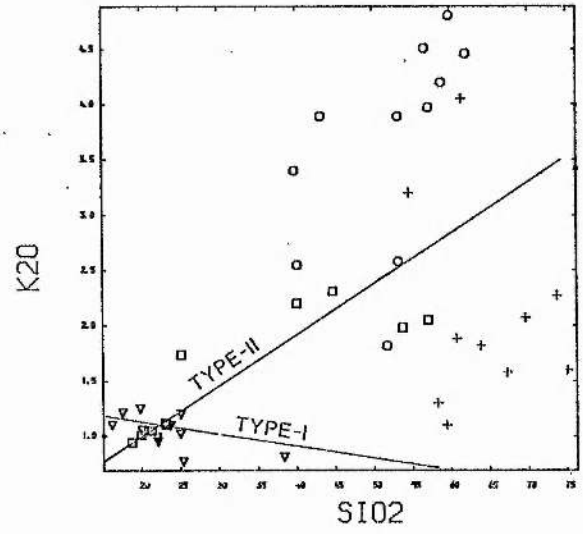

Fig 5.11

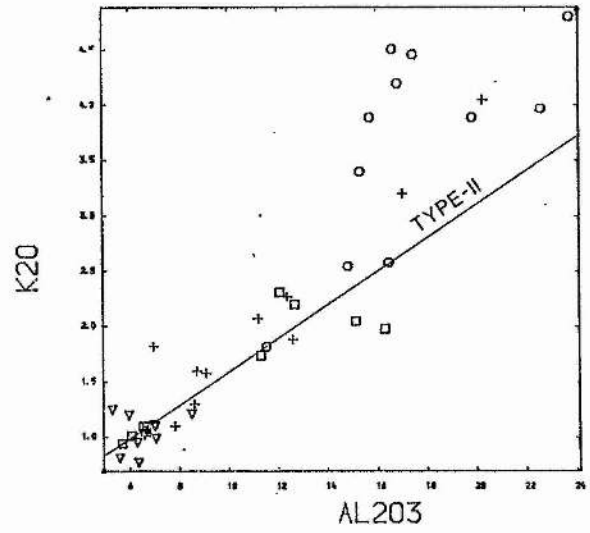

Fig 5.12

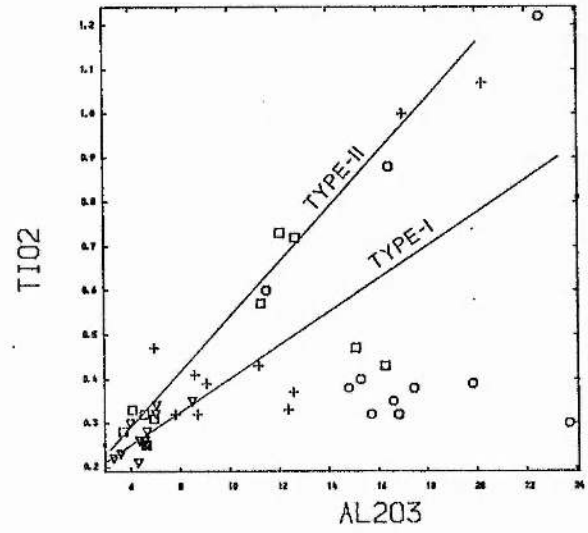

INDEX

▽ TYPE-I NODULES □ TYPE-II NODULES

\+ TYPE-I HOST ROCK o TYPE-II HOST ROCK

Fig 5.13

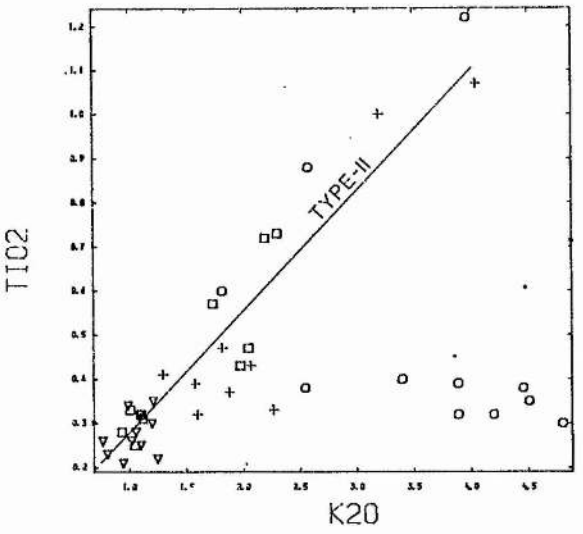

Fig 5.14

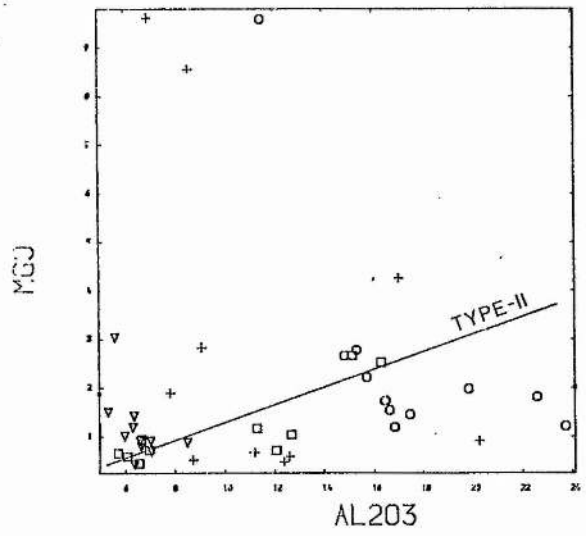

Fig 5.15

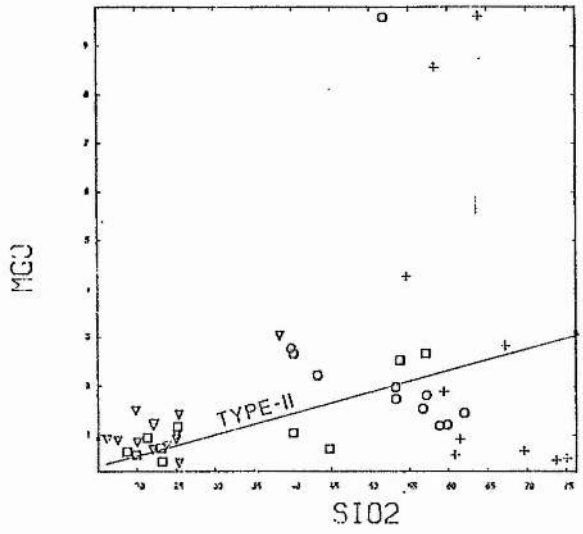

Fig 5.16

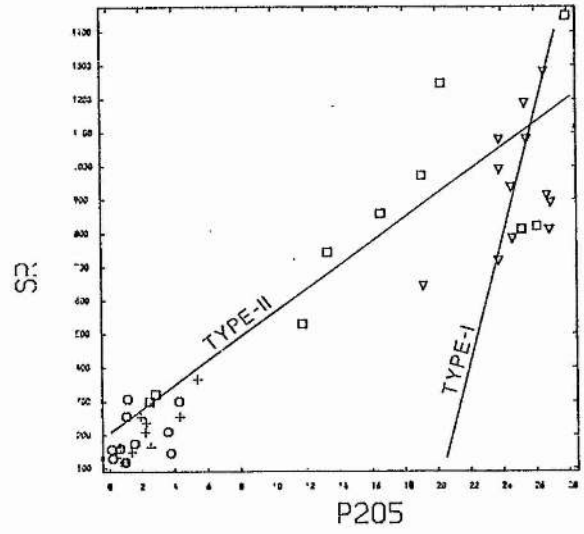

Fig 5.17

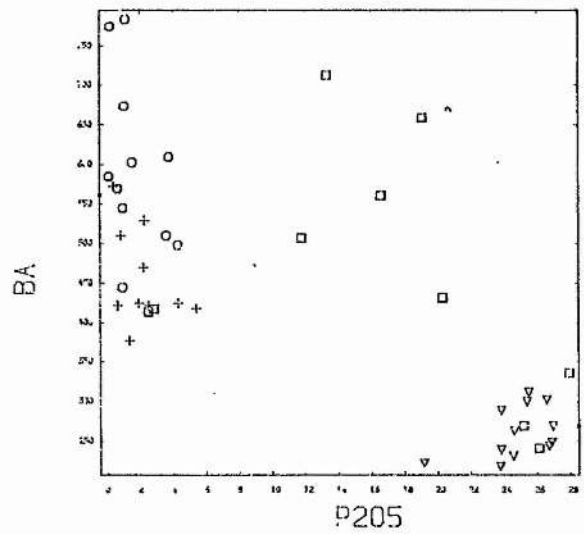

Fig 5.18

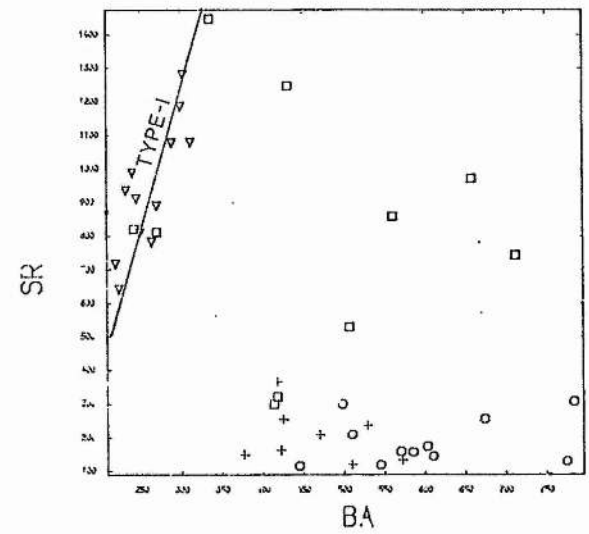

INDEX

▽ TYPE-I NODULES □ TYPE-II NODULES

\+ TYPE-I HOST ROCK o TYPE-II HOST ROCK

Fig 5.19

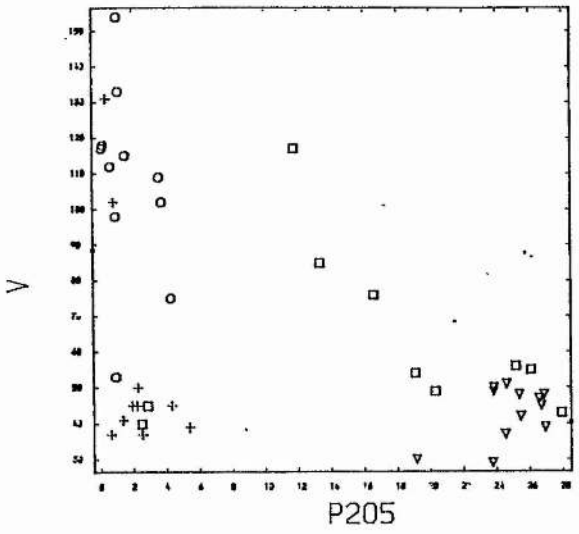

Fig 5.20

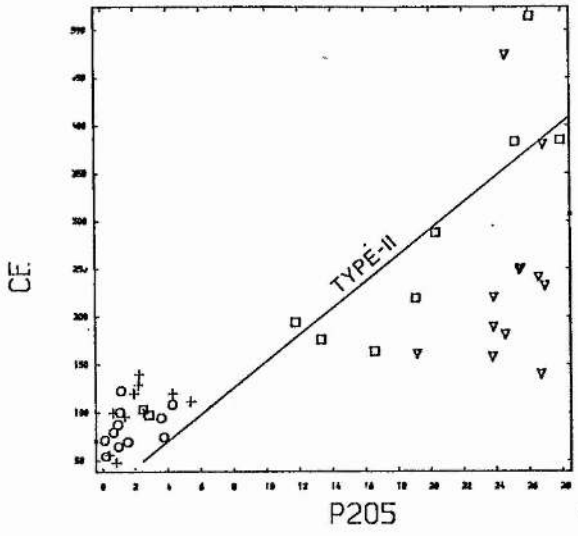

Fig 5.21

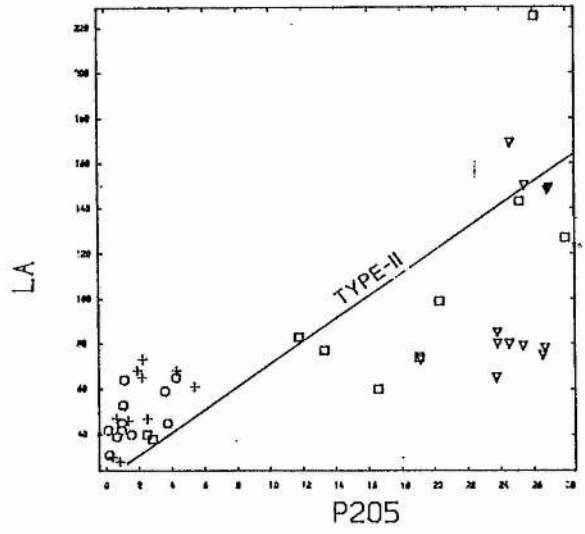

Fig 5.22

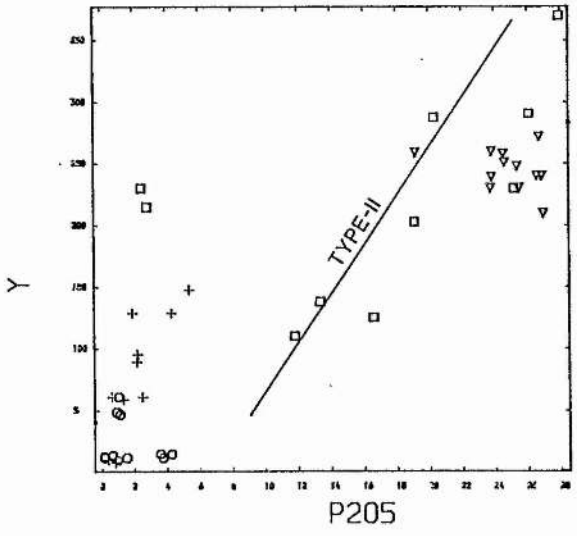

Fig 5.23

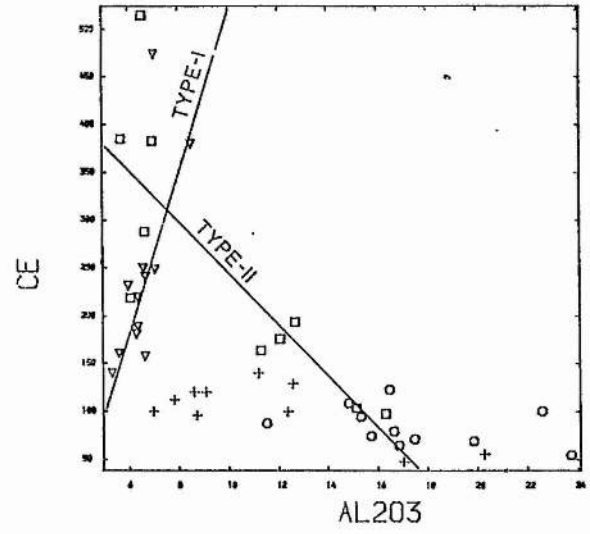

Fig 5.24

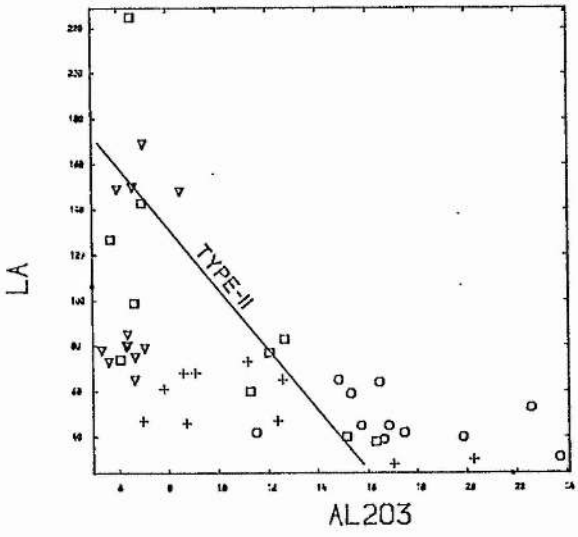

INDEX

▼ TYPE-I NODULES
□ TYPE-II NODULES
+ TYPE-I HOST ROCK
o TYPE-II HOST ROCK

Fig 5.25

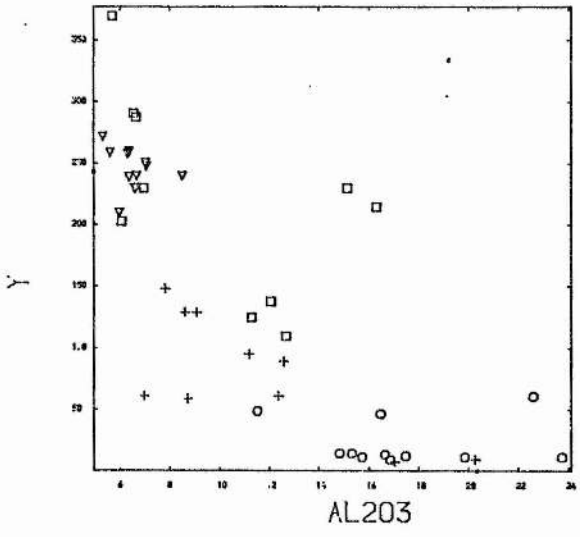

Fig 5.26

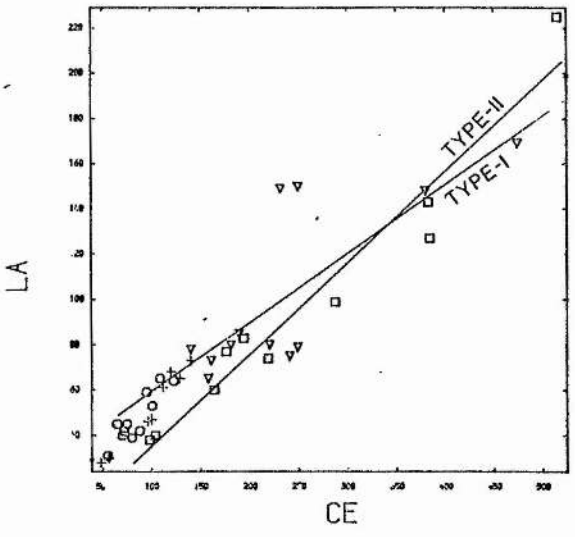

Fig 5.27

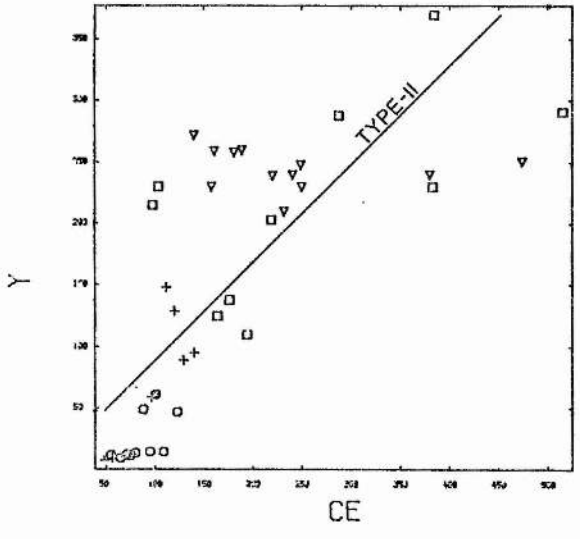

Fig 5.28

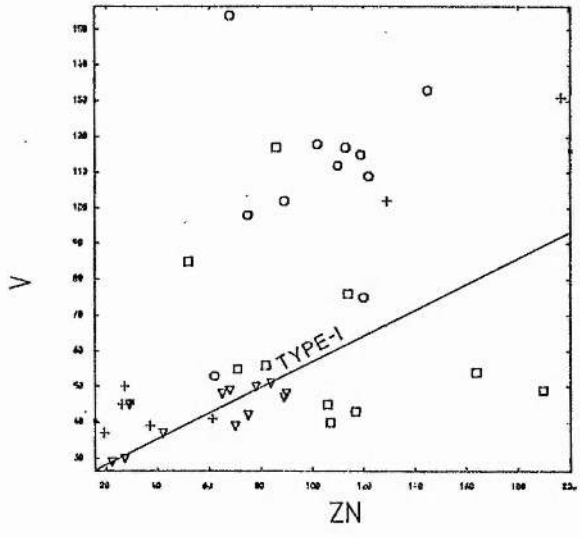

Fig 5.29

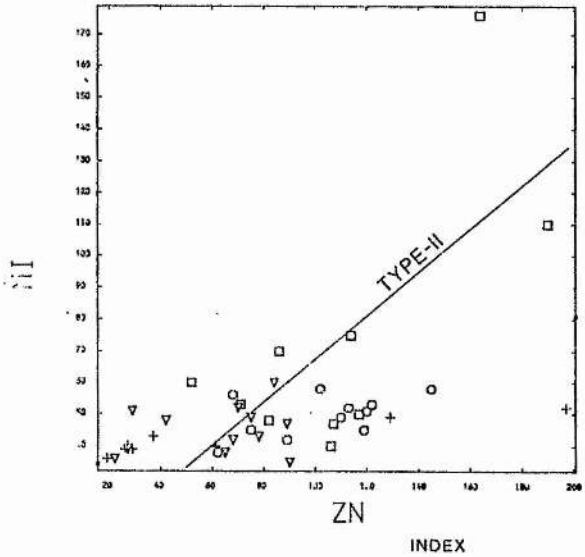

Fig 5.30

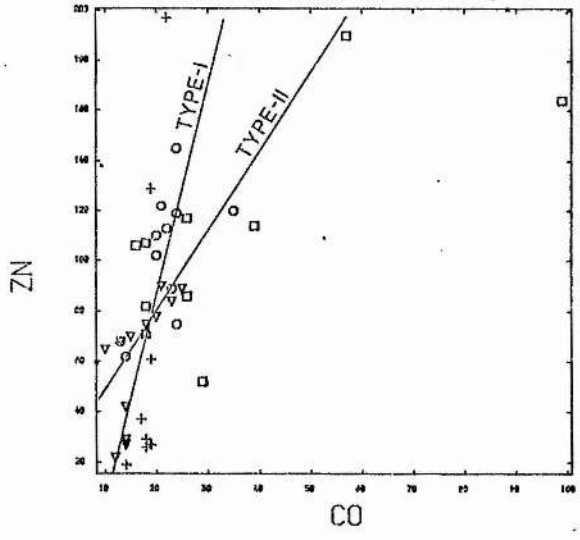

INDEX

▽ TYPE-I NODULES □ TYPE-II NODULES

\+ TYPE-I HOST ROCK ○ TYPE-Ii HOST ROCK

Fig 5.31

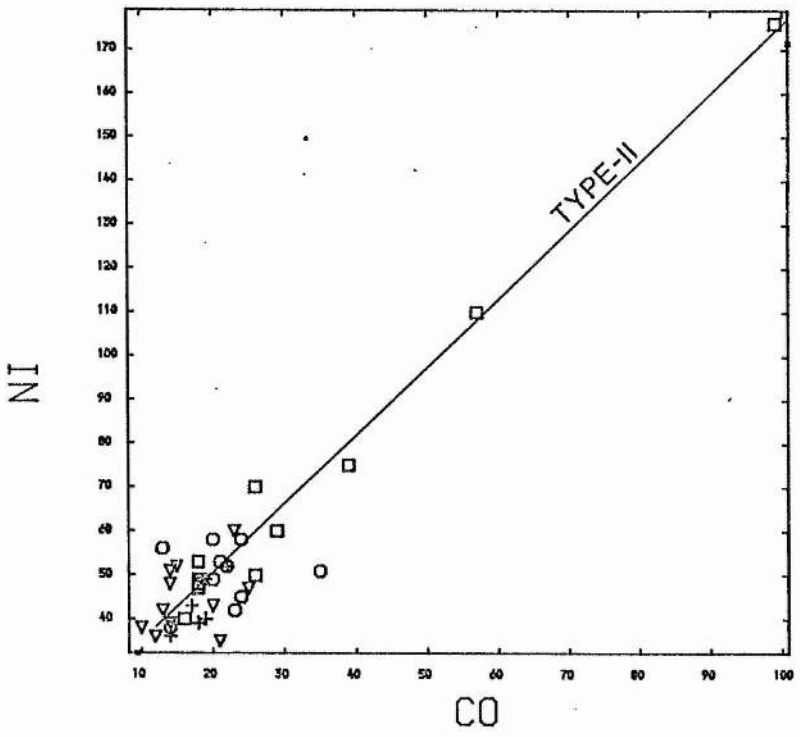

Fig 5.32

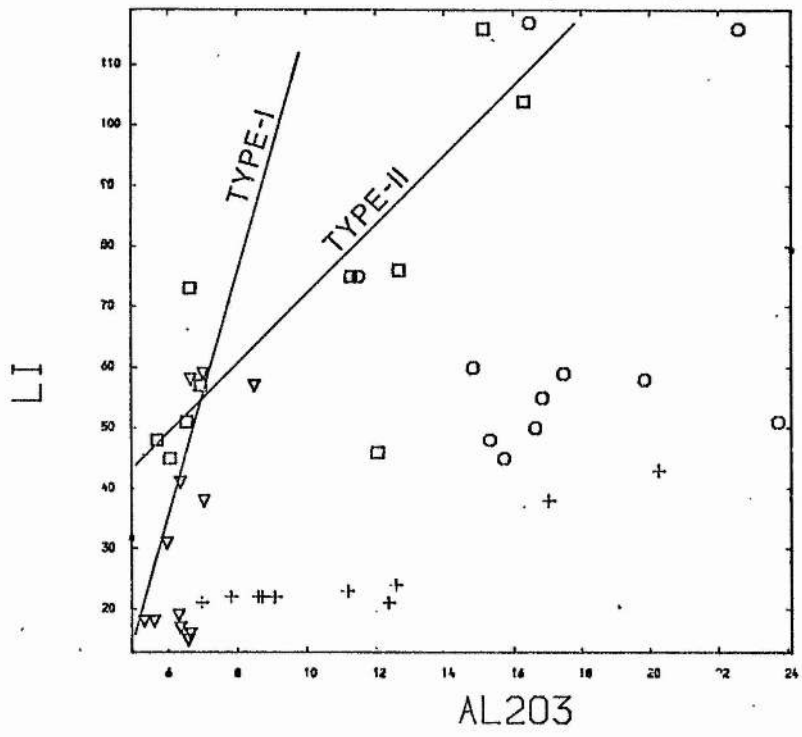

INDEX

▽ TYPE-I NODULES □ TYPE-II NODULES

\+ TYPE-I HOST ROCK o TYPE-II HOST ROCK

Table 5.1 Major (in weight percent) and trace (in ppm) element analyses of Type I nodular phosphorites and their host rocks

MAJOR ELEMENTS	Ph-5	Ph-6	Ph-10	Ph-12	Ph-15	Ph-31	Ph-57
	M A I N	B E D	O F	P H O S P H O R I T E			
SiO_2	38.38	25.42	22.11	23.81	19.87	17.58	16.19
TiO_2	0.23	0.26	0.21	0.25	0.22	0.35	0.32
Al_2O_3	5.60	6.36	6.31	6.65	5.31	8.51	7.02
Fe_2O_3	2.04	1.35	1.68	2.11	1.57	3.85	4.08
MgO	3.04	1.43	1.20	0.79	1.51	0.89	0.92
CaO	28.08	35.53	34.56	32.85	36.80	35.57	34.12
Na_2O	0.56	0.39	0.48	0.32	0.51	0.78	0.47
K_2O	0.81	0.77	0.95	1.10	1.25	1.21	1.10
P_2O_5	19.18	23.84	24.56	23.77	26.71	26.87	24.63
CO_2*	1.82	1.54	1.23	2.11	1.35	1.46	1.52
F•	1.526	1.97	2.02	1.99	2.09	1.97	1.82
C	nd	1.39	nd	nd	nd	nd	nd
LOI‡	nd	nd	2.10	2.10	nd	nd	1.69
Total	99.50	98.05	94.16	94.68	93.75	95.61	92.06
CaO/P_2O_5	1.464	1.490	1.407	1.381	1.377	1.32	1.38
F/P_2O_5	0.079	0.083	0.082	0.084	0.078	0.073	0.074
T R A C E	E L E M E N T S						
Ag	2	1	3	2	3	4	6
Ba	223	240	232	219	245	249	264
Ce	161	189	181	158	140	380	474
Co	14	13	14	12	14	10	23
Cr	162	101	160	120	158	240	346
Cy	22	20	20	30	25	27	30
La	73	85	80	65	78	148	169
Li	18	17	19	16	18	57	59
Mn	619	250	278	318	268	170	154
Mo	A	A	A	A	A	A	A
Nb	14	16	15	14	18	17	14
Ni	39	42	48	36	51	38	60
Sc	8	9	11	7	16	7	12
S	643	989	936	718	912	810	783
V	30	49	37	29	45	48	51
Y	259	260	258	230	272	240	251
Zn	27	68	42	22	29	65	84
Z	34	20	31	38	30	32	41

Note:- * By Peak Pair method of Gulbrandsen (1970)
• By Spectrophotometer
‡ Loss on Ignition at 1000 °C
nd = not determined

Table 5.1 Continued

MAJOR ELEMENTS	PG-1	PG-2	PG-3	Ph-48	Ph-49
	U P P E R B E D S				
SiO_2	25.08	25.11	22.05	25.42	20.04
TiO_2	0.26	0.30	0.34	0.26	0.28
Al_2O_3	6.59	5.97	7.05	6.36	6.67
Fe_2O_3	2.05	1.99	4.59	4.51	3.82
MgO	0.92	1.02	0.71	0.43	0.86
CaO	34.98	35.00	34.89	35.53	35.16
Na_2O	0.56	1.51	0.59	0.32	0.61
K_2O	1.02	1.20	0.99	0.77	1.06
P_2O_5	25.49	26.96	25.39	23.84	26.58
CO_2	0.645	1.65	1.235	0.58	0.65
F	1.97	2.11	2.31	2.28	4.77
C	nd	1.35	nd	nd	1.39
LOI			2.21		1.70
Total	99.25	100.41	100.70	97.44	100.61
CaO/P_2O_5	1.372	1.298	1.374	1.490	1.32
F/P_2O_5	0.077	0.078	0.090	0.096	0.179
T R A C E	E L E M E N T S				
Ag	1	1	3	3	6
Ba	312	270	300	289	303
Ce	250	232	249	220	241
Co	18	15	21	20	25
Cr	120	102	76	89	91
Cu	30	28	29	22	24
La	150	149	79	80	75
Li	15	31	38	41	58
Mn	250	310	271	269	232
Mo	A	A	A	A	A
Nb	14	16	13	15	15
Ni	49	52	35	43	47
Sc	10	12	9	7	11
S	1080	891	1187	1079	1281
V	42	39	48	50	47
Y	230	210	248	239	240
Zn	75	70	90	78	89
Z	69	25	22	34	19

Table 5.1 Continued

MAJOR ELEMENTS	Ph-5B	Ph-6B	Ph-10B	Ph-12B	Ph-57B	PG-1B	PG-2B
SiO_2	63.92	59.43	75.10	70.75	61.45	63.30	67.30
TiO_2	0.47	0.32	0.32	0.33	1.07	0.41	0.39
Al_2O_3	6.97	7.82	8.72	9.38	20.27	8.62	9.09
Fe_2O_3	3.51	2.35	2.55	2.14	7.27	2.41	2.83
MgO	9.62	6.90	3.56	4.48	0.92	0.56	0.83
CaO	7.00	11.92	2.75	6.11	0.25	10.15	6.47
Na_2O	0.77	1.50	0.67	1.73	0.72	0.81	1.00
K_2O	1.82	1.10	1.60	2.27	4.05	1.30	1.58
P_2O_5	2.53	5.41	1.36	0.64	0.40	4.31	1.94
CO_2	nd	nd	nd	nd	nd	nd	0.15
F	0.105	0.766	nd	nd	0.127	nd	nd
C	nd	nd	1.45	1.32	nd	nd	1.45
LOI	4.05	3.80	3.73	nd	2.87	3.89	4.55
Total	100.66	100.60	101.51	99.15	99.36	98.76	98.58
T R A C E E L E M E N T S							
Ag	1	1	64	1	1	3	1
Ba	422	418	377	422	572	425	450
Ce	100	112	96	101	56	120	98
Co	14	17	19	18	22	18	16
Cr	33	40	26	30	82	40	32
Cu	15	19	15	18	27	20	16
La	47	61	46	49	30	68	51
Li	21	22	22	20	43	22	20
Mn	400	464	852	774	155	305	312
Mo	17	15	16	16	22	22	16
Nb	10	8	10	9	29	10	9
Ni	36	43	40	35	52	39	36
Sc	10	9	10	8	17	10	9
Sr	164	365	149	155	133	254	165
V	37	39	41	42	131	45	36
Y	61	148	59	54	10	129	82
Zn	19	37	61	20	197	29	20
Zr	70	35	105	62	133	39	78

Table 5.1 Continued

MAJOR ELEMENTS	Ph-48B	Ph-49B	Ph-19 DOLOMITE	Ph-20	Ph-21 Black Shales
SiO_2	66.81	69.64	4.25	8.20	54.62
TiO_2	0.37	0.43	0.15	0.17	1.00
Al_2O_3	12.59	11.19	2.00	2.05	17.04
Fe_2O_3	4.89	4.28	0.93	2.27	3.94
MgO	0.59	0.67	19.00	20.32	4.26
CaO	3.77	4.71	28.70	27.49	6.19
Na_2O	1.05	1.07	0.30	0.05	0.90
K_2O	1.88	2.07	0.27	0.55	3.20
P_2O_5	2.19	2.25	0.21	0.11	0.83
CO_2	nd	nd	43.80	40.72	0.25
F	0.92	2.08	nd	nd	nd
C	nd	nd	nd	nd	2.00
LOI	nd	nd	nd	nd	nd
Total	95.06	98.39	99.61	101.93	94.23
T R A C E E L E M E N T S					
Ag	2	1	1	1	2
Ba	470	529	42	45	510
Ce	129	140	31	29	48
Co	18	19	12	14	19
Cr	35	39	32	47	65
Cu	15	24	14	13	32
La	65	73	4	1	28
Li	24	23	6	8	38
Mn	265	270	2456	2323	750
Mo	17	18	A	A	20
Nb	12	20	7	6	22
Ni	39	40	32	40	49
Sc	10	12	2	3	15
S	209	237	52	48	120
V	45	50	18	20	102
Y	89	95	9	11	8
Zn	26	27	18	15	129
Z	85	91	25	23	78

Table 5.2 Major (in weight percent) and trace (in ppm) element analyses of Type II nodular Phosphorites and their host rocks.

MAJOR ELEMENTS	B-1	B-2	Ph-28	Ph-35 Highly pyritized	Ph-36	Ph-37
SiO_2	23.22	40.11	23.08	19.92	44.76	18.73
TiO_2	0.32	0.72	0.31	0.33	0.73	0.28
Al_2O_3	6.55	12.69	6.96	6.07	12.07	5.69
Fe_2O_3	3.4	6.77	3.75	15.13	6.21	2.83
MgO	0.45	1.05	0.73	0.59	0.72	0.66
CaO	34.55	17.20	34.54	25.76	17.74	40.96
Na_2O	0.37	0.64	0.48	0.46	0.77	0.38
K_2O	1.10	2.20	1.12	1.01	2.31	0.94
P_2O_5	26.11	11.80	25.19	19.10	13.34	27.93
CO_2*	0.35	2.11	1.65	2.11	1.53	0.50
F•	2.31	1.23	2.09	1.31	1.12	1.92
C	1.68	nd	nd	nd	nd	1.35
LOI‡	2.45	nd	4.23	nd	nd	1.04
Total	101.89	96.52	102.04	91.79	100.3	103.24
CaO/P_2O_5	1.32	1.45	1.37	1.34	1.32	1.46
F/P_2O_5	0.088	0.104	0.083	0.070	0.099	0.070
T R A C E E L E M E N T S						
Ag	4	2	5	4	6	6
Ba	242	507	270	659	713	336
Ce	515	194	383	219	176	385
Co	18	26	18	99	29	26
Cr	48	83	103	40	43	90
Cu	21	29	25	66	36	20
La	225	83	143	74	77	127
Li	51	76	57	45	46	48
Mn	155	154	159	154	200	309
Mo	3	19	A	A	A	A
Nb	5	25	15	17	20	15
Ni	53	70	48	176	60	50
Sc	14	16	12	11	17	13
Sr	821	530	812	972	744	1448
V	55	117	56	54	85	43
Y	293	110	230	203	138	370
Zn	71	86	82	164	52	117
Zr	43	90	27	38	88	24

Note:- * By Peak Pair method of Gulbrandsen (1970)
• By Spectrophotometer
‡ Loss on Ignition at 1000 °C
nd = not determined

Table 5.2 Continued

MAJOR ELEMENTS	Ph-39	Ph-42	Ph-30	Ph-29
SiO_2	25.21	21.34	57.16	53.85
TiO_2	0.57	0.25	0.47	0.43
Al_2O_3	11.30	6.64	15.15	16.32
Fe_2O_3	7.36	6.85	12.12	13.26
MgO	1.17	0.96	2.67	2.53
CaO	23.22	29.88	3.70	4.65
Na_2O	0.81	0.47	0.72	0.65
K_2O	1.74	1.05	2.05	1.98
P_2O_5	16.61	20.32	2.50	2.85
CO_2	1.35	1.68	1.64	nd
F	1.34	4.46	0.37	0.25
C	nd	nd	nd	nd
LOI	nd	3.30	nd	nd
Total	92.68	93.16	96.54	96.77
CaO/P_2O_5	1.397	1.47	-	-
F/P_2O_5	0.081	0.219	-	-
T R A C E	E L E M E N T S			
Ag	5	4	2	1
Ba	561	432	414	418
Ce	164	288	104	98
Co	39	57	18	16
Cr	152	40	162	132
Cu	34	41	21	20
La	60	99	40	38
Li	75	73	116	104
Mn	154	1161	310	285
Mo	A	A	24	23
Nb	19	15	88	86
Ni	75	110	47	40
Sc	13	14	9	11
Sr	858	1248	300	321
V	76	49	40	45
Y	125	288	230	215
Zn	114	190	107	106
Zr	23	44	355	315

Table 5.2 Cont

MAJOR ELEMENTS	B-1B	B-2B	Ph-28B	Ph-35B	Ph-36B
SiO_2	62.07	59.90	58.86	40.19	43.28
TiO_2	0.38	0.30	0.32	0.38	0.32
Al_2O_3	17.47	23.73	16.85	14.84	15.74
Fe_2O_3	3.28	4.83	3.73	4.96	3.61
MgO	1.46	1.22	1.20	2.66	2.22
CaO	0.15	0.49	1.38	14.91	6.30
Na_2O	1.27	1.35	1.31	1.20	1.37
K_2O	4.46	4.80	4.20	2.55	3.89
P_2O_5	0.130	0.19	0.98	4.29	3.75
CO_2	nd	nd	nd	nd	nd
F	0.135	0.14	nd	nd	nd
C	nd	nd	nd	nd	nd
LOI	5.09	nd	6.55	7.76	7.89
Total	95.89	96.95	95.38	93.74	87.48
T R A C E	E L E M E N T S				
Ag	1	3	2	3	1
Ba	585	775	545	498	610
Ce	72	55	65	109	75
Co	22	20	24	35	23
Cr	73	60	70	89	65
Cu	31	22	25	40	35
La	42	31	45	65	45
Li	59	51	55	60	45
Mn	130	155	120	670	177
Mo	22	21	20	10	12
Nb	26	24	25	22	22
Ni	52	58	45	51	42
Sc	16	17	15	21	16
S	158	130	120	300	145
V	117	118	98	75	102
Y	13	12	10	15	12
Zn	113	102	75	120	89
Z	95	88	80	67	75

Table 5.2 Continued

MAJOR ELEMENTS	Ph-37B	Ph-39B	Ph-42B	Ph-25 Shales	Ph-26 Dolomitic Shales
SiO_2	56.75	53.29	39.87	53.30	51.81
TiO_2	0.35	0.39	0.40	0.88	0.60
Al_2O_3	16.65	19.85	15.32	16.48	11.52
Fe_2O_3	4.21	3.81	5.21	7.00	4.75
MgO	1.55	1.98	2.78	1.74	9.6
CaO	2.55	3.59	12.81	2.39	12.42
Na_2O	1.11	1.24	1.33	1.00	0.95
K_2O	4.51	3.89	3.40	2.58	1.82
P_2O_5	0.65	1.55	3.59	1.13	0.94
CO_2	nd	nd	nd	nd	nd
F	nd	nd	nd	nd	nd
C	nd	nd	nd	nd	nd
LOI	6.35	5.97	6.78	7.85	5.32
Total	94.68	95.56	91.49	94.35	99.73
T R A C E E L E M E N T S					
Ag	3	1	2	2	2
Ba	570	603	510	784	445
Ce	80	70	95	123	88
Co	20	24	21	24	14
Cr	78	65	72	91	64
Cu	22	30	24	21	16
La	39	40	59	64	42
Li	50	58	48	117	75
Mn	155	160	781	310	1549
Mo	25	22	9	26	17
Nb	24	25	27	31	34
Ni	49	45	53	58	38
Sc	17	16	17	20	10
S	160	175	210	308	116
V	112	115	109	133	53
Y	14	12	15	47	49
Zn	110	119	122	145	62
Z	92	85	98	117	101

Table 5.3 The average major element composition (in weight percent) for the Welsh phosphorites together with the average composition for the phosphorites from other deposits in the World.

Element	PERU-CHILE[1]	NAMIBIA[2]	AGULHAS[3] BANK	CALIFORNIA[4]	PHOSPHORIA[5]	WELSH[6] TYPE-I	WELSH[7] TYPE-II
SiO_2	22.3	1.4	12.84	nd	11.9	23.33	27.00
Al_2O_3	5.15	0.37	1.85	1.47	1.7	6.04	8.49
Fe_2O_3	2.85	0,88	8.24	nd	1.1	1.75	6.53
MgO	1.07	0.60	1.35	nd	0.3	1.59	0.79
CaO	33.93	51.25	37.29	44.91	44.0	33.56	27.98
Na_2O	0.85	nd	0.67	nd	0.6	0.45	0.54
K_2O	1.30	0.13	1.29	nd	0.5	0.97	1.43
P_2O_5	22.61	32.10	16.18	28.15	30.5	23.60	20.04
S	0.16	nd	0.40	nd	0.7	nd	nd
F	2.22	2.39	2.10	3.08	3.1	1.33	1.12
CaO/P_2O_5	1.50	1.596	2.30	1.59	1.44	1.48	1.396
F/P_2O_5	0.098	0.074	0.130	0.109	0.100	0.089	0.101

Note: nd = Not determined

1 Burnett (1977)

2 Price and Calvert (1978)

3 Parker (1971)

4 Dietz and others (1942)

5 Gulbrandsen (1966)

6), 7) This Study

Table 5.4A Varimax-rotated principal component factor matrix

Elements	TYPE-I NODULES FACTORS				Elements	TYPE-II NODULES FACTORS			
	1	2	3	4		1	2	3	4
SiO_2	-0.723	-0.315		-0.444	SiO_2	0.956			
TiO_2		0.659	0.528		TiO_2	0.926			-0.303
Al_2O_3		0.933			Al_2O_3	0.907		0.354	
Fe_2O_3		0.325	0.930		Fe_2O_3		0.973		
MgO	-0.687				MgO			0.844	
CaO	0.991				CaO	-0.893	-0.361		
Na_2O					Na_2O	0.780		0.515	
K_2O	0.339			0.908	K_2O	0.958			
P_2O_5	0.825				P_2O_5	-0.886	-0.345		
F	0.445				F	-0.372			0.907
Eigen Values	4.80	1.93	1.71	1.03	Eigen Values	12.98	6.54	3.05	2.49
% Variance	43.7	17.6	15.6	9.4	% Variance	46.4	23.4	10.9	8.9
Cumulative Variance	43.7	61.3	76.9	86.3	Cumulative Variance	46.4	69.8	80.7	89.6

Table 5.4B Varimax-rotated principal component factor matrix

Elements	TYPE-I (Host Rock)				Elements	TYPE-II (Host Rock)			
	F A C T O R S					F A C T O R S			
	1	2	3	4		1	2	3	4
SiO_2		-0.926			SiO_2	-0.967			
TiO_2	0.935				TiO_2		0.980		
Al_2O_3	0.932				Al_2O_3	-0.330		0.467	0.805
Fe_2O_3	0.762				Fe_2O_3		0.880		
MgO				0.914	MgO			-0.967	
CaO	-0.604	0.580		0.308	CaO	0.772		-0.529	
Na_2O			0.954		Na_2O		-0.913		
K_2O	0.972				K_2O	-0.392	-0.359	0.608	0.412
P_2O_5	-0.687	0.478			P_2O_5	0.983			
Eigen values	5.09	2.16	0.97	0.45	Eigen values	3.98	2.93	1.35	0.29
% Variance	56.6	24.0	10.9	5.0	% Variance	44.3	32.7	15.1	3.3
Cumulative Variance	56.6	80.5	91.5	96.5	Cumulative Variance	44.3	77.0	92.1	95.4

Table 5.5

	SiO_2	TiO_2	Al_2O_3	Fe_2O_3	MgO	CaO	Na_2O	K_2O	P_2O_5	CO_2	F	Ag	Ba	Ce	Co	Cr	Cu	La	Li	Mn	Nb	Ni	Sc	Sr	V	Y	Zn	Zr
SiO_2	1.000	0.921	0.874		0.830	-0.801		0.951	-0.789														0.874		0.854			0.915
TiO_2		1.000	0.974			-0.869	0.852	0.989	-0.864																0.920	-0.852		
Al_2O_3		0.772	1.000		0.840	-0.863	0.899	0.978	-0.870																0.923	-0.871		
Fe_2O_3		0.696		1.000											0.930		0.969					0.942						
MgO					1.000														0.890									
CaO	-0.767				-0.734	1.000	-0.810	-0.866	0.967				-0.799	0.835										0.707	0.841	0.925		
Na_2O							1.000	0.852	-0.814					-0.814												-0.859		
K_2O								1.000	-0.865														0.797		0.911	-0.831		0.796
P_2O_5	-0.802				-0.686	0.864		0.716	1.000				-0.802	0.878				0.800			-0.800			0.625	-0.848	0.894		
CO_2										1.000											0.811							
F									0.403		1.000									0.914								
Ag												1.000																
Ba										-0.806			1.000	-0.894				-0.830										
Ce		0.760	0.705											1.000				0.962			-0.875					0.780		
Co													0.746		1.000		0.959					0.989					0.761	
Cr														0.744		1.000												
Cu								0.627									1.000					0.959						
La														0.782				1.000			-0.864							
Li		0.734		0.629								0.828		0.783					1.000									
Mn	0.934				0.818	-0.851			-0.788											1.000								
Nb																					1.000							
Ni																0.573						1.000						
Sc																						0.742	1.000				0.740	0.859
Sr						0.589			0.588	-0.817	0.708		0.816			-0.558								1.000	-0.797	-0.820		
V						0.695														-0.726					1.000	-0.837		
Y															0.712											1.000		
Zn		0.678		0.672									0.833						0.659					0.697	0.771		1.000	
Zr																												1.000

TYPE - I

TYPE - II

Pearson correlation matrix of major and trace elements in Type I and Type II nodular phosphorites. Only significant values are shown

Table 5.6

TYPE - I

	SiO_2	TiO_2	Al_2O_3	Fe_2O_3	MgO	CaO	Na_2O	K_2O	P_2O_5	Ag	Ba	Ce	Co	Cr	Cu	La	Li	Mn	Mo	Nb	Ni	Sc	Sr	V	Y	Zn	Zr
SiO_2	1.000					-0.856			-0.960																		
TiO_2		1.000		0.834			-0.895												0.838								
Al_2O_3		0.900	1.000					0.700			0.719						0.949			0.767					0.932		0.930
Fe_2O_3		0.804	0.842	1.000			-0.699					0.763												0.758			
MgO					1.000			-0.735									0.841						0.729		0.783		0.719
CaO						1.000		-0.733	0.751									0.933				-0.697		-0.716			
Na_2O_3							1.000											0.790	-0.800					-0.693			
K_2O		0.935	0.963	0.856		-0.716		1.000				-0.700					-0.849			-0.791					-0.929		-0.817
P_2O_5			-0.707			0.909		-0.767	1.000									-0.817									
Ag										1.000									-0.859								
Ba		0.836	0.874	0.896				0.862			1.000										0.698			0.750			
Ce		-0.873	-0.759					-0.820				1.000		0.840		0.898							0.878				
Co		0.690	0.707	0.717							0.717		1.000		0.854												
Cr		0.962	0.906	0.816				0.906			0.866	-0.792	0.750	1.000		0.784						0.709	0.891				
Cu		0.848	0.734					0.713			0.788		0.689	0.836	1.000					-0.793							-0.707
La		-0.800	-0.719					-0.804				0.973		-0.690		1.000							0.868				
Li		0.981	0.943	0.842				0.943			-0.848	-0.857	0.770	0.974	0.818	-0.786	1.000			0.755					0.902		0.808
Mn																		1.000						-0.715			
Mo																			1.000								
Nb		0.920	0.921	0.895				0.939			0.955	-0.685	0.789	0.916	0.823		0.931			1.000					0.896		0.726
Ni		0.915	0.858	0.765				0.829			0.789	-0.800	0.834	0.945	0.840	-0.699	0.957			0.874	1.000	0.735		0.710			
Sc		0.972	0.939	0.858				0.965			0.902	-0.803	0.766	0.953	0.839	-0.744	0.975			0.981	0.910	1.000	0.808				
Sr						0.768		-0.720	0.889			0.688				0.771							1.000				
V		0.978	0.938	0.848				0.945			-0.862	-0.834	0.790	0.981	0.821	-0.759	0.995			0.946	0.952	0.983		1.000			
Y		0.804				0.741		-0.881	0.845			0.849				0.907	-0.783			-0.745		-0.808	0.927	-0.765	1.000		0.282
Zn		0.944	0.900	0.818				0.915			0.776	-0.876	0.802	0.948	0.750	-0.807	0.978			0.900	0.958	0.950		0.980	-0.770	1.000	
Zr			0.749	0.859		-0.819		0.800	-0.719		0.698						0.722			0.802		0.773	-0.718	0.729	-0.809	0.763	1.000

TYPE - II

Pearson correlation matrix of major and trace elements in Type I and Type II host rocks for phosphorites.
Only significant values are shown.

Table 5.7 Average Microprobe analyses of fine grain apatite within polished thin sections of phosphorite nodules from Welsh phosphorite occurrences.

AREA	Type - I. Nodule						Type - II Nodule				Oolite
Sample No	Ph-5	Ph-6	Ph-22	PG-1	PG-2	Ph-49	Ph34	Ph-35	Ph-36	Ph-37	Ph-30
SiO_2	9.98	7.60	nd	6.869	nd	14.48	nd	10.26	12.44	nd	4.40
$Al_{2*3}O$	nd	nd	nd	nd	nd	2.67	nd	3.29	3.55	nd	1.93
FeO	0.079	0.616	0.303	0.166	0.128	0.47	2.31	1.32	0.375	2.68	0.969
MgO	0.12	nd	0.039	nd	nd	0.251	0.08	0.459	0.149	0.78	0.151
CaO	49.25	48.00	50.86	51.69	49.10	43.76	49.55	43.08	44.18	41.39	47.39
Na_2O	0.06	0.05	0.068	0.035	nd	A	0.24	0.181	0.233	0.141	0.281
K_2O	nd	nd	0.387	nd	nd	0.46	nd	0.685	0.704	nd	0.434
P_2O_5	36.31	35.62	37.88	38.22	36.78	33.40	36.80	32.20	33.32	31.18	36.44
F	3.14	2.99	3.19	3.11	3.01	2.97	3.39	2.895	2.99	3.09	3.11
SO_4	nd	nd	0.965	nd	nd	0.15	nd	0.097	0.013	nd	0.92
Sr	nd	0.1453	0.1190	0.0948	0.1636	A	nd	0.277	nd	0.3420	nd
Mn	0.0045	0.0047	0.0050	0.0043	nd	0.0029	A	0.025	0.015	0.022	nd
Total	99.54	96.73	93.81	102.18	nd	98.61	nd	94.657	97.83	nd	96.02
CaO/P_2O_5	1.356	1.347	1.34	1.317	1.334	1.310	1.346	1.337	1.325	1.327	1.300
F/P_2O_5	0.086	0.084	0.084	0.081	0.081	0.089	0.092	0.090	0.090	0.099	0.085

Note:- 1) All Analyses in weight percent
2) * Total iron reported as FeO
3) nd = not determined
4) A = Absent

Table 5.8 Average Microprobe analyses of shell fragments within polished thin sections of phosphorite rocks from Welsh phosphorite occurrences.

AREA	Type - I Nodular Phosphorite			Type - II Nodular Phosphorite					Oolitic Phosphorite
Sample No	PG-3	Ph-22	Ph-49	Ph-34	Ph-35	Ph-36	Ph-37	B-1	Ph-30
No of spots Analysed	8	9	9	7	9	8	10	9	9
SiO_2	nd	A	nd	A	A	nd	A	nd	A
Al_2O_3	nd	nd	nd	A	nd	nd	A	nd	A
FeO*	0.025	A	0.452	1.137	1.168	0.163	3.884	2.31	3.458
MgO	0.010	0.012	0.063	0.085	0.053	0.018	0.025	0.148	0.080
CaO	54.20	54.164	48.08	50.19	52.199	53.851	47.01	46.33	48.116
Na_2O	0.021	0.042	0.066	0.219	0.185	0.122	0.152	0.343	0.362
K_2O	nd	nd	nd	nd	nd	nd	nd	nd	nd
P_2O_5	40.79	40.171	35.89	36.15	38.130	38.49	35.684	34.19	38.979
F	3.705	3.387	3.039	3.579	3.596	3.710	3.265	3.41	3.257
SO_4	nd	nd	nd	nd	nd	nd	nd	nd	nd
Sr	A	0.088	0.119	A	A	nd	0.212	A	0.1387
Mn	nd	0.005	0.009	0.0017	0.0038	0.008	0.005	nd	0.016
Total	98.74	97.86	nd	91.36	95.33	96.36	90.237	nd	94.40
CaO/P_2O_5	1.33	1.35	1.34	1.39	1.37	1.40	1.317	1.36	1.234
F/P_2O_5	0.090	0.084	0.085	0.099	0.094	0.096	0.091	0.099	0.083

Note: 1) All Analysed in weight percent
2) * Total iron reported as FeO
3) nd = notdetermined
4) A = Absent

Table 5.9 Average Microprobe analyses of secondary phosphorite minerals within polished thin sections of phosporite nodules from Welsh phosphorite occurrences.

AREA	SECONDARY PHOSPHORITE MINERALS (STRENGITE?)					WAVELLITE			
Sample No	Ph-22 (Red)	Ph-22 (Orange)	Ph-33 (Red)	Ph-33 (Orange)	Ph-36 (Red)	Ph-35	Ph-36	Ph-39	Ph-40
SiO_2	0.983	2.15	0.809	0.458	1.41	0.079	0.104	0.197	-
Al_2O_3	8.276	14.45	1.44	9.43	3.91	34.267	28.23	23.86	28.73
FeO*	57.89	37.55	55.40	37.32	51.94	1.71	3.90	1.874	1.747
MgO	0.014	0.298	nd	0.298	nd	0.033	0.097	0.001	0.008
CaO	0.262	1.55	nd	1.35	nd	0.147	0.147	0.035	0.042
Na_2O	nd	A	A	A	A	A	A	0.014	0.007
K_2O	A	0.48	A	A	nd	0.045	0.055	0.005	0.024
P_2O_5	11.92	19.93	15.23	24.07	13.44	37.82	28.27	25.46	35.86
F	0.30	0.45	0.169	0.44	0.23	0.638	0.475	0.115	0.21
SO_4	1.36	0.84	5.04	0.868	6.88	4.40	3.197	2.71	3.67
Sr	A	0.132	A	nd	nd	nd	nd	nd	nd
Mn	0.011	A	nd	A	0.015	A	A	A	A

Note:- 1) All Analyses in weight percent
2) * Total iron reported as FeO
3) nd = not determined
4) A = Absent

Table 5.10 Concentration of trace elements in Type-I and Type-II nodular phosphorites relative to marine shale and sea-water (All values in ppm except sea water which is in ppb)

Elements	Sea Water	Average Shale	TYPE-I	Enrichment Factor*	Depletion Factor	TYPE-II	Enrichment Factor	Depletion Factor
Ag	0.07	0.07	3	Ag 43		5	Ag 71	
Ba	425	580	262		Ba 2	465		
Ce	0.0012	91	240	Ce 3		291	Ce 3	
Co	0.39	19	17			39		Co 2
Cr	0.2	90	147	Cr 2		75		
Cu	0.9	45	26		Cu 2	34		
La	0.0034	40	103	La 3		111	La 3	
Li	170	66	32		Li 2	59		
Mn	0.4	850	282		Mn 3	183		Mn 5
Mo	10	2.6	A		Mo 3	11	Mo 4	
Nb	nd	nd	15			16		
Ni	6.6	68	45		Ni 2	80		
Sc	0.004	13	10			15		
Sr	8100	300	942	Sr 3		929	Sr 3	
V	1.9	130	43		V 3	67		V 2
Y	0.013	26	245	Y 9		194	Y 7	
Zn	5	95	62			110		
Zr	nd	160	33		Zr 5	47		Zr 3

Note:- Sea Water abundance - Turekian (1969)
Average Shale - Turekian and Wedepohl (1961)
* An element is considered "enriched" if its abundance is at least 2x that of shales, and "depleted" if its abundance is ½ or less. Abundances between these limits are classed as "normal" following Tooms et al, (1969).

Table 5.11A Varimax-rotated principal component factor matrix

Elements	TYPE-I NODULES FACTORS				Elements	TYPE-II NODULES FACTORS			
	1	2	3	4		1	2	3	4
Ag			0.936		Ag	0.980			
Ba	0.934				Ba		0.481	0.738	-0.357
Ce		0.815	0.471		Ce	0.49		-0.832	
Co	0.684		0.459		Co		0.961		
Cr	-0.413	0.688	0.451		Cr	-0.359	-0.411	0.308	
Cu					Cu		0.931		
La		0.859			La	0.392		-0.865	
Li	0.346	0.418	0.779		Li	-0.795			
Mn	-0.361				Mn				
Mo					Mo	-0.934			
Nb					Nb	-0.792		0.423	0.342
Ni		0.345		0.878	Ni		0.985		
Sc				0.925	Sc	0.408			-0.750
Sr	0.911				Sr	0.796			
V	0.672	0.369			V				-0.972
Y					Y			-0.450	0.704
Zn	0.839	0.398			Zn		0.673		
Zr					Zr	-0.828		0.352	0.310
Eigen Values	5.91	3.10	2.58	1.79	Eigen Values	7.32	4.28	3.30	1.18
% Variance	34.8	18.3	15.2	10.6	% Variance	40.7	23.8	18.4	6.6
Cumulative Variance	34.8	53.1	68.3	78.8	Cumulative Variance	40.7	64.5	82.9	89.5

Tab le 5.11B Varimax-rotated principal components factor matrix

Elements	TYPE-I (Host Rock) FACTORS				Elements	TYPE-II (Host Rock) FACTORS			
	1	2	3	4		1	2	3	4
Ag			0.953		Ag				0.989
Ba	0.769	0.345	-0.336	0.346	Ba			0.772	
Ce	-0.600	-0.600			Ce	0.933			
Co	0.854		0.311	0.300	Co	0.401	-0.879		
Cr	0.837	0.326			Cr	0.926			
Cu	0.868				Cu		-0.922		
La	-0.476	-0.728			La	0.933			
Li	0.833	0.464			Li	0.608	0.655		
Mn			0.305	-0.860	Mn			-0.851	
Mo	0.420				Mo			0.327	
Nb	0.812	0.470			Nb		0.919		
Ni	0.940				Ni	0.330		0.718	0.352
Sc	0.806	0.516			Sc	0.656	-0.374	0.572	
Sr		-0.962			Sr	0.931			
V	0.832	0.448			V			0.930	
Y	-0.436	-0.893			Y	0.437	0.840		
Zn	0.824	0.448			Zn	0.386	-0.405		
Zr	0.523	0.686			Zr		0.830	0.394	
Eigen Values	12.12	2.75	1.12	0.88	Eigen Values	6.37	4.85	3.38	1.24
% Variance	67.4	15.3	6.2	4.9	% Variance	35.4	27.0	18.8	6.9
Cumulative Variance	67.4	82.7	88.9	93.8	Cumulative Variance	35.4	62.4	81.2	88.1

CHAPTER VI

STABLE ISOTOPE GEOCHEMISTRY

6.1 Introduction

In this chapter, stable carbon and oxygen isotopic compositions of structural carbonate present in francolite, are examined for the following reasons -

1) To establish possible differences in the origin of the 2 types of nodular phosphorites.
2) to compare these nodular phosphories with the well known authigenically precipitated phosphorites and phosphatized limestones of the World.
3) to calculate palaeotemperatures.

Many studies have been made on stable isotopes in phosphorites (Kolodny and Kaplan, 1970; Al-Bassam 1980; McArthur et al 1980; Benmore, et al 1983, Benmore, 1984). Kolodny and Kaplan (1970) have analysed the carbon and oxygen isotopes within francolite CO_3^{2-} and in coexisting calcite. They found that both C and O in francolite are enriched in the respective light isotopes relative to calcite. Another important point of the 3 publications (Kolondy and Kaplan, 1970; Al-Bassam, 1980 and McArthur et al, 1980) was that the samples which have $\delta^{18}O$ depletion are also depleated in $\delta^{13}C$. As the authors point out this may represent the effect of terrestrial ground water. Other data also indicate that a Schizohaline environment is favourable for phosphate deposition (Kolodny, 1980). The structural carbonate in francolite was also used for ^{14}C dating purposes

(Haynes, 1968).

6.1.1 Carbon Isotopes

Carbon has 2 stable isotopes: ^{12}C and ^{13}C which have average terrestrial abundances of 98.9% and 1.1% respectively (Hoefs, 1980). The carbon isotope composition of naturally occurring substances varies quite considerably from $\delta^{13}C_{PDB}$ values of over +20 °/oo to -90 °/oo (Hoefs, 1980).

Sea water bicarbonate has a fairly uniform carbon isotope composition with a $\delta^{13}C_{PDB}$ value of approximately 0 °/oo (Craig 1953). It is enriched by around 8 °/oo with respect to atmospheric carbon dioxide at 20 °C (Hoefs, 1980). A much greater variation in $\delta^{13}C$ values in carbon reservoirs is produced by kinetic fractionation which operates during photosynthesis. The fractionation by marine phytoplanktons is related to oceanic surface temperature: $\delta^{13}C_{PDB}$ values vary from around -30 °/oo at 2 °C to about -20 °/oo at 15 °C and over (Sackett et al, 1973).

It is the carbon reservoir of sea water and organic matter which ultimately provide the source of carbon which is incorporated into the structure of sedimentary francolite. Seawater bicarbonate is the predominant source of carbon in marine limestones which have been phosphatized in seawater whilst porewater bicarbonate containing organically derived carbon is an important supply for structural carbonate in authigenic francolite forming in anoxic sediments. Since the two carbon reservoirs have distinctly different isotopic compositions, it should be possible to distinguish between the 2 types of francolite by the $\delta^{13}C$ values of their structural carbonate (McArthur et al, 1980).

In contrast to the narrow seawater range in $\delta^{13}C$ values, porewater bicarbonate can vary considerably in carbon isotope composition (Presley and Kaplan, 1968; Nissenbaum et al, 1972; Claypool and Presley, 1973). Isotopically light carbon is released to the porewater from organic matter as it oxidized by aerobic bacteria in oxic sediments; by dysaerobic bacteria in suboxic sediments, or by sulphate reducing bacteria in anoxic sediments. Since the original seawater bicarbonate concentration in solution as porewater is small (seawater (HCO_3) = 142 mg/1 (Culkin, 1965)), it is isotopicaly sensitive to such inputs. Thus one would expect the carbon isotope composition of porewater bicarbonate to range from marine values (0 °/oo) to that of organic matter (-25 °/oo) (Irwin et al, 1977).

$\delta^{13}C$ values between 0 °/oo and -12 °/oo are not only characteristic of carbonates formed from sulphate reducing porewater during marine burial diagenesis but also of freshwater carbonates as defined by Keith and Weber (1964). Indeed Al Bassam (1980) suggested that the light carbon isotopic composition (-5.8 to -9.6 °/oo) of marine phosphorites in Iraq is indicative of a low salinity formational environment. It is unlikely that francolite can form at the expense of limestone in freshwater environments in view of the fact that the bicarbonate: phosphate ratio of riverwater is approximately double that of normal seawaters which itself favours the precipitation of $CaCO_3$ to that of francolite (Gulbrandsen, 1969).

In light of the above, carbon isotope composition of the structural carbonate in unaltered francolite discriminates between phosphatized limestones and authigenic phosophorites, the

former preserving the $\delta^{13}C$ value of its precursor and latter containing a stubstantial proportion of lighter organic carbon generated by bacterial degradation of organic matter, (McArthur 1980 and Benmore et al, 1983).

6.1.2 Oxygen Isotopes

Oxygen has 3 stable isotopes whose average natural abundances are: ^{16}O = 99.8%, ^{17}O = 0.04%, ^{18}O = 0.2%. Only $^{18}O/^{16}O$ ratios are normally measured because of their greater abundance and mass differences (Hoefs, 1980). At equilibrium the partition of ^{18}O relative to ^{16}O between 2 oxygen-bearing phases varies with temperature and is effectively independent of pressure. For any particular pair of phases it is therefore possible to use the isotopic fractionation as a thermometer. The calcite-water isotopic temperature scale was determined by McCrea (1950), developed by Epstein et al (1951, 1953) and modified by Craig (1965). The relationship between fractionation and temperature is given by

$$t = 16.9 - 4.3 (\delta c - \delta w) + 0.13 (\delta c - \delta w)^2$$

where t = temperature

$\delta c - \delta w$ = difference between $\delta^{18}O$ PDB calcite (c) and $\delta^{18}O$ PDB water (w)

(PDB = International carbonate standard - a Cretaceous Belemnite, Belemnitella americana from the Pedee Formation, S Carolina, USA).

This equation is used to obtain palaeotemperatures of ancient seas using the $\delta^{18}O$ value of marine calcite. The derivation of such palaeotemperature relies on 3 basic assumptions:

1) The estimated $\delta^{18}O$ value used for ancient sea water is correct.

2) Isotopic fractionation has occurred in equilibrium

3) The calcite has not isotopically re-equilibrated during diagenetic or weathering processes.

Present-day sea water has a narrow range of oxygen isotopic composition ($\delta^{18}O$ PDB $\sim$ 0 °/oo). Palaeotemperatures calculated in this study assume $\delta^{18}O$ PDB value of -1.2 °/oo for ancient sea water (Shackleton and Kennet, 1975). Since the fractionation factor between francolite and water is unknown it has been assumed to be the same as for the calcite water (Kolodny and Kaplan, 1970). If this assumption is seriously incorrect the $\delta^{18}O$ values for francolite are in systematic error. This can be tested to a certain extent, however by comparing the determined palaeotemperatures of modern francolites with the temperatures of the waters in which they formed. In McArthur et al, (1980) it was shown that formational temperatures calculated for authigenic Namibian francolite fall within the temperature range of upwelled water off the Namibian coast although that range (6-16 °C) is rather large.

In spite of the aforementioned uncertainties it is useful to calculate palaeotemperatures for francolite because very unrealistic values are likely to be indicative of formation from water of an oxygen isotope composition different from sea water. A significant decrease in $\delta^{18}O$ in porewaters which are isolated from their original sea water source can be caused by diagenetic reactions (Lawrence et al, 1976; Irwin et al, 1977) or mixing with isotopically light groundwater of meteoric origin (Hudson,

1978) and so francolite precipitated in this environment will probably have an excessively high palaeotemperature. It could alternatively result from $\delta^{18}O$ exchange with isotopically light meteoric water during weathering.

6.1.3 Post Depositional Alteration

A trend of lighter oxygen isotope composition with increasing age has been observed in limestones and dolomites (Keith and Weber, 1964; Veizer and Hoefs, 1976), in cherts (Knauth and Epstein, 1976) and in PO_4 in francolites (Longinelli and Nutti, 1968). This could reflect a cooling and/or an evolution in the oxygen isotopic composition of sea water to heavier values over geological time. Alternatively, the trend could be interpreted as evidence for post depositional equilibration with isotopically light meteoric waters or with waters at high temperatures, since increasing age gives greater chance of such interaction occurring. It is now the general consensus that post depositional processes are responsible for the observed variation. This assumption has been confirmed by systematic decreases in $\delta^{18}O$ seen in diagenetic transformation from metastable to stable carbonate assemblages in Quaternary to Tertiary profiles (eg Gross, 1964). Veizer (1977) suggested that the majority of alteration occurs during this period (n x 10^7 yrs) before carbonate mineralogy has been stabilized, and that further post depositional modification is of a much smaller magnitude. He also showed that relatively stable calcite is probably less susceptible to such isotopic alteration than metastable aragonite and Mg-calcite.

Since francolite is metasable with respect to fluorapatite (see Chapter IV) by analogy one might expect considerable $\delta^{18}O$ fractionation to occur in its structural carbonate as its mineralogy is stabilized. In contrast to calcite, however, the mineralogy of the francolite-fluorapatite series is not usually stabilized by n x 10^7 years. It is still metastable as a lithified onshore deposit. It follows that equilibration with meteoric water during weathering is probably far more important for francolite than calcite. If this is so, the chance of altering the carbon isotope composition of structural carbonate in francolites is probably greater than for limestone. This is because diagenetic stabilization usually proceeds in a partially closed microsystem and since the amounts of bicarbonate in solution is small there is little scope for appreciable modification of $\delta^{13}C$ values of precursor carbonate. Consequently the $\delta^{13}C$ values of carbonates do not appear to show any secular variation (Keith and Weber, 1964; Veizer and Hoefs, 1976). In the case of francolite, further stabilization during weathering would increase the water-rock ratio and thus the capacity for equilibration with meteoric water.

In view of the variable isotopic composition of meteoric waters the precise effect of continuous equilibration is hard to determine. The carbon in the bicarbonate of groundwater is derived from carbon dioxide from the soil zone and from dissolved carbonate. Meteoric water has a wide global variation in $\delta^{18}O$ composition ($\sim$0 to -55 °/oo, Craig, 1961) but a narrow range in any particular locality. In general post depositional equilibration with meteoric water result in a systematic lowering

of $\delta^{13}C$, and $\delta^{18}O$. The possibility of post depositional alteration must always be borne in mind when interpreting isotopic compositions even in samples which appear unaltered petrographically. Fortunately post depositional transformation of francolite to fluorapatite also results in changes in bulk geochemical composition so it is possible to identify the severely altered samples.

6.1.4 Carbon dioxide extraction

Carbon dioxide was extracted from phosphorite samples by reacting with excess 100% orthophosphoric acid in vacuo (McCrea, 1950) at a constant temperature of 25 $^{o}C \pm 0.05$.

The francolite samples were treated in exactly the same way as calcite samples but a greater amount of sample was needed due to the lower structural carbonate content. For calcite samples (standards) approximately 10 mgs was used and for francolite samples between 300-400 mgs. The reaction was considered complete when evolution of gas from the sample has ceased. Few francolite samples took upto 72 hours of reaction. Type I nodules present in the Main bed of phosphorite contain accessory dolomite. This could not be removed as the Silverman's citrate extractin technique does not completely dissolve dolomite (Smith and Lehr, 1966). Samples containing free dolomite are marked with an asterisk in the Table 6.1.

6.1.5 Accuracy and Precision of isotopic measurement

Isotopic measurement of the extracted carbon dioxide was made on mass spectrometer at the Scottish Universities Research

and Reactor Centre (SURRC), East Kilbride, Glasgow. Samples were run with respect to laboratory secondary standards Tct-2 which is calibrated for both $\delta^{13}C$ and $\delta^{18}O$ with respect to international carbonate standard PDB from direct measurments against primary international carbonate standards NBS-19 and NBS-20 (Solenhofen Limestone). Technical details are given in Appendix -6.1.

6.1.6 Isotope notation

The abundance of stable isotopes in a substance is measured by the ratio of the trace isotope to the predominant isotope. This ratio (R) is measured with respect to a standard and expressed as a del value (δ) in per mil ($^{o}/oo$) where

$$\delta(^{o}/oo) = \left(\frac{R\ Sample}{R\ Standard} - 1\right) \times 1000$$

A positive value indicates enrichment in the heavy isotope relative to the standard and a negative value indicates depletion.

6.2 RESULTS AND DISCUSSION

The isotopic composition of structural carbonate in Type I and Type II nodular phosphorites is plotted as a $\delta^{13}C$ versus $\delta^{18}O$ scatter plot (fig 6.1). Other deposits plotted in this figure for comparision purposes are phosphatized carbonates of Agulhas Bank and Peru-Chile, authigenically precipitated phosphorite of the Namibian Shelf (SW Africa) and weathered authigenic phosphorites of Georgina Basin and Amadeus Basin of Australia (McArthur et al, 1980; Benmore, 1984). The well known phosphatized carbonates of Agulhas

Bank have $\delta^{13}C$ values of about -1 °/oo which is within the range of 'normal' marine limestones (Veiser & Hoefs, 1976). The Namibian authigenic (concretionary) francolites have $\delta^{13}C$ values of -7 °/oo to -8 °/oo, values characteristic of sulphate reduction processes (McArthur et al, 1980). The Welsh phosphorites show similar marked depletion in $\delta^{13}C$ values in contrast to unweathered replacement phosphorites of Agulhas Bank and Catham Rise suggesting authigenic origin for Welsh phosphorites. All the samples from Welsh deposit lie in between the fields of primary marine carbonate and sulphate reduction carbonate. This reflects the input of isotopically light organically derived carbon to the formational environment. It is also clear from this plot that $\delta^{18}O$ values are much lighter in Welsh phosphorites than the Namibian phosphorites. If this represents equilibration with isotopically light meteoric water any sample which were originally replacement phosphorites will have presumably become lighter in both $\delta^{13}C$ and $\delta^{18}O$. Weathered samples of authigenic origin may have only become lighter in $\delta^{18}O$, however, because authigenic francolite already possess light $\delta^{13}C$ signatures.

It is also evident that Type II nodular phosphorite contain lighter carbon and oxygen isotopic composition than Type I (Table - 6.1). This difference is probably because of the presence of some free carbonate (which could not be removed as Silverman's citrate extraction technique does not completely dissolve dolomite) in Type I nodules. Georgina Basin (Cambrian) and Amadeus Basin (Ordovician) phosphorites of Australia are very much more similar to Welsh phosphorites in their C and O isotope

values. These deposits were plotted because they are comparable in age with Welsh phosphorites and hence the effects of ageing should be very similar. In view of the fact that francolite is metastable with respect to fluorapatite over geological time (McClellan, 1980) apatite samples from these deposits are likely to have undergone considerable structural crystallographic changes since their formation in comparison to Namibian phosphorites which is forming at present. Indeed Welsh phosphorites have low substituent levels, in some cases characterizing fluorapatite rather than francolite, hence this isotopic interpretation is tentative.

6.2.1 Post-Depositional Alteration Trends

As discussed in Chapter V, Sr is a very mobile element and during weathering it becomes progressively depleted in the apatite lattice. As different samples contain different values of Sr it was thought to be useful to plot Sr/P_2O_5 ratio against their C and O isotopic values. The Sr/P_2O_5 versus $\delta^{13}C$ strongly suggests that samples most depleted in Sr (greatly altered) are enriched in ligher C-isotopes (fig 6.2). This reflects progressive degree of equilibration with meteoric water which is isotopically lighter than the original formational waters. $\delta^{13}C$ modifications are surprising because of the low concentration of exchangeable bicarbonate in meteoric waters (McArthur et al, 1980). The relationship of Sr/P_2O_5 versus $\delta^{18}O$ is more difficult to interpret (fig 6.3). Benmore (1984) has shown that different weathered phosphorite deposits of the world, initially having reasonably similar Sr/P_2O_5 ratios, form discrete groups when

plotted against $\delta^{18}O$ because of the interplay of five variables: 1) initial francolite $\delta^{18}O$ compostion, 2) degree of equilibration with meteoric water, 3) temperature of local meteoric water during equilibration, 4) isotopic composition of local meteoric water, 5) strontium content of local metemoric water. Since these variables are likely to have different values for each deposit it is not surprising that samples suites from each deposit plot as discrete groups. Most of these deposits including Welsh phosphorites show ligher $\delta^{18}O$ compostions with lower Sr/P_2O_5 ratios. This must reflect progressive degrees of equilibration with meteoric water which is isotopically ligher and/or at a higher temperature than the original forwational waters.

6.2.2 Palaeotemperatures

Palaeotemperatures calculated using Craig's (1965) equation for Welsh phosphorites give temperature range of 65-80 ^{o}C. These high temperatures are likely to be due to a significant decrease in $\delta^{18}O$ in porewaters which are isolated from their original sea water sources because of diagenetic reactions (Lawrence et al, 1976; Irwin et al, 1977) or mixing with isotopically light groundwater of meteoric origin (Hudson, 1978). It is difficult to prove these possibilities in view of the fact that these phosphorites are much older and have undergone some weathering. It is probably during the leaching with meteoric water that $\delta^{18}O$ isotopic exchange has occurred. Sr/P_2O_5 versus $\delta^{18}O$ plotting (Fig 6.3) also reflect a progressive degree of equilibration with meteoric water which is istopically lighter and/or at a higher

temperature than the original formational waters.

Another strong possibility of isotopic exchange is during burial of these rocks. The petrographic and SEM studies showed the transformation of smectite into illite suggesting that these sediments were buried to a maximum depth of approximately 2500 m. The observed lighter isotopic values are probably the result of changes occurred during this burial. The temperatures due to geothermal gradient at this depth are compatible with calculated values.

Legend

Figure 6.1 Scatter plot of the structural carbon and oxygen isotopic composition of Welsh phosphorites along with other deposits of the world.

Figure 6.2 Sr/P_2O_5 ratio versus $\delta^{13}C$ for Welsh phosphorites.

Figure 6.3 Sr/P_2O_5 ratio versus $\delta^{18}O$ for Welsh phosphorites.

- □ Agulhas Bank, S.W. Africa
- ● Peru-Chile Phosphorites
- ○ Namibian Shelf (Authigenic Concretionary phosphorites)
- △ Georgina Basin, Australia
- ▲ Amadeus Basin, Australia
- ■ Welsh Phosphorites

Fig.6.1

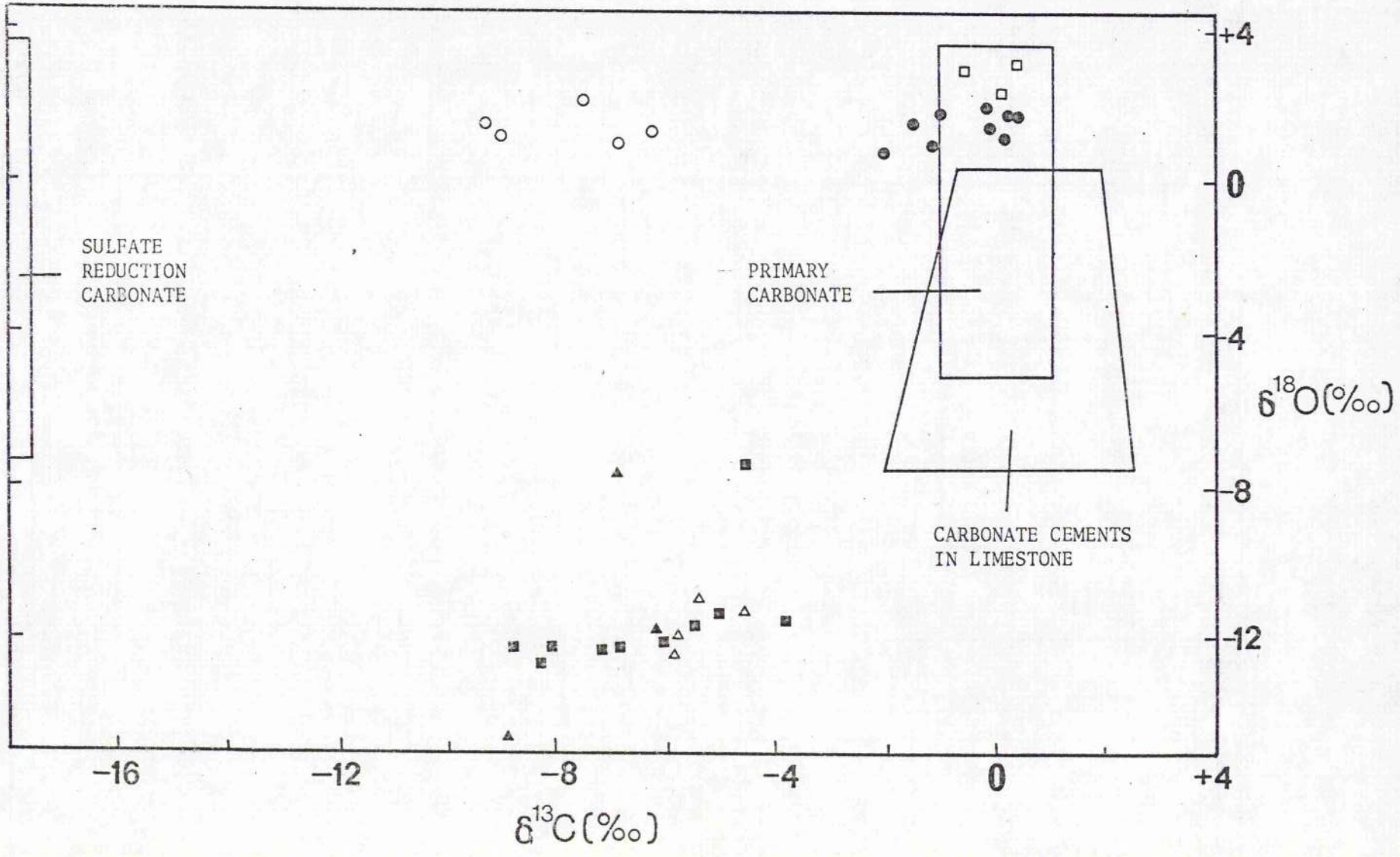
SULFATE
REDUCTION
CARBONATE
PRIMARY
CARBONATE
CARBONATE CEMENTS
IN LIMESTONE
+4
0
-4
-8
-12
δ18O(‰)
-16
-12
-8
-4
0
+4
δ13C(‰)

Fig.6.2

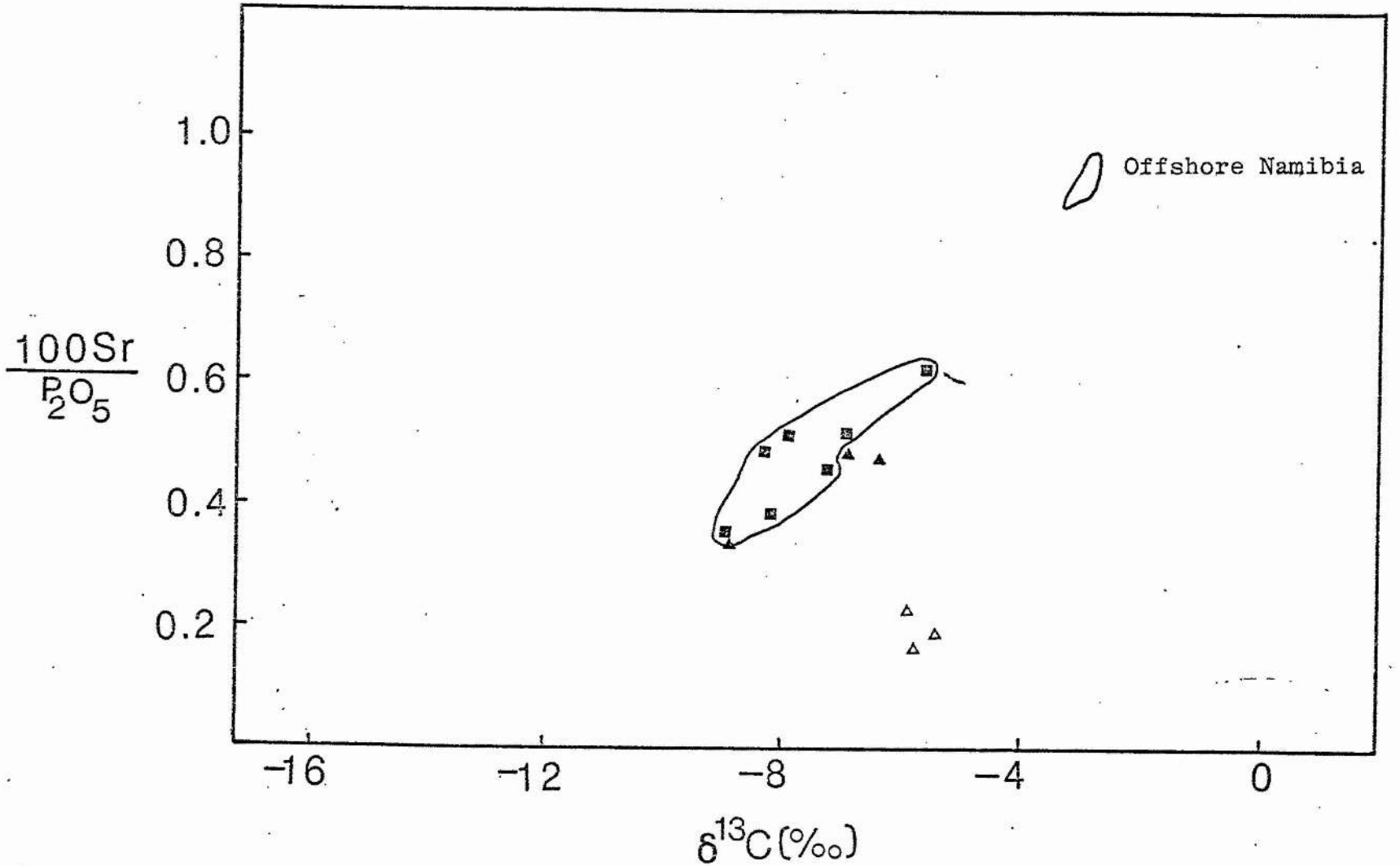

Fig.6.3

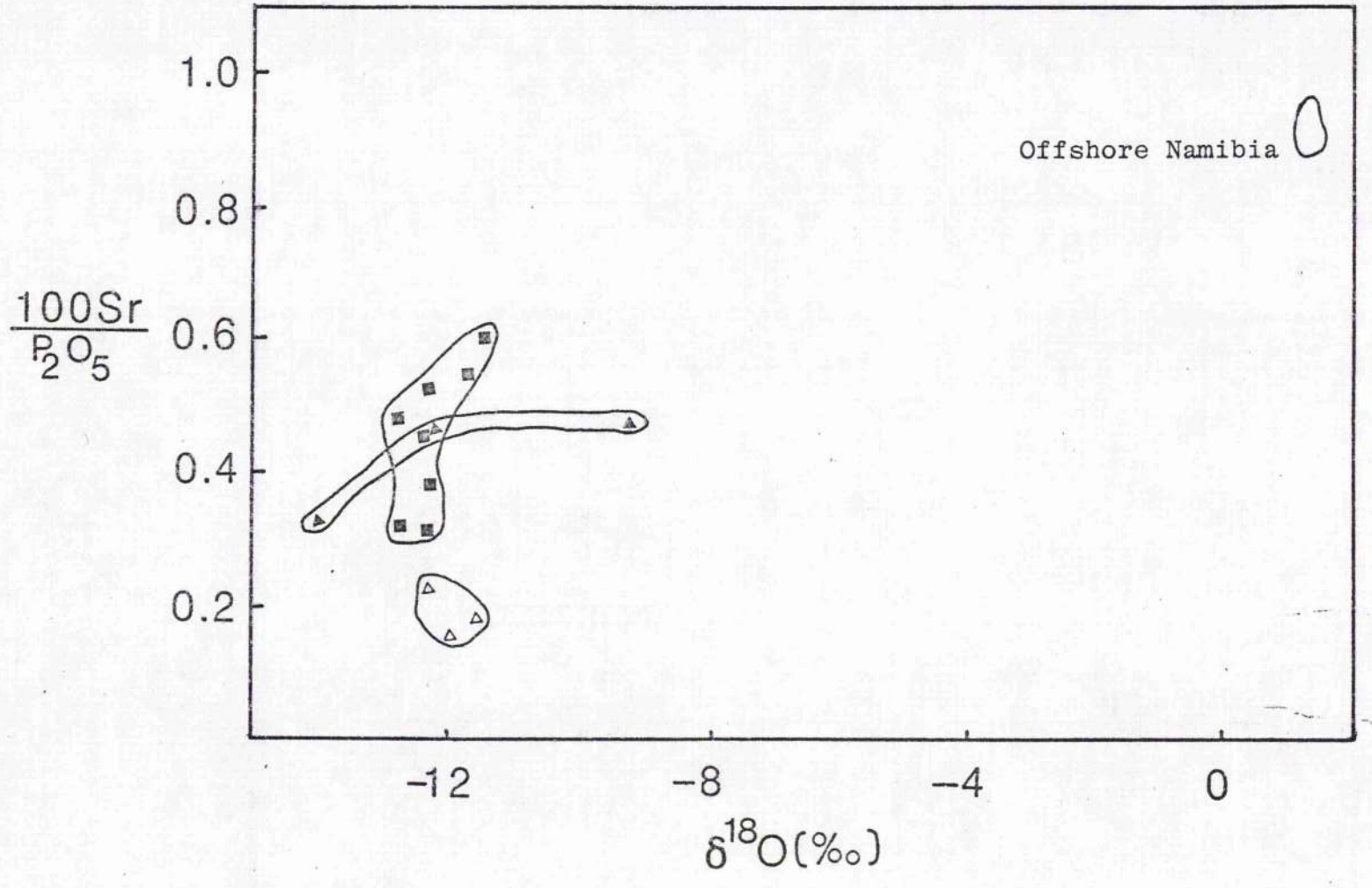

Table 6.1 Isotopic composition of francolite -CO_2 in Welsh phosphorite

Sample No	Reaction Time (hours)	$\delta^{13}C$ °/oo (PDB)	$\delta^{18}O$ °/oo (PDB)
Ph-5*	24	-4.58	-7.04
Ph-6*	24	-5.69	-7.89
Ph-31	48	-6.89	-11.76
Ph-57	48	-5.08	-11.22
PG-1*	24	-3.87	-11.30
	48	-3.80	-11.03
Ph-49	24	-8.3	-12.79
	48	-7.24	-12.34
	72	-8.18	-12.33
Ph-28	24	-6.09	-12.66
Ph-35	24	-7.88	3.89
Ph-37	24	-6.30	-12.29
	48	-6.76	-12.31
	72	-6.89	-12.27
Ph-42	24	-5.47	-11.53

Note: * Sample containing some carbonates

CHAPTER VII

SUMMARY AND CONCLUSIONS

Caradocian phosphorite occurrences of Powys county, N Wales, present in the lower portion of the Nod Glas Formation are examined mineralogically, petrographically and geochemically. Former underground workings at Berwyn, Cwmgwnen and Pwll-y-Wrack are now inaccessible but exposures of phosphorite bed are still largely accessible at Pen-y-Garnedd and Nant Achlas areas. The phosphorite bed about 40-45 cms thick, contains closely packed nodules which show large variation in their size. Nodules are the main form of phosphorite although phosphatized organic fragments and oolitic grains are also present. On the basis of petrographic characteristics, nodules are grouped into two types. Type I nodules contain abundant organic material whereas Type II nodules are rich in clay minerals. The most striking sedimentological features of Type I nodular phosphorites is the scarcity of detrital sediments. Fine quartz sand is the most abundant detrital sediment and it is present only in minor amounts.

The biogenic material present in Type I nodules is largely sponge spicules of Hexactinellida and Demospongiae and rarely molluscs, crustaceans and Hystrichosphaeridium tests around Pen-y-Garnedd area. A few miles south-east of Pen-y-Garnedd around Gwern-y-Brain area, nodules are however, rich in ostracod valves and rarely contain spicules and other organic remains. The almost absence of organic remains in the Type II nodular phosphorite indicate that the physico-chemical conditions were different during the formation of the 2 types of nodular

phosphorites. Though the presence of algae/fungi and bacteria like bodies suggests existence of some organic life even in the western part of the basin.

Scanning electron microscopic examination of phosphorites revealed that apatite occurs as well developed crystals cementing mainly organic fragments in Type I and clay minerals in Type II nodules. Apatite crystals are found to be variable in size; generally they are of the order of 4-5 μm along the c-axis although they can be as big as 8-10 μm. Often, apatite needles are seen to be present in intercrystalline spaces. Apatite appears to favour certain types of surfaces for nucleation. For instance, siliceous sponge spicules and various other organic fragments present appear to be favourable sites for the authigenic apatite growth. The availability of suitable nucleation sites for apatite growth has not been much discussed in the literature. Stumm and Morgan (1970) showed experimentally that calcite acts as a well matched surface for the nucleation of apatite. Presumably, the apatite forms epitaxially on the calcite. Stumm and Leckie (1970) demonstrated that the precipitation of apatite is greatly accelerated by calcite, the surface of which acts as a nucleation agent for crystallization. Berner (1974) verified this by showing that pore waters from high carbonate (>95 percent $CaCO_3$) fine grained sediments are in equilibrium with apatite at all depths. In the absence of calcite, the PO_4^{3-} content of a solution may reach values greatly in excess of equilibrium. However, from the SEM studies reported here, it appears that other surfaces may serve as nucleation sites in the absence of carbonate. Siliceous skeletal material

and various detrital clay minerals appear to be favoured sites for the initiation of authigenic apatite growth when calcite is not present. SEM studies also showed the presence of organic forms which could be bacterial; fungal and/or algal bodies. The presence of these organic forms may suggest some direct or indirect biological control in creating favourable physico-chemical conditions for the precipitation of apatite. However, the SEM studies are significant since there appears to have been direct precipitation of apatite in these nodules.

Mineralogical and electron microprobe studies of phosphorites revealed that a fluorine-rich variety of apatite (francolite) is the major phosphate component. Besides francolite, various secondary phosphorite minerals were also identified. X-Ray diffraction patterns showed sharp, well defined diffraction lines suggesting a high degree of crystallinity for the francolite. The francolite however, has a tendency to be poorer in carbonates (an average of 1.8%) with unit cell dimensions varying between francolite and pure fluorapatite. Type I nodular phosphorite showed lower a^{o}-values (consistent with higher CO_2 contents) than nodules present in the upper beds and Type II nodules which showed higher a^{o}-values (consistent with lower CO_2 contents). While these phosphorites maintained a basic mineralogy reflected as francolite, the loss of considerable amounts of CO_2 (as francolite forming at present on the ocean floor contain as high as 8.4% CO_2) has been interpreted largely as the effects of weathering because this is an old deposit which has had longer periods to undergo leaching. The possibility of formation of francolite authigenically in

carbonate-poor environment has not been ruled out in view of the presence of free carbonates and absence of any secondary phosphorite minerals especially in Type I nodules. Similar examples of authigenically derived phosphatic rocks are Saldanha Bay and the South African Shelf containing an average of 2.6 percent and 1.8 percent CO_2 respectively (Birch, 1980). These values are markedly different from the CO_2 content of the apatite phase in phosphatic rocks of the replacement type which has been determined by both Parker (1971) and Birch (1975) to be 5.5%. However, impoverishment of CO_2 in Type I nodules present in upper beds of phosphorite and in Type II nodules, may support the possibility of leaching during weathering as these nodules showed the presence of secondary phosphorite minerals which only form during weathering.

Structural formulae of apatite (Chapter IV) indicate that these francolites are pure carbonte fluorapatite with meagre amounts of other substituents including CO_2, F, Na and Mg. Average structual formalae are as follows:

Type I phosphorite - $Ca_{9.95}Mg_{.02}Na_{.02}/(PO_4)_{5.66}(CO_3).34/F_{1.77}$.

Type II phosphorite - $Ca_{9.81}Mg_{.12}Na_{.08}(PO_4)_{5.7}(CO_3).31F_{.05}/F_2$

Structural formula of Type I nodules show characteristic deficiency of F in contrast to Type II nodules containing higher amounts than required for fluorapatite structure. An original deficiency of F in the depositional environment is suggested during the formation of Type I nodules as these phosphorites contain abundant free carbonate and some structural carbonate as well protecting it from leaching. The absence of secondary phosphorite minerals also negates any leaching. It was difficult

to imagine the removal of much F without affecting any other associated minerals/elements. Another factor which supports the idea of low F content during the formation of the Type I nodules, is the presence of abundant organic activity during the precipitation of francolite. It is well known that F is a toxic element and its deficiency implies a non-toxic environment which would allow luxuriant growth of organisms (Riggs, 1979).

Higher than normal amounts of F in Type II nodular phosphorites, inspite of visible leaching effects (including decarbonation of phosphorites, low contents of Ca and presence of secondary phosphorite minerals) is probably due to abnormally high concentrations of F in the depositionsal environment. The abnormal concentrations of F inhibited life and thesefore these nodules do not contain any organic remains.

Geochemical studies showed significant impoverishment of lattice elements and enrichment of non-lattice elements in both types of nodules. Large variations in CaO/P_2O_5 ratio in Type I nodules is explained by the presence of accessory dolomite, whereas variation of this ratio in Type II nodules is mainly due to differential weathering processes. High contents of free silica around Pen-y-Garnedd is ascribed to the higher activity of siliceous sponges since the saturation of sea water with silica is very unlikely. Higher contents of silica in Type II nodules attributed mainly to the alteration of smectite to illite during diagenesis. Both types of nodules contain very insignificant amounts of Na and K in the apatite lattice. The concentration of these elements is comparatively higher in Type II nodules than Type I. This higher concentration of elements is either due to

the original differences in the salinity conditions of depositional sites or to the diffusion of these elements into apatite lattice from the more abundant clays of Type II nodules. Very insignificant concentration of Mg, however, in both types of nodules also support the authigenic origin of phosphorite. It has been shown experimentally (Bachra et al, 1965; Martens and Hariss, 1970) that Mg^{2+} ions inhibit the precipitation of apatite, probably because Mg^{2+} competes with Ca^{2+} for sites in the apatite structure. In view of these results, it is difficult to explain how apatite could possibly form in the ocean, since Mg^{2+} is so abundant in sea water. According to the work of Martens and Hariss (1970), there is probably some threshold value for the Ca/Mg ratio above which crystalline apatite may precipitate. This ratio remains almost invariant in normal sea water, even in near shore areas. Pore-water compositions, however, are known to vary greatly from sea water values (Brocker, 1973). It seems plausible therefore, that diagenetic reactions occurring within anoxic sediments could raise the Ca/Mg ratio to the point where apatite may precipitate. Drever (1971), for example has suggested that Mg^{2+} may replace Fe^{3+} in clays under anoxic conditions. The Fe^{3+} is then reduced and combines with sulphides. Other mechanisms to remove interferring Mg^{2+} ions may include ion exchange, substitution of Mg^{2+} for Ca^{2+} in carbonates and the authigenic formation of Mg-rich silicates such as sepiolite or chlorite.

Many of the trace elements studied during the present investigation, show different behaviour in the two types of nodules. Average concentration of trace elements were compared

with an average concentration in marine shales, and enrichment or depletion of trace elements similar to that of a sea water would suggest a sea water source. It has been found that both types of nodules are enriched in Ag, Ce, Cr, La, Sr and Y relative to marine shales. Type I nodules show depletion in Ba, Cu, Li, Mn, Mo, Ni, V and Zr whereas Type II nodules showed depletion in only a few elements such as Co, Mn, V and Zr. This enrichment and/or depletion largely suggests precipitaton from sea water source.

Only a few trace elements showed significant positive correlations with P_2O_5 such as Sr, Ce, La and Y. Inspite of significant correlations Sr/P_2O_5 ratios were found to be low in both types of nodules. Low concentrations of Sr in the depositional environment is difficult to explain at least during the formation of Type I nodules in view of the fact that they contain abundant organic remains and it is well known that Sr concentrates in tests and shells of micro-organisms (Kulp et al, 1952). It has been suggested that both types of nodules have lost Sr during a long span of time since their formation as its substitution in apatite lattice requires no balancing of charges, it is free to enter or leave the structure compared to Na, CO_3 or SO_4 which require couple substitution to maintain charge imbalance. This would also suggest that Sr may be affected both by weathering and secondary enrichment processes. McArthur (1978) suggested that Sr is most affected by weathering and that the secondary enrichment processes are of minor importance. Present data support McArthur's observation and it is suggested that Sr is more mobile than P_2O_5.

Ce, La and Y are enriched in the nodules in comparison to

marine shales. The enrichment of Y in these francolites is normal and suggests precipitation or fixation of apatite from a sea water source as the rare-earth distribution patterns for sea water show a marked enrichment of yttrium (Hogdahl, 1967). A striking feature of the nodules is the Ce/La ratio which is higher than one, paralleling that of crustal abundance (Goldberg, et al, 1963). Their significant positive correlations with P_2O_5 especially in Type II nodules suggests their presence in the apatite lattice. In view of the fact that Ce is impoverished in sea water, its higher than normal content suggested some abnormal conditions. As indicated by Blokh and Kochenov (1964) and Kholodov (1963) higher than normal contents of Ce represent hyposaline and/or euxinic conditions.

Mineralogical, petrographical and geochemical studies have also shown that these phosphorites have undergone differential leaching during weathering processes with the development of secondary phosphate[illegible] minerals. It is certain that the weathering processes depend on the mineral association, but anyhow one of its first results is a loss of CO_2 from the apatite lattice ie decarbonation of francolite with concomitant increase of the lattice constants (McClellan and Lehr, 1967). The decarbonation is associated with the removal of many major and minor elements. The apatite lattice becomes depleted in Ca, F, Na and Sr. As long as free carbonates are present in the rock they protect the associated apatite, stopping the evolution from going further than the fluorapatite stage. Type I nodules, present in the lower main bed of phosphorite, are a good example of this stage. They contain considerable amounts of free

dolomite which is protecting francolite from dissolving further down than the fluorapatite stage. It has also lost considerable amounts of Na and Sr.

The further effects of weathering on phosphorites leads, after leaching of the free carbonates and decarbonation of apatite, to the appearance of aluminous and ferruginous phosphorites. Type I nodules present in the upper beds of phosphorite, are a very typical example of this stage. The nodules are deficient in both structural carbonate and free carbonates and show the presence of secondary Fe-Al phosphates. The secondary phosphate minerals are present in fractures replacing pyrite and/or as scattered pyrite pseudomorphs. All these Fe-Al phosphates are rich in Fe and poor in Al as these rocks are rich in pyrite and poor in clay minerals.

Francolite present in Type II nodular phosphorites is highly susceptible to dissolution during leaching as free carbonates are absent to protect it. Very low contents of CaO, CO_2, Sr and Na along with the presence of wavellite and hydrated Fe-Al phosphorite minerals indicate that these rocks have undergone strong leaching during weathering. These secondary phosphate minerals are present mainly along fractures and also as pyrite pseudomorphs. Overall they are rich in Al, because of the fact that these phosphorites are rich in clay minerals.

Stable C and O-isotopic composition of structural carbonate present in francolite was examined to compare these phosphorites with other well known authigenically precipitated phosphorites and phosphatized limestones. The Welsh phosphorites show marked depletion in $\delta^{13}C$ values, similar to the Namibian concretionary

francolites, suggesting an authigenic origin for these apatites. $\delta^{18}O$ values are much lighter in Welsh phosphorites than the Namibian phosphorites. Sr/P_2O_5 versus $\delta^{13}C$ and $\delta^{18}O$ plot show progressive equilibration with meteoric water which is isotopically lighter and/or at a higher temperature than the original formational waters. This supports the earlier conclusion, on the basis of petrography, mineralogy and geochemistry, that these phosphorites have undergone leaching during weathering.

The question of the source of the phosphate in the Welsh deposit is open to speculation. Oceanic upwelling such as Kazakov (1937), McKelvey et al, (1953) and Sheldon (1963) applied so successfully to Phanerozoic deposits is not entirely satisfactory. There is abundant evidence of very shallow water deposition and restricted circulation in the 1) presence of Hexactinellida and Demospongiae which thrive only in shallow water; 2) the unbroken nature of very fragile spicules suggesting quiet waters; 3) the restriction of very few species of organisms at different points or their entire absence at places; 4) the presence of oolites; 5) the abnormal concentration of elements like Ce suggesting euxinic environment.

An all-pervading shallow sea and restricted circulation of water give very little scope to the postulation of any upwelling water hypothesis. A biogenic origin for the phosphorite would seem reasonable in view of the abundant fossil material present in the deposit although it may be argued that abundant biogenic material is the effect rather than the cause of abundant phosphatic nutrient. However, a direct proof of the possibility

that organic phosphorus may be easily recycled to form inorganic apatite was given by Lucas and Prevot (1981) who succeeded in synthesizing francolite, starting from calcite and phosphorus in organic matter (ribonucleic acid). In general, organic matter in phosphorites appears to be the main results of anoxic microbial degradation of marine plankton. A predominant organic source of phosphate for Welsh phosphorites would also help to explain why their structural carbonate $\delta^{13}C$ values show contribution from organically derived carbon.

The presence of some volcanic fragments in phosphorites of the western part of the Welsh deposit may indicate a volcanic source of P as suggested by Blackwelder (1916). Immediately underlying rocks in the Welsh basin contain much volcanic ash and it is possible that some of this has been reworked into the phosphorite as there is no other firm evidence to suggest volcanicity during the deposition of the Nod Glas (William and Bulman, 1931).

Most of the francolite have pecipitated directly from solution and not by phosphatization/replacement. The various factors in favour of direct precipitation are

1) The euhedral crystal forms and the growth of apatite on the surfaces of biogenic fragments and minerals.
2) Low CaO/P_2O_5 ratio,
3) Low structural carbonate content,
4) Low MgO/CaO ratio,
5) Petrographic evidence of replacement such as pseudomorphism, embayed contacts and crystals transecting earlier structures are completely lacking and

6) Very light $\delta^{13}C$ values support authigenic origin.

The SEM examinations clearly showed that the phosphorites described here were formed authigenically by chemical precipitation. Whether the precipitation was truly inorganic or was influenced by biological activity is a matter of detail, but the phosphorites did not originate (at least most of it) by the process of replacement. The elemental ratios reported earlier in this thesis are close to those expected for pure apatite, thus implying that there are no unreplaced residuals, which might be expected if the apatite had formed by replacement of calcite.

The source of the phosphate was mainly the abundant organic material present within the sediments. The organic phosphate released from organisms, in areas of stagnant water or from quiet current movement, can be easily recycled to form inorganic apatite (Lucas & Prevot, 1981). These processes are proposed here to account for phosphate genesis along shallow restricted zones (lagoonal) which possibly were the environment of deposition of the Caradocian phosphorites. The view that apatite was formed exclusively within the pore water of organic rich sediments and not in the overlying waters is based on the following considerations:

1) the phosphate content within pore waters is very high in comparison to the overlying bottom waters [direct measurements from the Namibian Shelf muds where phosphate is forming today have shown phosphate concentrations upto 2500 ppb (Baturin, 1972) and normal marine water contains about only 75 ppb phosphate (Birch, 1980)].

2) there is no reasonable mechanism to raise the Ca/Mg ratio in sea water to the point where apatite may precipitate, but diagenetic reactions could significantly deplete Mg^{2+} in pore waters.

3) surfaces for apatite nucleation are more readily available within the sediments.

REFERENCES

Al-Bassam, K.S., 1980. Carbon and oxygen isotopic composition of some marine sedimentary apatites from Iraq. Econ. geol., 75, p. 1231-1233.

Altschuler, Z.S., 1967. Rare earths in phosphorites. U.S. Geol. Survey Prof. Pap. 575-B, p. 1-9.

, 1973. The weathering of phosphate deposits. Geochemical and environmental aspects. In: Griffith et al (eds.). Environmental Phosphorus Handbook. Wiley & Sons, New York, 33-96.

, 1980. The geochemistry of trace elements in marine phosphorites. Part I. Characteristic abundances and enrichment. In: Bentor, Y.K. (ed.) SEPM Spec. Pub. 29, p. 19-30.

, Cisney, E.A., and Barlow, I.H., 1953. X-ray evidence of the nature of carbonate-apatite. Amer. Mineral., 38, p. 328.

, Clarke, R.S., and Young, E.J., 1958. Geochemistry of uranium in apatite and phosphorite: U.S. Geol. Survey Prof. Paper 314-D, p. 45-90.

, Berman, S., Cuttitta, F., 1976. REE in phosphorites - geochemistry and potential recovery: U.S.G.S. Prof. Paper 575-B, p. 1-9.

Atlas, E.L. and Pytkowicz, R.M., 1977. Solubility behaviour of apatites in sea water. Limnol. Oceanogr.,22, p. 290-300.

Azad, H.S., and Borchardt, J.A, 1970. Variations in phosphorus uptake by algae: Environ. Sci. Technology, 4, p. 737-743.

Bachra, B.N., Trautz, O.R. and Simon, S.L., 1965. The effect of magnesium and fluoride ions on the spontaneous precipitation of calcium carbonates and phosphates. Arch. Oral. Biol., 10, p. 731-738.

Bailey, S.W., 1972. Determination of chlorite compositions by X-ray spacings and intensities. Clays and Clay minerals, 20, p. 381-88.

Baird, G.C., 1978. Pebbly phosphorite in shale: a key to recognition of a widespread submarine discontinuity in Middle Devonian of New York. J. Sediment.Petrol., 48, p. 545-555.

Bancroft, B.B., 1945. The brachiopod zonal indices of the Stages Costonian to Onnian in Britain. J. Paleont., 19, p. 181-252.

Baturin, G.N., 1969. Authigenic phosphate concentration in Recent sediments of the southwest African Shelf. Dokl. Acad. Sci. U.S.S.R., Earth Sci. Sect., 189, p. 227-230.

, 1971. Stages of phosphorite formation on the sea floor. Nature (Phys. Sci.) 232, p. 61-62.

, 1972. Phosphorus in interstitial waters of sediments on

the South West Africa Shelf: Oceanology, 12, p. 849-855.

, Kochenov, A.V. and Petelin, V.P. 1970. Phosphorite formation on the shelf of S.W. Africa. Lith. and Min. Res., 3, p. 266-276.

Benmore, R.A., 1984. Stable isotopic and geochemical evidence for the origin of phosphorites. Ph.D. Thesis, University College London, 242 pp. (Unpublished).

, Coleman, H.L. and McArthur, J.M., 1983. Carbon and sulphur isotopes in phosphorites: evidence of origin. Nature, 302, p. 601-603.

, McArthur, J.M. and Coleman, H.L., 1984. Carbon and oxygen isotopic composition of phosphorite. Proc. 4th Int. Field Workshop and Sem. on Phosphorites, Udaipur, India, 1981 (in press).

Bentor, Y.K., 1979. Modern phosphorites - not a sure guide for the interpretation of ancient deposits: Rep. Marine Phosphatic Sediments Workshop. Eds: W.C. Burnett and R.P. Sheldon, Honolulu, p. 29.

, 1980. Phosphorites - The unsolved problems in marine phosphorites. In: Bentor, Y.K. (ed.) SEPM Spec. Publ. 29, p. 3-18.

Berner, R.A., 1964. An idealized model of dissolved sulphate distribution in recent sediments. Geochim. Cosmochim.

Acta, 28, p. 1497-1503.

, 1969. The synthesis of framboidal pyrite. Econ. Geol., 64, p. 383-384.

Birch, G.F., 1975. Sediments on the continental margin off the west coast of South Africa. Thesis, Ph.D., Univ. of Cape Town (unpublished).

, 1979a. Phosphorite pellets and rock from the western continental margin and adjacent coastal terranes of South Africa. Mar. Geol., 33, p. 91-116.

, 1979b. Phosphatic rocks on the western margin of South Africa. J. Sed. Petrol. 49, p. 93-110.

, 1980. A model of penecontemporaneous phosphatization by diagenetic and authigenic mechanisms from the western margin of southern Africa. SEPM Spec.Publ.,29, p. 79-100.

, Thomson, J., McArthur, J.M. and Burnett, W.C., 1983. Pleistocene phosphorites off the west coast of South Africa. Nature, 302, p. 601-603.

Biscaye, P.B., 1964. Distinction between kaolinite and chlorite in Recent sediments by X-ray diffraction. Amer. Mineral.,49, p. 1281-89.

Blokh, A.M. and Kochenov, A.B. 1964. Element admixture in bones of fossil fish. Geol. mestorozhd. redkii elementov.,24,

p. 1-100 [In Russian].

Bostrom, K., 1970. Submarine volcanism as a source for iron. Earth Planet. Sci. Lett., 9, p. 348-354.

Bremner, J.M., 1978. Sediments on the continental margin off South West Africa between latitudes 17° and 25°S. Thesis, Ph.D., Univ. of Cape Town (Unpublished).

, 1980. Concretionary phosphorite from southwest Africa. J. geol. Soc. London, 137, p. 773-786.

Brenchley, P.J., 1966. The Caradoc rocks of the north and west Berwyns, North Wales. Thesis (Ph.D.), Liverpool University.

Brindley, G.W., 1961. Kaolin, serpentine and kindred minerals. In Brown, G. (ed.). The X-ray identification and crystal structures of clay minerals, p. 51-131.

Brown, G. (Ed.), 1961. The X-ray identification and crystal structure of clay minerals. Mineral. Soc. (Clay Mineral Group), London, 544 p.

Broecker, W.S. 1973. Interstitial water studies, Leg 15 - introduction and summary, in Heezen, B.C., MacGregor, I.G. and others. Initial reports of the Deep Sea Drilling Project, Vol. 20: Washington, D.C., U.S. Govt. Printing Office, P. 751-755.

Burnett, W.C., 1977. Geochemistry and origin of phosphorite deposits from off Peru and Chile. Geol. Soc. Amer. Bull., 88, p. 813-823.

, 1980. U-series, oceanographic and sedimentary evidence in support of recent formation of phosphate nodules off Peru. SEPM Spec.Publ. 29, p. 61-72.

, and Veeh, H.H. 1977. Uranium-series disequilibrium studies in phosphorite nodules from the west coast of South America. Geochim. Cosmochim. Acta, 41, p. 755-764.

, Veeh, M.H. and Soutar, A., 1980. U-series oceanographic and sedimentary evidence in support of recent formation of phosphate nodules off Peru. Soc. Econ. Paleontol. Mineral., Spec. Publ., 29; p. 61-71.

Bushinskii, G.I., 1935. Structure and orgin of the phosphorites of the U.S.S.R., J. Sed. Petrol., 5, 81.

, 1966. The origin of marine phosphorites. Lith. & Min. Res., 3, p. 293-311.

, 1966. Old phosphates of Asia and their Genesis. Akad. Nauk SSSR. Geol. Inst. Translations. 49, p. 1-192.

, 1969. Old phosphorites of Asia and their Genesis. Transal. from Russian, Israel Prog. of Sci. Transl., 266 p.

Calvert, S.E., 1976. The mineralogy and geochemistry of near-shore sediments. Chemical Oceanogr. Ed. Riley & Chester, V.G., Acad. Press, p. 187-280.

Cathcart, J.B. and Gulbrandsen, R.A., 1973. Phosphate deposits: In United

State mineral resources, U.S. Geol. Surv., Prof. Paper. 820, p. 515-525

Cave, R., 1965. The Nod Glas sediments of Caradoc age in North Wales. Geol. Jour. 4, 2, p. 279-298.

CAYEUX, L. 1932. Existence d'un phosphate à spicules de calcisponges dans l'Ordovician de Pays de Galles. C.r. hebd. Séanc. Acad. Sci., Paris, Vol. 195, No 25, pp 1158-1190.

Clarke, F.W. and Wheeler, W.C., 1922. The inorganic constituents of marine invertebrates. U.S. Geol. Survey, Prof. Paper, 124, 62 p.

Claypool, G.E., and Presley, B.J., 1973. Generation of light hydrocarbon gases in deep sea sediments (abstr.) Am. Assoc. Pet. Geol. Bull., 57, p. 773.

, Love, A.H. and Maughan, E.K., 1978. Organic geochemistry incipient metamorphism and oil generation in black shale members of Phosphoria Formation, western interior United States. Amer. Assoc. Pet. Geol. Bull. 62, p. 98-120.

Cook, P.J., 1972. Petrology and geochemistry of the phosphate deposits of north-west Queensland, Australia, Econ. Geol., 67, p. 1193-1213.

, and McElhinny, M.W., 1979. A reevaluation of the spatial and temporal distribution of sedimentary phosphate deposits in the light of plate tectonics. Econ. Geol., 74, p. 315-330.

Cossa, 1878. "Sur la diffusion du Cerium, du lanthane et du didyme," extract of a letter from Cossa to Sella, presented by Frency: C.R. Ac. Sc., Paris, V. 87, p. 378-388.

Craig, H., 1953. The geochemistry of the stable carbon isotopes.

Geochim. Cosmochim. Acta, 3, p. 53,

, 1961. Isotopic variations in meteoric waters. Science, 133:1702.

, 1965. The measurement of oxygen isotope palaeotemperatures. In: Tongiorgi, E. (ed.). Stable Isotopes in Oceanographic Studies and Palaeotemperatures. p. 3-14. Consighe Nazionale delle Ricerche, Pisa.

Criddle, A.J., 1974. A preliminary description of microcrystalline pyrite from the nannoplankton ooze at site 251, Southwest Indian Ocean. In: Lyendyk, B.P., Davies, T.A. et al. Initial Rep. Deep Sea drill proj., Leg 26. U.S. Govt. Printing Office, Washington, 603-7.

Cullen, D.J., 1980. Distribution, composition and age of submarine phosphorites on Catham Rise, east of New Zealand. SEPM Spec. Publ. 29, 139-48.

Culkin, F., 1965. Chemical Oceanography (eds. Riley, J.P. and Skirrow, G.). Academic, London.

Davies, D.C., 1967. On a bed of phosphate of Lime, N.W. of Llanfyllin, North Wales. Geol. Mag., 252.

, 1875. The phosphorite deposits of North Wales Quart. Jour. Geol. Soc. xxxi, 357.

Deer, W.A., Howie, R.A., and Zussman, J. 1963. Rock forming minerals - Non silicates. Vol. 5; Longmans, edit. London, 363 p.

, 1966. An introduction to the rock-forming minerals: New York, John Wiley & Sons, 528 p.

Dietz, R.S., Emery, K.O., and Shepard, F.P., 1942. Posphorite deposits on the sea floor off Southern California: Geol. Soc. Amer. Bull., p. 815-847.

Doubinger, J., 1979. Dinokystes et Acritarches des sediments phosphates de Ganntour (Maroc): Sci. geol. Bull., 31, p. 3.

Doyle, L.J., Blake, N.J., Woo, C.C. and Yevich, P., 1978. Recent biogenic phosphorite: concretions in mollusk kidneys. Science,199, 1431-1433.

Drever, J.I. 1971. Magnesium-iron replacement in clay minerals in anoxic marine sediments: Science,172, p. 1334-1336.

Epstein, S., Buchsbaum, R., Lowenstam, H.A., and Urey, H.C., 1951. Carbonate-water isotopic temperature scale, Geol. Soc. Amer. Bull., 62, p. 417-426.

, 1953. Revised carbonate-water isotopic temperature scale. Bull. geol. Soc. Amer. 64, p. 1315.

Fang, J.H. and Bloss, F.D. 1966. X-Ray Diffraction Tables. Southern Illinois University Press/Carbondale and Edwardsville. London.

Fauconnier, D. 1977. Les Dinoflagelles de l'Albien et du Cenomanien inferieur du Bassin de Paris. Repartition stratigraphique et relations avec la nature du depot: These (Doctorat d'Univ.)

Orleans, 229 p.

Foster, M.D., 1962. Interpretation of the composition and classification of the chlorites. U.S.G.S. Prof. Pap. 414-A.

Garcia, S.G. and Camazano, M.S. 1968. Differentiation of kaolinite from chlorite by treatment with dimethyl-sulphoxide. Clay Minerals, 7, p. 447-50.

Goldberg, E.D. Koide, Minoiu, Schmitt, R.A. and Smith, H.V., 1963. Rare earth distribution in the marine environment. Jour. Geophys. Research, 68, p. 4209-4217.

Gross, G.A., 1964. Variation in the O^{18}/O^{16} and C^{13}/C^{12} ratios of diagenetically altered limestones in the Bermuda Islands. J. Geol.,71, p. 170.

Gulbrandsen, R.A., 1960. Petrology of the Mead Peak phosphatic shale member of the Phophoria Formation at Coal Canyon, Wyoming: U.S.G.S. Geol. Bull. IIIIC, p. 71-146.

, 1966. Chemical composion of phosphorite of the Phosphoria Formation. Geochim. Cosmochim. Acta, 30, p. 769-778.

, 1969. Physical and chemical factors in the formation of marine apatite. Econ. Geol., 64, 4, p. 365-382.

, 1970. Relation of carbondioxide content of apatite of Phosphoria formation to regional facies. U.S. Geol. Surv. Prof. Paper 700B, p. 9-13.

Gusev, G.M., Zanin, Y.N., Krivolutskaya, L.M., Lemina, N.M., and Yusupov, T.S. 1976. Transformation of apatite during weathering and leaching. Dokl Akad. Nauk SSSR, 229, p. 971-973.

Haynes, C.V. Jr. 1968. Radiocarbon analyses of inorganic carbon of fossil bones and enamel. Science, 161, p. 687-688.

Hey, M.H. 1954. A new review of the chlorites. Mineral. Mag. London, 30, p. 277-92.

Hoefs, J., 1980. Stable isotope Geochemistry. Wyllie, P.J., Goresy, A.El., Engelhardt, W. von, and Hahn, T. (Eds.) Springer-Verlag, 208 p.

Hogdahl, Ove, 1967. Distribution of the rare earths in sea-water. Prog. Rept. no. 4. to NATO, Central Instit. for Ind. Res., Blindern, 34 p.

Howie, R.A., and Broadhurst, F.M., 1958. X-ray data for dolomite and ankerite. Amer. Mineral., 43, p. 1210-1211.

Haung, W.H. and Johns, W.D. 1967. "Simultaneous determination of fluorine and chlorine in silicate rocks by a rapid spectrophotometric method." Anal. Chim. Acta, 37. p. 508-515.

Hudson. J.D., 1978. Concretions, isotopes and the diagenetic history of the Oxford Clay (Jurassic) of central England. Sedimentology, 25, p. 339-370.

Hutchison, C.S. 1974. Laboratory handbook of petrographic techniques. New York.

Irwin, H., Curtis, C. and Coleman, M. 1977. Isotopic evidence for source

of diagenetic carbonates formed during burial of organic rich sediments. Nature (London), 269, p. 209.

Jarvis, I., 1980. Geochemistry of phosphatic chalks and hardgrounds from the Santonian to early Campanian (Cretaceous) of Northern France. J. geol. Soc. (Lond.), 137. p. 705-721.

Jehu, R.M., 1926. The Geology of the District around Towyn and Abergynolwyn (Merioneth). Quart. Jour. geol. Soc. London, 102, 465.

Kazakov, A.V., 1937. The phosphorite facies and the genesis of phosphorites in Geological investigations of agricultural ores, U.S.S.R. Trans. Sci. Inst. Fertilizers and Insectofungicides, no. 142, p. 93-113.

Keith, M.L. and Weber, J.N., 1964. Isotopic composition and environmental classification of selected limestones and fossils. Geochim. Cosmochim. Acta, 28, 1787.

Kennedy, W.J. and Garrison, R.E., 1975. Morphology and genesis of nodular phosphates in the Cenomanian Glauconitic Marl of South East England. Lethaia, 8, p. 339-360.

Kholodov, V.N., 1963. On rare and radioactive elements in Phosphorites. Akad. nauk. Inst. Mineral. Geokgm. Kristallokhim Reak. Elem., Tr., V. 17, p. 67-108 (in Russian).

, 1973. Trace element distribution in the Kurumsak-Chulaktau Deposits of Karatau. English translation. Geoch. Intern., V. 10, p. 795-802.

King, W.B.R., 1923. The Upper Ordovician Rocks of the southwestern Berwyn Hills. Quart. Jour. Geol. Soc. London, 79, 487.

, 1928. The geology of the District around Meifod (Montgomeryshire). Quart. Jour. Geol. Soc. London, 84, 671.

, and Williams, A., 1948. On the Lower Part of the Ashgillian Series in the North of England. Geol. Mag., 85, 205.

Kolodny, Y., 1980. The origin of phosphorite deposits in the light of occurrences of Recent sea-floor phosphorites. SEPM Spec. Publ., 29, p. 249.

, 1981. Phosphorites. In: Emiliani C. (ed.). The Sea. Wiley & Sons, New York 7, p. 981-1023.

, and Kaplan, I.R., 1970. Carbon and oxygen isotopes in apatite - CO_2 and co-existing calcite from sedimentary phosphorites. J. Sediment. Petrol., 40, p. 954-959.

Knauth, L.P. and Epstein, S., 1976. Hydrogen and oxygen isotope ratios in nodular bedded cherts. Geochim. Cosmochim Acta, 40: 1095.

Kramer, J.R. 1964. "Sea Water - saturation with Apatites and carbonates." Science, 146 (3644), p. 637-638.

Krauskopf, K.B., 1955. Sedimentary deposits of rare metals. Econ. Geol., 50, p. 411-463.

Kulp, J.L., Turekian, K., and Boyd, D.W., 1952. Strontium content of limestones and fossils. Bull. geol. Soc. Am., V. 63, p. 701-716.

Lawrence, J.R., Gieskes, J.M., and Broecker, W.S. 1967. Oxygen isotope and cation composition of DSDP pore waters and the alteration of Layer II basalt. Earth Planet. Sci. Lett., 27, p. 1-10.

Lewis, H.P., 1940. The microfossils of the Upper Caradocian Phosphate Deposits of Montgomeryshire. North Wales, Ann. Mag. Nat. Hist.,5, 11, 1.

Longinelli, A. and Nutti, S., 1968. Oxygen isotopic composition of phosphorites from marine formations. Earth Planet. Sci. Lett.,5, p. 13-6.

Lovell, J.P.B., 1977. The British Isles through Geological time. A northward drift. Cox & Wyman Ltd. London, 40 p.

Lowell, W.R., 1952. Phosphatic rocks in the Deer Creek Wells Canyon area, Idaho. Bull. U.S. Geol. Surv., 982-A, 51 pp.

Lucas, J., Flicoteaux, R., Nathan, Y., Prevot, L., Shahar, Y., 1980. Different aspects of phosphorite weathering. SEPM, Spec. Publ., 29, p. 41-51.

, and Prevot, L., 1981. Synthese d'apatite a partir de matiere organique phosphoree (ARN) et de calcite par voie bacterienne. c.r. hebd. Seanc Acad. Sci., Paris, 192, p. 1203-1208.

Mabie, C.P. and Hess, H.D., 1964. Phosphate study and classification of western phosphate ores. U.S. Bur. Mines. Rept. Inv. 6468, 95 p.

Manheim, F.T., and Gulbrandsen, R.A., 1979. Marine phosphorites,

in Burns, R.G., ed., Marine minerals: Mineralog. Soc. America Short Course Notes. V. 6, p. 151-170.

, Pratt, R.M., and McFarlin, P.F. 1980. Composition and origin of phosphorite deposits of Blake Plateau. SEPM Spec. Publ. 29, p. 117-137.

Marshall, J.F. and Cook, P.J., 1980. Petrology of iron and phosphorus rich nodules from the E. Australian continental shelf. J. geol. Soc. London, 137, p. 765-771.

Martens, C.S. and Harris, D.C. 1970. Inhibition of apatite precipitation in the marine environment by magnesium ions. Geochim. Cosmochim. Acta, 34, p. 621-625.

McArthur, J.M., 1978. Systematic variations in the contents of Na, Sr, CO_3 and SO_4 in marine carbonate-fluorapatite and their relation to weathering. Chem. Geol., 21, p. 89-112.

, 1980. Post depositional alteration of the carbonate-fluorapatite phase of Moroccan phosphates. SEPM Spec. Publ. 29, p. 53-60.

, Coleman, H.L. and Bremner, J.M., 1980. Carbon and oxygen isotopic composition of structural carbonate in sedimentary francolite. J. geol. Soc. London, 137, p. 669-673.

McClellan, G.H., 1980. Mineralogy of carbonate fluorapatite. J. geol. Soc. London, 137, p. 675-681.

, and Lehr, J.R., 1967. "Crystal chemical investigation of natural apatites." presented at Geol. Soc. Am. Annual meeting, Nov. 10-22, New Orleans, La.

McCrea, J.M., 1950. The isotopic chemistry of carbonates and a palaeotemperature scale. J. Chem. Phys., 18, p. 849-857.

McConnell, D., 1938. A structural investigation of the isomorphism of the apatite group. Amer. Mineral., 23, p. 1-19.

, 1960. The crystal chemistry of dahllite. Amer. Mineral., 45, p. 209-21

, 1963. Inorganic constituents in the shell of living brachiopod Lingula, Geol. Soc. Amer. Bull., 74, p. 363-364.

, 1973. Apatites: Its Utilization and Geologic and Biologic Occurrence. Springer Verlag, Berlin, 111 p.

McKelvey, V.E., Swanson, R.W. and Sheldon, R.P., 1953. The Permian Phosphoria deposits of Western United States, 19th Int. Geol. Congr. Algier, Section XI, p. 45-64.

Nathan, Y., 1980. Structural positions of trace elements in Apatites; Implications for their recovery. Proceedings 2nd International Congress on Phosphorous Compounds. Institute Mondial du Phosphate (IMPHOS), Boston, April 21-25, p. 1-6.

, and Neilson, H., 1980. Sulphur isotopes in phsophorite. In: Bentor, Y.K. (ed.) SEPM Spec.Publ. 29, p. 19-30.

, and Saas, E., 1981. Stability relations of apatites and calcium carbonates. Chem. Geol., 34, p. 103-111.

Nissenbaum, A., Presley, B.J., and Kaplan, I.R. 1972. Early diagenesis in a reducing fjord, Saanich Inlet, British Columbia. I. Chemical and isotopic changes in major components of interstitial water. Geochim. Cosmochim. Acta, 36, p. 1007-1028.

Notholt, A.J.G., 1980. Economic phosphatic sediments: mode of occurrence and stratigraphical distribution. J. geol. Soc. London, 137, p. 793-805.

O'Brien, G.W., and Veeh, H.H., 1980. Holocene phosphorite on the East Australian continental margin. Nature, 288, p. 690-692.

, Harris, J.R., Milnes, A.R. and Veeh, H.H., 1981. Bacterial origin of east Australian continental margin phosphorites, Nature, 294, p. 442-444.

Odin, G.S. and Letolle, R., 1980. Glauconitization and phosphatization environments: A tentative comparison, In: Bentor, Y.K. (ed.) SEPM. Spec. Publ. 29, p. 227-237.

Parker, R.J., 1971. The petrography and major element geochemistry of phosphorite nodule deposits on the Agulhas Bank, South Africa: SANCOR Mar. Geol. Prog. no. 2, Dept. Geol., Univ. Cape Town, 92.

, and Seisser, W.G. 1972. Petrology and origin of some phosphorites from the South African continental margin.

J. Sed. Pet., 42, p. 434-440.

Presley, B.J. and Kaplan, I.R. 1968. Changes in dissolved sulphates, calcium and carbonate from intersitial water on near shore sediments. Geochim. Cosmochim. Acta, 32, 10, p. 1037-1048.

Prevot, L., Lucas, J., Nathan, Y., and Shilonim, Y, 1979. Repartition des elements traces dans les Phosphorites Marines in origin and distribution of the elements, Second symposium. L.H. Ahrens, (Ed.) Physics and Chemistry of the Earth. Pergamom Press, p. 293-304.

, and , 1980. Behaviour of some trace elements in phosphatic sedimentary formations, SEPM Spec. Publ. 29, p. 31-39.

Price, N.B. and Calvert, S.E., 1978. The geochemistry of phosphorites from the Namibian Shelf. Chem. Geol., 23, p. 151-170.

Pugh, W.J., 1923. The Geology of the District around Corris and Aberllefenni (Merionethshire). Quart. Jour. geol. Soc. London, 79, p. 508.

, 1928. The Geology of the District around Dinas Mawddwy (Merioneth). Quart. Jour. geol. Soc. London, 84, p. 345.

Pytkowicz, R.M. and Kester, D.R., 1967. Relative calcium phosphate saturation in two regions of the North Pacific. Limonology and oceanography, 12, p. 714-718.

Reeves, M.J. and Saadi, T.A.K., 1971. Factor controlling deposition of phosphate bearing strata. Econ. Geol.,66, p. 451-465.

Riggs, S.R., 1979a. Phosphorite sedimentation in Florida - A model phosphogenic system. Econ. Geol., 74, p. 285-314.

, 1979b. Petology of the Tertiary Phosphorite System of Florida. Econ. Geol., 74, p. 195-220.

Robertson, C.E., 1966. Solubility implications of apatite in sea water. U.S.G.S. Prof. Paper, 550-D, p. D178-D185.

Rooney, T.P., and Kerr, P.F., 1967. Mineralogic nature and origin of phosphorite, Beaufort Country, North Carolina. Bull. Geol. Soc. Am., 78, p. 731-748.

Sackett, W.M., Eadie, B.J., and Exner, M.E., 1973. Stable isotope composition of organic carbon in Recent Antarctic sediments. Adv. Org. Geochem., 661.

Shackletton, N.J., and Kennet, J.P., 1975. Palaeotemperature history of the Cenozoic and the initiation of Antarctic glaciation; Oxygen and carbonate isotope analysis in DSDP sites 277,279, and 281: Init. Rep. Deep Sea Drill. Proj. V. XXIX, p. 743-755.

Sheldon, R.P. 1963. Physical stratigraphy and mineral resources of Peruvian rocks in Western Wyoming. U.S. Geol. Survey Prof. Paper 313B, p. 49-272.

Sheldon, R.P., 1964(a). Paleolatitudinal and Paleogeographic distribution of phosphorite. U.S. Geol. Survey Prof. Paper 501-C, p. 106-113.

, 1964b. Exploration for phosphorite in Turkey. A case history. Econ. Geol., 59, p. 1159-1175.

, 1981. Ancient marine phosphorites. Ann. Rev. Earth Planet. Sci., 9, p. 251-284.

Shishkina, O.V., and Pavlova, G.A., 1973. Iodine in the phosphorite nodules and bone phosphate of Recent shelf deposits: Geokhimia, p. 1573-1527. (English: p. 1161-1165)

Siesser, W.G., and Rogers, 1976. Authigenic Pyrite and gypsum in South West Africa continental slope sediments. Sedimentology, 23, p. 567-577.

Smith, J.P. and Lehr, J.R., 1966. An X-ray investigation of carbonate-apatites. J. Agric. Food Chem., 14, no. 4, p. 342-349.

Stumm, W. and Leckie, J.O., 1970. Phosphate exchange with sediments; its role in the productivity of surface waters: Water Poll. Res. Conf., III, 26, p. 1-16.

, and Morgan, J.J. 1970. Aquatic chemistry - An Introduction Emphasizing Chemical Equilibria in Natural Waters. Wiley - Interscience, New York, N.Y., 583 pp.

Summerhayes, C.P., 1972. Aspects of the mineralogy and geochemistry of Agulhas Bank sediments. Parts I and II: SANCOR Mar. Geol. Prog. Tech. Rept. Geol. Dept. Uni of Cape Town, 4, p. 83-95.

Swaine, D.J., 1962. The trace element content of fertilizers: Commonwealth Bureau of Soils, Technical Communication, No. 52, Harpenden, England, 306 p.

Sweet, K. and Crowder, R.K. 1982. Primary phosphatic oolites from the Lower Cambrian of Spitsbergen, J. Sediment. Petrol., 52, p. 587-593.

Tankard, A.J., 1974. Petrology and origin of the phosphorite and aluminium phosphate rock of the Langebaanweg-Saldanha area, southwestern Cape Province. Ann. S. Afr. Mus., 65, p. 217-249.

Thewlis, J., Glock, G.E. and Murray, M.M., 1939. Chemical and X-ray analysis of dental, mineral and synthetic apatites. Trans. Faraday Soc., 35, p. 358-363.

Thorez, J., 1976. The practical identification of clay minerals. G. Lelotte, Dison, Belgique.

Tooms, J.S., Summerhayes, C.P. and Cronan, D.S., 1969. Geochemistry of marine phosphate and manganese deposits. Oceanogr. Mar. Biol. Ann. Rev., 7, p. 49-100.

Turekian, Karl K., and Wedepohl, Karl Hans, 1961. Distribution of elements in some major units of the Earth's crust. Geol. Soc. Am. Bull., 72, p. 175-192.

, 1969. The oceans, streams, and atmosphere: in Handbook of

geochemistry (K.H. Wedepohl, Ed.) Springer-Verlag, Vol 1, p. 297-323.

Veizer, J. and Hoefs, J. 1976. The nature of O^{18}/O^{16} and C^{13}/C^{12} secular trends in sedimentary carbonate rocks. Geochim. Cosmochim. Acta, 40, p. 1387-1395.

Voelcker, A. 1866. On phosphatic deposits recently discovered in North Wales. Rep. Brit. Ass. Adv. Sci. Trans.,37.

Wade, A. 1911. The Llandovery and associated rocks of North-eastern Montgomeryshire. Quart. Jour. geol. Soc. London, 67, p. 415.

Walsh, J.N., and Howie, R.A. 1980. An evaluation of the performance of an inductively coupled plasma source spectrometer for the determination of the major and trace constituents of silicate rocks and minerals. Min. Mag., 43, p. 967-74.

Wedd, C.B., Smith, B., King, W.B.R., and Wray, D.A. 1929. The country around Oswestry. (Explanation of Sheet 228). Mem. geol. Surv. Engl. Wales.

William, H. and Bulman, O.M.B., 1931. The geology of the Dolwyddelan Syncline (North Wales). Quartr. Journ. Geol. Soc. London, 87, p. 425.

APPENDIX 4

4.1 X-ray diffraction settings used for Mineral scans

Radiation	Scan Speed	Range (C.P.S.)	Time constant (secs.)
Cu K alpha	$1^{o}2\theta$/min	4×10^{2}	4

4.2 Mineralogy

The X-ray reflection (peaks) were measured and the minerals were identified by conversion of 2θ values to 'd' values using the tables of Fang and Bloss (1966). The mineralogical identification was done by measuring the intensity of each reflection against their respective 'd' values. The maximum reflection of apatite was then taken as a hundred and each reflection was converted to the nearest whole number with respect to this hundred percentile maximum reflection. This was done to obtain a definite intensity ratio. The mineral identification was subsequently done following the X-ray identification charts of Brown (1961), McConnell (1960, 1973), Howie and Broadhurst (1958) and Thewlist et al (1939).

4.3 Clay mineral identification

The clay fraction of the phosphorite was identified by the following: Bailey (1972), Biscay (1964), Brindley (1961), Foster (1962), Hey (1954), Hutchison (1974) and Thorez (1976). The most favoured methods of clay mineral determination by XRD involve comparison of the intensities of especially basal reflection in the untreated state, with their intensities following a range of chemical and physical treatments outlined below:-

(a) Untreated Sample: The presence of a well ordered kaolinite is

indicated by narrow, symmetrical and relatively intense 7A and 3.5 A reflections. The intensity of the (001) reflections decreases with disordered kaolinite dislay fewer reflections than that of fully ordered kaolinite. The quartz peak can be used throughout as internal standards to correct peak portions.

(b) HCl-treatment - A portion of the sample was digested with 2N HCl in a 50 ml flask over a sand bath for 8 hours, maintaining a temperature of 80 ^{o}C (Biscay, 1964). The peaks are seen to be unaffected, eliminating the possibility of the presence of chlorite. The digested sample was washed in distilled water and allowed to dry and mounted on a slide with ethylene glycol and a diffractogram run under the previous conditions. Kaolinte, quartz, mica and feldspars are all resistant to solution in hot dilute HCl, whilst chlorite is removed.

(c) Heat treatment - Another portion of the sample was heated to 600 ^{o}C for 1 hour mounted by the standard method and run under the previous conditions in furnace for 1 hour. At around 550 ^{o}C kaolinite loses water from its structure. This amorphous transformation is indicated by the elimination of the kaolinite peaks, those for the other component minerals remaining intact (Brindley, 1961).

(d) DMSO treatment - The clay fraction was refluxed in 50 ml dimethyl sulphoxide (DMSO) at 180 ^{o}C for approximately 70 hours The (001) reflection at 7.15 A is expanded to 11.18 A and (002) peak at 3.56 A. Another peak appears at 3.63 A whilst the 3.56 A peak remains unaffected. This response is considered as a positive diagnosis of kaolinite (Garcia and Camazano, 1968).

4.4 Determination of structural CO_2 by X-ray Diffraction

Following the X-ray diffraction peak-pair method of Gulbrandsen (1970), the amount of structual CO_2 was determined in representative samples. The pair of peaks selected here are the (410) and the (004) which occur at about 51.6° and 53.1° 2θ respectively, for Cu-radiation. Each sample was scanned three times between the two X-ray diffraction peaks. The angular difference between these values was used to calculate the strutural CO_2 content of francolite using the emphirical relationship wt % CO_2 = 23.6341 - 14.7361 x where x = Δ 2θ (410) for Cu-radiation.

4.5 Determination of Unit-cell Dimensions by X-ray Diffraction

Unit cell dimensions were calculated using the following equation:

$a^{\circ} = 1.3333\ d^2\ \sqrt{h^2 + k^2 + hk}$ with (210), (310), (320) and (410) planes

$c^{\circ} = 1 \times d$ with (004) and (002) planes

APPENDIX 5

Technical Details of Analytical Methods used for Geochemistry

5.1 Inductively Coupled Plasma Source Spectrometer

It is necessary to prepare stable solutions for all the elements to be determined in ICP spectrometery (Walsh and Howie, 1980). Two solutions were prepared one for major element work and the other for trace element work.

5.1.2. Major Element Procedure (Solution -A)

0.1 gms of sample was fused for 30 minutes at 900 ^{o}C in a platinum crucible with 0.6 gms of lithium metaborate (100%). Crucible was allowed to cool. The resultant fusion bead was then completely dissolved in 200 mls of 5% nitric acid and made upto 250 mls with distilled water.

5.1.3. Trace Element Procedure (Solution -B)

0.5 gms of sample was evaporated to dryness in a platinum crucible along with 4 ml of perchloric acid and 15 ml of hydrofluoric acid. The crucible was allowed to cool. 4 ml of hydrochloric acid and distilled water was half filled in the crucible and it was heated till the salt dissolved and made upto 50 ml with distilled water. Si is removed in the evaporation, but all the other major and trace elements can be determined on this more concentrated solution.

5.1.4 Instrumental Settings used for ICP analysis

a) for major elements

b) for trace elements

Table 5.1.4

Instrumental settings used for ICP analysis

a) for major elements

b) for trace elements

	a	b
R.F. generation	1.4 kw	1.2 kw
Gas flows (all high purity argon)	litres/min	
Plasma (and coolant)	20	18
Auxiliary	0.5	0
Carrier	1.3	1.3
Sample uplate rate	2.3	

Table 5.1.5 Detection limit for trace elements

Trace element	Line (nm)	Detection limit (3σ) - ppm in rock
Zn	202.55	4
Ni	231.60	4.5
Co	228.62	2
V	290.88	4
Nb	309.42	3
Cu	324.75	4.5
Zr	339.20	3
Y	371.03	5
La	398.85	4
Sr	407.77	5

Ce	418.66	7
Cr	425.44	5
Ba	455.40	5
Li	670.78	1
Sc	361.38	1

5.1.6. Standards: Sample solutions were calibrated with KC11, USGS-22, USGS-47, and University College London Laboratory phosphate rock standards P-1, P(Ca)-1, P(Fe)-1 and P(Fe)-2.

5.2 Determination of F using Spectrophotometer

5.2.1 Solution Preparation

Weigh 0.05-0.1 gm sample in a platinum crucible. Add 4.0 gm flux mixture ($Na_2 CO_3$: ZnO 6:1). Mix well with a plastic rod. Tap crucible to settle powder. Weigh out 0.5 gm sodium carbonate powder and scatter it evenly over the sample + flux powder mixture. Cover with lid and heat for 20 minutes. Allow to cool. Half fill the crucible with deionised distilled water and add 3 drops ethanol. Place the crucible on the hot plate, bring temperature to 100 ^{o}C and leave to stand overnight. With a flat ended glass rod, crush the solids in the crucible. Filter the solution by passing through approximately 10 ml 20% nitric acid followed by 3 rinses with near boiling d.d. water. Discard the rinsing. Filter the solution through the washed filter paper into the plastic beaker. Rinse filter paper and solids, five times with approximately 2 ml squirts of near boiling d.d. water. Cover beaker with watch glass and slowly add by syringe pipette through the pouring lip 4.7ml concentrated nitric acid. Allow effervescence to subside and gently swirl solution.

Transfer solution to a 50 ml volumetric flask.

5.2.2 Fluorine Measurment

Take 1 ml sample solution (for F range 250-5000 ppm) or 5 ml sample solution (for F range 50-1000 ppm) into a 50 ml volumetric flask. Add 3 drops 6N sodium hydroxide and mix well. Add 3 ml (syringe pipette) erichrome Cyanine R reagent. Add 5 ml zirconyl chloride reagent. Dilute to volume and allow sample solution to stand for 11/2 hours before measureing absorbence. Prepare standard solutions and reference solution. Reference solution is prepared to set the absorbence zero on the spectrophotometer. Set wavelength to 532 nm. Fill cell with reference solution and set absorbence to 1.000. Run blank and samples, followed by standards. Plot the calibration curve from the standard absorbence vs concentration to obtain the net value for sample (Huang and Johns, 1967).

5.3 Electron Probe Microanalysis

The electron microprobe analyzer at the Grant Institute of Geology, Edinburgh was used for the analysis of individual apatite crystallites. Epoxy resin mounted, polished thin sections were used for the study. Spot analyses of the dispersed phosphate grains concentrated in the nodules were performed on 30 thin sectin of phosphorites. Spot sizes varies from 1 to 10 microns.

5.3.1 Standards

The standards used were apatite, periclase and wollastonite for P, Mg and Ca; Wollastonite and pure metals for Si and Mn; and (Co, Zn) F_2 pure metals and corrundum for F, Fe and Al.

Calibration was monitored by a cobalt standard; accuracy was estimated by analysing a jadeite standard prior to the commencement of each session. Precision is 1% at 50% concentration level, 2% at 10% concentration level and 10% at 2% concentration level.

APPENDIX 6

6.1 Technical Details of Carbon and Oxygen Isotope Analysis

The isotope composition of extracted carbon dioxide was measured on a mass spectrometer which was operated automatically using the computer at the Scottish Universities Research and Reactor Centre (SURRC), East Kilbride, Glasgow. Samples were measured relative to a laboratory secondary standards Tet-2 calcite which is calibrated for both $\delta^{13}C$ and $\delta^{18}O$ with respect to International carbonate standard PDB (a Cretaceous belemnite, Belemnitella americana from the Pedee Formation, S. Carolina, USA) from direct measurement against primary International carbonate standards NBS-19 and NBS-20 (Solenhofen Limestone).

6.2 Carbon dioxide Extraction

Carbon dioxide was extracted from samples by reacting with excess 100% orthophosphoric acid in vacuo (McCrea, 1950) at a constant temperature of 25 ^{o}C. For calcite samples approximately 20 mgs of sample was used and for francolite samples between 300-400 mgs. The francolite samples were treated in exactly the same way as calcite samples. The reaction was considered complete when evolution of gas from the sample had ceased. For calcite several hours are usually sufficient reaction time but francolite samples took upto 72 hours.